

Transport through interacting quantum dots with Majorana fermions or phonons

INAUGURAL DISSERTATION



zur Erlangung des Doktorgrades
der Mathematisch-Naturwissenschaftlichen Fakultät
der Heinrich-Heine-Universität Düsseldorf

vorgelegt von

ROLAND HÜTZEN

aus Düsseldorf

Düsseldorf, Juli 2013

Aus dem Institut für Theoretische Physik IV
der Heinrich-Heine Universität Düsseldorf

Gedruckt mit der Genehmigung der
Mathematisch-Naturwissenschaftlichen Fakultät der
Heinrich-Heine Universität Düsseldorf

© Roland Hützen

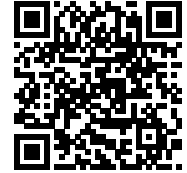
Referent: Prof. Dr. Reinhold Egger
Koreferent: Prof. Dr. Jürgen Horbach

Tag der mündlichen Prüfung: 04.07.2013

This thesis is based on the following original publications:

Part I:

Majorana single-charge transistor,
R. Hützen, A. Zazunov, B. Braunecker,
A. Levy Yeyati and R. Egger,
Phys. Rev. Lett **109**, 166403 (2012).



Original abstract: We study transport through a Coulomb blocked topologically non-trivial superconducting wire (with Majorana end states) contacted by metallic leads. An exact formula for the current through this interacting Majorana single-charge transistor is derived in terms of wire spectral functions. A comprehensive picture follows from three different approaches. We find Coulomb oscillations with universal halving of the finite-temperature peak conductance under strong blockade conditions, where the valley conductance mainly comes from elastic cotunneling. The nonlinear conductance exhibits finite-voltage sidebands due to anomalous tunneling involving Cooper pair splitting.

This work was awarded with the “INC Young Researchers Prize in Materials Science”, founded by the Instituto Nicolás Cabrera, Universidad Autónoma de Madrid, Spain.

Part II:

*Iterative summation of path integrals
for nonequilibrium molecular quantum transport*,
R. Hützen, S. Weiss, M. Thorwart and R. Egger,
Phys. Rev. B **85**, 121408(R) (2012).



Original abstract: We formulate and apply a nonperturbative numerical approach to the nonequilibrium current, $I(V)$, through a voltage-biased molecular conductor. We focus on a single electronic level coupled to an unequilibrated vibration mode (Anderson-Holstein model), which can be mapped to an effective three-state problem. Performing an iterative summation of real-time path integral (ISPI) expressions, we accurately reproduce known analytical results in three different limits. We then study the crossover regime between those limits and show that the Franck-Condon blockade persists in the quantum-coherent low-temperature limit, with a nonequilibrium smearing of step features in the IV curve.

Summary

Recent advances in the search for Majorana fermions within condensed matter systems inspired the first part of the thesis. These hypothetical particles which are their own antiparticles are predicted to arise in the form of quasi-particle excitations called Majorana bound states at the surface of engineered condensed matter systems. An experimental detection is challenging since their defining property also implies that they possess no charge, no energy and no spin. This significantly reduces the possibilities to interact with them and get a proof of their existence from a measurement. The most promising experimental results are based on transport measurements where current-voltage-characteristics play the role of a spectroscopy signal. In this thesis, we investigate a single electron transistor setup which hosts a spatially separated pair of Majorana fermions with respect to their influence on its transport characteristics. We focus on a master equation approach including sequential and cotunneling contributions. After deducing all relevant rates we solve the system numerically over a broad parameter regime. For some limits, we also elaborate analytical solutions. In comparison with collaboratively worked out other methods we provide a broad understanding of the setup and make a proposal how our results could be used as a detection scheme for Majorana fermions.

The second part of the thesis investigates the spinless Anderson-Holstein model which is the minimal model for molecular transport. It models a molecule with electronic and vibronic degrees of freedom which is placed between metallic leads at different chemical potentials to investigate again its transport properties. Also here we intended to gain access to a broad parameter regime and successfully extended the numerical “iterative summation of path-integrals” scheme to this model. It is based on a real-time path-integral approach in combination with the nonequilibrium Keldysh technique and is numerically exact. Within a finite memory time the scheme fully takes into account all time-nonlocal correlations within the self energies of the leads and we extended it to also handle time-nonlocal interactions originating from the electron-phonon coupling. The latter was possible by exactly mapping the Anderson-Holstein model to an effective three-state-system and the introduction of a spin 1 auxiliary field within each short-time propagator of the real-time path-integral. An extrapolation scheme which is based on a least dependence approach then allows to eliminate the errors introduced by the finite memory time and the time discretization in a systematic way. We benchmarked our scheme against three other analytical methods, valid in three different corners of the parameter space where approximative expansions are possible. Finally we could demonstrate with our method the persistence of the Franck-Condon blockade in a deep quantum regime, inaccessible by the other methods.

Zusammenfassung

Der erste Teil dieser Arbeit wurde durch neue Fortschritte auf der Suche nach Majorana Fermionen in Festkörpersystemen inspiriert. Die Existenz dieser hypothetischen Teilchen, die ihre eigenen Antiteilchen sind, wurde in Form von Quasiteilchen, sogenannten gebundenen Majorana Zuständen, an der Oberfläche speziell konstruierter Festkörpersysteme vorhergesagt. Ihr experimenteller Nachweis gestaltet sich jedoch als schwierig, da ihre definierende Eigenschaft impliziert, dass sie ladungs-, energie- und spinlos sein müssen. Die Möglichkeiten sie zu detektieren werden dadurch entschieden reduziert. Die bisher vielversprechendsten Experimente basieren auf Transportmessungen, bei denen eine charakteristische Strom-Spannungs Relation als spektroskopisches Signal dient. In dieser Arbeit untersuchen wir an einem Einzelelektronentransistoraufbau, der zwei räumlich getrennte Majorana Fermionen beherbergt, deren Einfluss auf seine Strom-Spannungs Charakteristik. Den Schwerpunkt legen wir hierbei auf einen Mastergleichungsansatz, der sequentielle Raten sowie Kotunnelraten berücksichtigt. Nachdem wir alle Raten hergeleitet haben, lösen wir die Mastergleichung numerisch über einen weiten Parameterbereich und in einigen Bereichen auch noch analytisch. Durch den Vergleich mit noch anderen kollaborativ ausgearbeiteten Methoden, ergänzen wir abschließend das physikalische Verständnis des Aufbaus zu einem möglichst großen Gesamtbild. Basierend auf unseren Erkenntnissen schlagen wir dann ein Detektionsschema für Majorana Fermionen mit Hilfe unseres Aufbaus vor.

Im zweiten Teil dieser Arbeit untersuchen wir das spinlose Anderson-Holstein Modell, welches das minimale theoretische Studienobjekt für die Untersuchung molekularen Transports ist. Es modelliert ein Molekül mitsamt seinen elektronischen und vibronischen Freiheitsgraden, welches von zwei Seiten durch metallische Elektroden unterschiedlichen chemischen Potentials kontaktiert ist. So wird wiederum die Untersuchung von Transporteigenschaften ermöglicht. Ziel war es diese Eigenschaften über einen großen Parameterbereich zu charakterisieren. Hierzu erweitern wir erfolgreich die Methode der “iterativen Summation von Pfadintegralen” auf dieses Modell. Sie basiert auf einem Echtzeit Pfadintegralansatz zusammen mit der Nichtgleichgewichts Keldyshtechnik und ist numerisch exakt. Alle zeitlich nicht lokalen Korrelationen des Modells werden innerhalb einer endlichen Gedächtniszeit vollständig berücksichtigt. Wir erweitern die Methode, um neben den Korrelationen innerhalb der durch die Kontakte induzierten Selbstenergie auch Korrelationen einer nicht lokalen Wechselwirkung, in unserem Falle der Elektron-Phonon Kopplung, mitzunehmen. Letzteres gelingt uns durch die exakte Abbildung des spinlosen Anderson-Holstein Systems auf ein effektives Drei-Zustandssystem. Hierzu führen wir ein Spin 1 Hilfsfeld innerhalb jedes Kurzzeitpropagators des Pfadintegrals ein. Alle Fehler, die durch die endliche Gedächtniszeit und die Diskretisierung der Zeit auftreten, werden systematisch durch ein Extrapolationsschema, basierend auf der Methode minimaler Abhängigkeiten, eliminiert. Wir testen unser entwickeltes Schema gegen drei analytische Methoden, welche jeweils in anderen Bereichen des Parameterraumes gültige Approximationen darstellen. Zum Abschluss, demonstrieren wir, dass eine Frank-Condon Blockade auch im tiefen Quantenregime, welches den anderen Methoden unzugänglich ist, weiter Bestand hat.

Introduction

Almost 60 years ago, the invention of the transistor marked the beginning of a new age. A first working example was a huge macroscopic device but soon it was miniaturized and finally integrated circuits became possible. From there on the race for a further miniaturization started and by today structural sizes of 22 nanometer are standard and quantum mechanical effects will become relevant within the design of further miniaturized devices. Up to now connections between different functional parts of an integrated circuit are assumed to behave classical and potential quantum mechanical effects are unwanted sources of errors.

Approaching this problem from another perspective is to ask what are the smallest possible structures which might be used as functional electronic devices. This gave rise to the field of molecular electronics which is still under fundamental research and represents the context of the second part of the thesis but historically the beginning of our research. A lot of experimental and theoretical effort is made to understand for example transistor setups where the active region consists of a single molecule. It is attached from two sides by metallic leads playing the role of the source and the drain for electrons. The transport behavior is strongly influenced by the internal structure of the molecule which possesses beside its electronic structure also vibronic degrees of freedom. Both can be tuned by attaching specially designed functional groups to the molecule or changing external parameters like electric fields or the presence of a surrounding solvent. A minimal theoretical model of such a molecular transistor setup is presented in the second part of this thesis and its transport properties are analyzed by extending a numerically exact method to it.

The typical transport setup used to study the conductivity of a molecule can be seen from two different points of view. On one hand the results of fundamental research will lead to an understanding how to design a molecule in the way that it will later behave as miniaturized functional device exactly in an intended way. On the other hand the analysis of current measurements can also help to understand internal structures of a molecule and therefore the whole setup also serves as a spectroscope.

Following this perspective, we get a motivation for the first and more recent part of the thesis, where we investigate a single electron transistor constructed out of a semiconductor and a superconductor in a way to give rise to Majorana bound states. They are a delocalized pair of Majorana fermions. However, their existence has not been proven yet experimentally, although there are promising experiments. Majorana fermions correspond to particles which are their own antiparticles and this property is also the reason why they are so hard to detect. It implies that they must be spinless, chargeless and possess no energy but their presence within a transistor setup modifies its differential conductance and might open a spectroscopic way to detect them. Beside of proposing a detection scheme the general transport properties of our investigated device within a large parameter regime are of fundamental interest and will be covered by different methods.

In addition to this general introduction each part will begin with a second detailed introduction motivating each part within its special field of research.

Contents

I	The Majorana Single-Charge Transistor (MSCT)	1
1	Introduction	3
1.1	Majorana fermions (MF)	4
1.2	Majorana bound states (MBS)	5
1.2.1	Kitaev’s toy model: The spinless p-wave chain with MBS	6
1.2.2	MBS in spin-orbit coupled semiconducting wires	7
1.2.3	Electron “teleportation” through MBS	9
2	The Majorana single-charge transistor	11
2.1	The MSCT Hamiltonian	12
2.2	Master equation approach	13
2.2.1	Rate derivation up to second order from golden rule	14
2.2.2	Compact rate expressions	20
2.2.3	Expectation value of the current	21
2.3	Numerical solution of the master equation	22
2.4	Analytical solutions of the master equation	23
2.4.1	Current through the grounded wire	24
2.4.2	Linear conductance from analytics	26
2.4.3	Low temperature strong Coulomb blockade limit	28
2.5	Other methods used for comparison	31
2.5.1	Exact expression for the current	31
2.5.2	Equation-of-motion (EOM) approach	32
2.5.3	Zero-bandwidth model (ZBWM)	32
2.5.4	Weak coupling limit	32
3	Results	33
3.1	Peak conductance halving	33
3.2	Coulomb blockade	34
3.2.1	Coulomb oscillations	34
3.2.2	Finite-voltage sidebands	35
4	Conclusions	39
II	Iterative Summation of Path-Integrals (ISPI) for nonequilibrium molecular quantum transport	41
5	Introduction	43
5.1	The spinless Anderson-Holstein (AH) model	44
5.2	The Hamiltonian	45
5.3	The current operator	46

6	The Keldysh path-integral formalism	47
6.1	The Keldysh formalism	47
6.1.1	The initial equilibrium partition function	48
6.1.2	The Keldysh generating function	49
6.2	The real-time coherent state path-integral	49
6.2.1	Fermionic and bosonic coherent states	50
6.2.2	The Trotter Suzuki break-up	51
6.2.3	Generating function from real-time path-integral	52
6.3	The AH short-time propagators	53
6.4	Gaussian integration and matrix notation	57
7	Fourier transformation of the free lead Green's function (GF)	63
7.1	General expression in continuum limit	63
7.2	Flat infinite band limit	64
7.3	Flat finite band (hard cut-off)	65
7.4	Comparison of flat wide and flat finite band	66
7.4.1	Finding the optimal cut-off	67
8	The resonant level (RL) model	69
8.1	Discrete solution for the RL model	69
8.2	Continuous solution for the RL model	70
8.2.1	Continuous time representation of GFs	71
8.2.2	Continuous frequency representation of GFs	72
8.2.3	The Meir Wingreen formula	72
8.2.4	The GF of the RL model	73
8.2.5	The analytical current for the RL model	74
9	Extension of the ISPI scheme to the AH model	75
9.1	Change to the ISPI basis-ordering	76
9.2	Cut-off scheme	76
9.3	Construction of the ISPI scheme - fermionic part	77
9.4	Construction of the ISPI scheme - bosonic part	81
9.5	Data handling, extrapolation and convergence	82
10	Analytical approaches to the AH model	85
10.1	Perturbative expansion in the phonon coupling	86
10.2	Sequential tunneling approximation	87
10.3	Nonequilibrium Born Oppenheimer approximation (NEBO)	90
11	Numerical results	93
11.1	Check against the RL model	93
11.2	Benchmark against approximative analytics	94
11.3	Franck-Condon (FC) blockade	96
12	Conclusions	99

Appendix MSCT

A Regularization scheme for cotunneling rates	103
A.1 General structure of the cotunneling rates	103
A.2 Isolation of divergent residuals	104
A.3 The regularization scheme - Physical motivation	105
A.4 The regularized integral	105
A.5 Special limits	107

Appendix ISPI

B Perturbation theory at finite temperature	111
B.1 Green's function of the "free" phonon	111
B.1.1 Time representation	111
B.1.2 Frequency representation	111
B.2 The second order retarded self-energy	112
B.2.1 The causal component of the self energy	112
B.2.2 The lesser component of the self-energy	113
B.2.3 The retarded self-energy	113
B.3 Solving the remaining integrals	114

Part I

The Majorana Single-Charge Transistor (MSCT)

1 Introduction

Topologically nontrivial insulators and superconductors exhibit many remarkable nonlocal features such as non-Abelian statistics or teleportation ([1, 2] & Sec. 1.2.3). For a one-dimensional topological superconductor (TS) wire, such effects can be traced back to the existence of a zero-energy Majorana bound state (MBS) localized at each end ([3, 4, 5, 6, 7] & Sec. 1.2).

When a grounded TS is weakly contacted by a normal metal, the MBS is expected to produce a characteristic zero-bias anomaly peak in the tunnel conductance [8, 9, 10, 11, 12]. Recently, such a feature has been experimentally observed in tunnel spectroscopy using InSb or InAs nanowires [13, 14, 15, 16], where Majorana fermions are theoretically expected due to the interplay of strong spin-orbit coupling, Zeeman field, and proximity-induced superconducting pairing ([17, 18, 19], Sec. 1.2.1 and 1.2.2) Recent reviews [1, 2, 6, 7, 19] have also summarized alternative MBS proposals.

In this thesis we discuss an interacting variant of previously studied Majorana wire set-ups, the floating “Majorana single-charge transistor” (MSCT) which consists of a TS wire hosting two MBS which is tunnel coupled with two metallic leads at both ends and Josephson coupled to a superconducting substrate (see also Fig. 2.1). A comprehensive picture of its transport properties in the presence of interactions emerges from our later analysis in Sec. 2.2 and 2.5. Noting that the experimentally observed peak features could be related to a disorder-induced spectral peak [20, 21], our results should help to distinguish the Majorana state from alternative explanations in future experiments.

Previous works [22, 23, 24] have studied electron-electron interactions in an isolated TS wire and found that Majoranas still exist under rather general conditions. We study instead a generalization of the set-up in Ref. [13], where source and drain metallic electrodes contact the TS wire. We stress that the MSCT could be realized not only with nanowires but using most other Majorana proposals as well. In such a geometry, Coulomb blockade effects due to the finite charging energy E_c of the TS can play a decisive role. For instance, one expects Coulomb oscillations of the conductance as a function of a gate voltage parameter n_g , with peaks (valleys) near half-integer (integer) n_g , while in the noninteracting ($E_c = 0$) limit, the MBSs pinned to zero energy cause resonant Andreev reflection (AR) [8, 9, 10, 11], with n_g -independent linear conductance $G = 2e^2/h$ at temperature $T = 0$. Resonant AR also survives for $E_c \lesssim \Gamma = \Gamma_L + \Gamma_R$, albeit with reduced conductance [25]. For $E_c \gg \Gamma$, Coulomb blockade is firmly established, and the peak conductance approaches the (spinless) resonant tunneling value $G = e^2/h$, which has been pointed out as a signature of electron teleportation [26].

In this work, we consider Coulomb blocked charge transport through the MSCT; for a variant with one superconducting and one metallic lead, see Ref. [27]. We provide an exact expression for the current in this interacting system, and develop three different approximation schemes to study Coulomb oscillations in the MSCT both for $T = 0$ and finite T . We quantitatively describe the $T = 0$ crossover of the peak conductance from $G = 2e^2/h$ to e^2/h as E_c/Γ increases, which constitutes a characteristic signature of Majorana

ranas. Remarkably, this “halving” of the peak conductance is universal and found to hold for arbitrary T . For the valley conductance, we find that elastic cotunneling dominates while AR is subleading. We predict finite-voltage sidebands in the nonlinear differential conductance which are directly related to anomalous tunneling processes where the Majorana state and the Cooper-pair number change simultaneously. The presence of Majoranas can be unambiguously identified in experiments by the magnetic field dependence of the sideband location.

If not explicitly stated otherwise, we set $e = \hbar = k_B = c = 1$ throughout the whole thesis and before we explicitly introduce the MSCT setup, we will first provide the necessary background information which directly leads to the MSCT setup and also explains a possible way for its experimental realization. Since all of the interesting features of the MSCT are based on the MBS, which are nothing else than a condensed matter realization of Majorana Fermions we start from their definition.

1.1 Majorana fermions

The relativistic extension of quantum mechanics by Dirac led to the prediction [28] of the existence of antiparticles. The most prominent and also first observed example is the positron as the antiparticle of the electron. Dirac’s prediction was in 1928 and the discovery [29] in 1932 within the cosmic radiation. From his framework antiparticles naturally arise as an always existing second complex conjugate solution of the Dirac equation with respect to an existing one. They always possess the negative energy of the corresponding particle and the opposite charge but the same spin. This symmetry imposes the question if there are particles which are their own antiparticles. The mathematical possibility requires a real solution to the Dirac equation which was found in 1937 by Ettore Majorana [30]. Since the equation itself describes spin-1/2-particles they are called Majorana fermions (MF). Within the framework of the second quantization, a fermionic creation operator γ_i^\dagger and its conjugate annihilation operator γ_i must be equal for a Majorana state

$$\gamma_i^\dagger = \gamma_i . \quad (1.1)$$

These Majorana operators still obey a fermionic anticommutation relation but generate an unconventional algebra since the definition of a number operator leads to a constant and leaves the occupation number of a single Majorana state undefined

$$\{\gamma_i, \gamma_j^\dagger\} = \delta_{i,j} \quad \Rightarrow \quad \gamma_i^\dagger \gamma_i = \gamma_i^2 = 1/2 . \quad (1.2)$$

The only way to associate an occupation number to Majorana states is to use their relation to a conventional Dirac fermion state composed of two Majorana fermion states. Formally, one can construct Majorana fermion operators from the real and imaginary part of a conventional Dirac fermion operator

$$\left. \begin{array}{l} \gamma_B = \frac{1}{\sqrt{2}}(d + d^\dagger) \\ \gamma_A = \frac{1}{i\sqrt{2}}(d - d^\dagger) \end{array} \right\} \Leftrightarrow \left\{ \begin{array}{l} d = \frac{1}{\sqrt{2}}(\gamma_B + i\gamma_A) \\ d^\dagger = \frac{1}{\sqrt{2}}(\gamma_B - i\gamma_A) \end{array} \right. . \quad (1.3)$$

but without a mechanism to spatially separate such Majorana pairs, this remains a local purely mathematical transformation.

Up to now, we only argued from a mathematical point of view that Majorana fermions are an allowed solution to the Dirac equation. But if there really exist fundamental particles which are Majorana fermions is still an open question. One possible candidate is the neutrino. A consequence would be the possibility of a neutrinoless double beta decay. This extremely seldom process consists of a decay of two neutrons into two electrons, two protons, and usually two electron antineutrinos. If the neutrino is a Majorana fermion, the two (anti)neutrinos could annihilate each other and represent a purely virtual excitation, rendering the double beta decay neutrinoless.

Opposed to searching for MFs among elementary particles, there are different proposals how to generate them as quasi-particles within engineered condensed matter systems. A very good review on this is given in Ref. [19] and we will now follow the argumentation from there.

In metallic systems, excitations are described by the creation and annihilation of electrons and holes in certain states with the possibility of electron hole annihilation. But since they always carry opposite charge, they are no candidates for MFs. If they exist in condensed matter systems they must be nontrivial excitations constructed out of fundamental building-blocks.

Based on (1.3) we can already claim that they can only appear in pairs and must be linked to superpositions of electrons and holes which are charge-neutral and naturally arise for example as excitations in superconductors. In a s-wave superconductor, forming singlet Cooper-pairs, these excitations schematically take the form

$$\tilde{\gamma} = uc_{\uparrow}^{\dagger} + vc_{\downarrow} \quad \Rightarrow \quad \tilde{\gamma}^{\dagger} = v^*c_{\downarrow}^{\dagger} + u^*c_{\uparrow} \neq \tilde{\gamma} \quad \forall \quad u, v \in \mathbb{C} , \quad (1.4)$$

in terms of electron creation and annihilation operators c_{\uparrow}^{\dagger} and c_{\downarrow} with opposite spins. Therefore the spin prevents these excitations from being candidates for MFs. Avoiding this problem is possible in “spinless” superconductors, i.e. systems with only one active spin species. Due to the Pauli exclusion principle their pairing must occur with odd parity like in exotic p-wave superconductors forming triplet Cooper-pairs. Schematically the desired excitations have the form of Eq. (1.5) after dropping spin indices $\{\uparrow, \downarrow\}$.

$$d = uc^{\dagger} + vc \quad \Rightarrow \quad d^{\dagger} = v^*c^{\dagger} + u^*c = d \quad \text{for} \quad u = v^*, v = u^* . \quad (1.5)$$

We will now proceed with a minimal 1D model which includes a p-wave pairing term and allows for the existence as well as for the spatial separation of a MF pair.

1.2 Majorana bound states (MBS)

Next, we deal with a 1D toy model proposed by Kitaev in [3]. His work was motivated by quantum computation. Since MF in condensed matter systems always appear as pairs, only these pairs possess a defined occupation number. A spatial separation of such a pair still can store information in the form of a conventional fermion, but its delocalization will render the state immune to local perturbations and thus protect it from most types of decoherence. Although his model is quite simple, it allows to understand how a spatially separated pair of MF can arise.

1.2.1 Kitaev's toy model: The spinless p-wave chain with MBS

Kitaev's toy model is a finite 1D tight-binding chain of spinless fermionic sites, including a nearest neighbor hopping term and proximity induced p-wave superconductivity

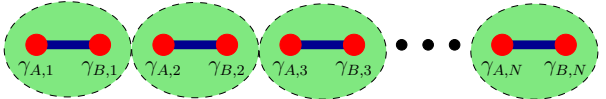
$$H = -\mu \sum_{n=1}^N c_n^\dagger c_n - \frac{1}{2} \sum_n (t c_n^\dagger c_{n+1} + \Delta c_n c_{n+1} + \text{H.c.}) . \quad (1.6)$$

Operators c_n^\dagger refer to conventional Dirac fermions and the index labels the chain sites. The occupation of the sites is determined by the chemical potential μ . The formation of Cooper-pairs involving adjacent sites is governed by the superconducting gap $\Delta = |\Delta|e^{i\chi}$ including the superconducting phase χ . The next neighbor hopping is proportional to the hopping amplitude t . Without loss of generality we choose $\chi = 0$ in this section¹. The interesting properties of the chain arise after decomposing each fermionic site into its real and imaginary part using the identity from Eq. (1.3)

$$c_n = \frac{1}{\sqrt{2}}(\gamma_{B,n} + i\gamma_{A,n}) . \quad (1.7)$$

By choosing appropriate parameters one can now drive the system into two different phases. The first is reached by switching off the superconductivity $\Delta = 0$ and setting a negative chemical potential $\mu < 0$. It is topologically equivalent to the vacuum and therefore called "trivial". Topologically equivalent in this context means, that by still respecting the parameter definition of the phase, there exists the smooth transformation $\mu \rightarrow -\infty$ which completely empties the chain and establishes the equivalence to the vacuum. The Hamiltonian (1.6) reduces to be

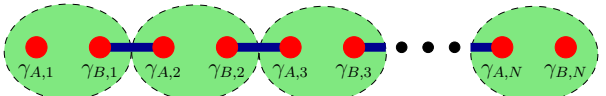
(a) topologically trivial: (1 ground state: "vacuum"): $t = \Delta = 0 ; \mu < 0$

$$H = -\mu \sum_{n=1}^N i\gamma_{B,n}\gamma_{A,n} .$$


The schematic illustration right to the Hamiltonian emphasizes the local pairing of Majorana operators on each site resulting in a conventional fermionic chain.

The second and topologically nontrivial phase of the system is reached by setting the chemical potential to zero and the finite hopping equal to the superconducting gap. Again by decomposing all fermionic operators into their real and imaginary parts the Hamiltonian now reduces to be

(b) topologically nontrivial: (2 ground states: "differ by parity") $t = \Delta > 0 ; \mu = 0$

$$H = 0d^\dagger d - t \sum_{n=1}^{N-1} i\gamma_{B,n}\gamma_{A,n+1} .$$


The schematic illustration shows again the Majorana operator pairings which now always

¹For arbitrary χ see Ref. [3] or [19].

involve adjacent sites. Due to the two ends of the chain there are two locally unpaired Majorana operators left which correspond to two Majorana bound states (MBS) forming a highly nonlocal fermionic level fixed at zero energy, represented by the operator

$$d = (\gamma_{A,1} + i\gamma_{B,N})/\sqrt{2}. \quad (1.8)$$

The occupation number of this level is called parity of the system. Since it can be occupied at no cost of energy it causes a parity degenerate ground state. For this second phase, there is no continuous transformation into the vacuum, without closing the superconducting gap which contradicts its definition. Consequently, both phases are topologically different [1]. The topological invariant which distinguishes the two phases is the existence of the two MBS. They only disappear after a topological phase transition to the trivial phase. Regarding conductivity, in the topological phase the wire is superconducting in the bulk but metallic at its surface, the ends. This difference between the bulk to surface properties also gave rise to the name topological superconductor (TS). This concept is an extension of the classification of insulators based on topological invariants to superconductors. For more details on this classification we refer to [1].

We derived the existence of MBS from a “spinless” chain model. Allowing for a second spin species doubles the chain and leads to the formation of MF pairs at the ends of the chain. These pairs would form local conventional fermions again and destroy the nontrivial topological phase of the system.

1.2.2 MBS in spin-orbit coupled semiconducting wires

Kitaev’s chain is a theoretical toy model and the most crucial point is that the model is spinless, but also involves a term creating Cooper-pairs. An experimental realization must be based on an energetic separation of the different spin species to enter a “spinless” regime. Consequently a pairing in this regime must occur within the same spin species. This is only possible for an intrinsic p-wave superconductor or a system which effectively behaves like one. The first option faces serious problems since p-wave superconductivity is extremely rare in nature and also not long-ranged ordered enough as assumed in Kitaev’s model. But due to the proposals [17, 18] based on engineering the desired system out of well known and controllable building-blocks the second option became feasible and is promising.

The fundamental setup behind the proposals is depicted in Fig. 1.1 (a) and consists of a 1D wire with strong intrinsic spin-orbit coupling in the proximity of an ordinary s-wave superconductor and an external magnetic field B perpendicular to the wire. The corresponding wire Hamiltonian reads

$$H_{wire} = \int dx \psi^\dagger \left(\frac{k^2}{2m} - \mu + \alpha k \sigma_y + E_z \sigma_z \right) \psi \quad ; \quad \psi = \begin{pmatrix} \psi_\uparrow \\ \psi_\downarrow \end{pmatrix} \quad (1.9)$$

and includes the usual kinetic term along the x -direction, a Rashba spin-orbit term [31] with coupling constant $\alpha > 0$ that favors a spin alignment along the y -direction and a Zeeman term introducing an energy split of $2E_z \geq 0$ due to the magnetic field B in z -direction. As long as the magnetic field axis is perpendicular to the spin-orbit axis, their absolute position is irrelevant. The $\sigma_{x,z}$ are Pauli matrices and ψ_σ^\dagger adds an electron

with effective mass m , chemical potential μ and spin σ to the wire. The proximity to the underlying s-wave superconductor additionally induces an electron pairing mechanism proportional to the superconducting gap Δ . The complete Hamiltonian of the setup from Fig. 1.1 (a) is phenomenologically modeled by

$$H = H_{wire} + \int dx (\Delta \psi_{\uparrow} \psi_{\downarrow} + \text{H.c.}) . \quad (1.10)$$

Despite of the following qualitative explanation why this setup is one possible realization of Kitaev's chain, the exact mapping is given in [32].

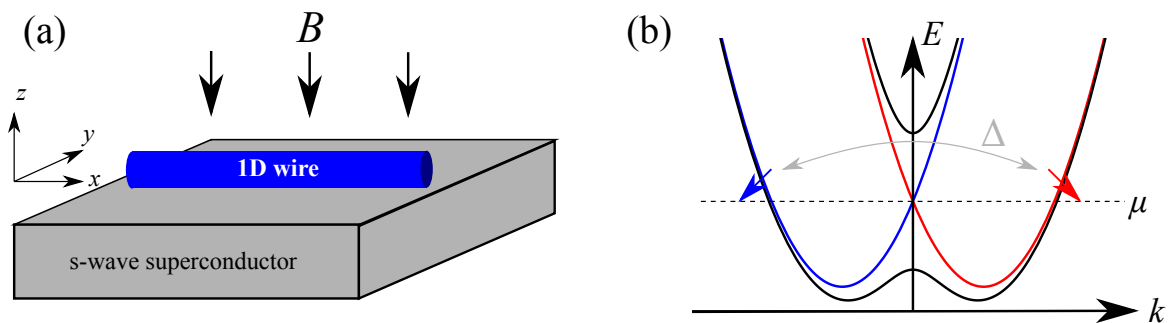


Figure 1.1: (a) Experimental setup: Semiconducting InAs or InSb wire with large g-factor and large Rashba spin-orbit coupling on top of a s-wave superconductor in a magnetic field B perpendicular to the wire. (b) Schematic illustration of the effective dispersion relation $E(k)$ between energy E and momentum k . Red and blue with Rashba field only, black for Zeeman and Rashba field present. If the chemical potential μ is tuned into the gap at $k = 0$, the wire appears “spinless” (cf. text below). The gray arrow indicates the effective p-wave pairing. Figure based on [19].

The fundamental idea is illustrated in Fig. 1.1 (b). Without a magnetic field ($E_z = 0$) and without spin-orbit coupling ($\alpha = 0$) the wire Hamiltonian corresponds to a spin degenerate parabolic dispersion. Switching on the spin-orbit coupling will result in a horizontal shifting of the two parabolas associated with the two spin species and locks the spin to the momentum at a given energy. This situation is represented by the red and blue parabola in Fig. 1.1 (b). Adding now the magnetic field also lifts the spin degeneracy at $k = 0$ and will result in the gapped dispersion shown in black. The band energies are

$$\epsilon_{\pm}(k) = \frac{k^2}{2m} - \mu \pm \sqrt{(\alpha k)^2 + E_z^2} . \quad (1.11)$$

By tuning the chemical potential to somewhere within this gap it only intersects the dispersion twice instead of four times like in a high energy situation above the gap. This halves the number of available states of the system and corresponds to a projection of the system onto the lower band. In this limit, spin is not anymore a good quantum number and we end up with an effectively spinless system. For the full Hamiltonian which also

includes the proximity induced s-wave pairing, a similar argumentation holds and the spinless phase is defined by the criterion

$$E_z > \sqrt{\Delta^2 + \mu^2} \quad (1.12)$$

which ensures that the chemical potential has only two intersections with the dispersion relation. Formally the connection between Eq. (1.10) and Kitaev's chain can be established by introducing new field operators ψ_{\pm}^{\dagger} which add electrons with energies $\epsilon_{\pm}(k)$ to the wire, using them as a new basis for Eq. (1.10) and then projecting the resulting Hamiltonian on its lower band. What remains is a "spinless" Hamiltonian and the basis rotation also creates the essential p-wave pairing term ($\propto \alpha k \Delta / E_z$) within the new basis from the initial proximity induced s-wave pairing term in the old basis. To conclude, one needs materials with a strong Rashba spin-orbit field and a large g-factor to access the topological phase of this setup. Both can be fulfilled by using InAs and InSb wires.

1.2.3 Electron "teleportation" through MBS

Before we introduce our transistor setup in the next chapter, let us first consider the following: if the wire is only weakly coupled to the superconducting substrate, Coulomb interactions will become important. Their influence on a TS wire has been studied first by Fu in Ref. [26]. A simple way to model them is to idealize the setup from Fig. 1.1 as an "floating" (not grounded) TS wire with a capacitance C which introduces a charging energy $E_c = \frac{e^2}{2C}$. We label the MBS by γ_i with an index referring to the both ends $i = L/R$ of the wire and remember the definition of the associated nonlocal fermion operator $d = (\gamma_L + i\gamma_R)/\sqrt{2}$ which defines the parity operator of the wire $\hat{n}_d = d^{\dagger}d$. Together with the number of Cooper-pairs in the wire, counted by the operator \hat{N} , its instantaneous charge state is defined by the corresponding set (N, n_d) of eigenvalues. Additionally also taking into account the influence of a gate potential V_g by a dimensionless parameter $n_g \propto V_g$, we arrive at the effective wire Hamiltonian

$$H_c = E_c(2\hat{N} + d^{\dagger}d - n_g)^2. \quad (1.13)$$

Without the nonlocal single fermion state at zero energy, we assume that there are only single fermion states above the superconducting gap Δ . Whenever the total number of electrons on the wire is even, an additional one must occupy a state above the superconducting gap and must at least possess the gap energy Δ to tunnel in. On the other hand, when the total number of electrons on the wire is odd and another one enters from the leads, a Cooper-pair can be built and this electron doesn't need to exceed the gap in energy. This separation in energy between charge states involving an even or odd total number of electrons is independent of the concept of a charging energy and vanishes with the presence of a MBS pair forming a level at zero energy, cf. Fig. 1.2. The intrinsic ground state degeneracy of a TS wire, like depicted in Fig. 1.2 (b) on the left gets also lifted by the additional inclusion of interactions in the form of a charging energy. The presence of a back-gate potential can be used to restore a single parity degenerate ground state if it is tuned to a half integer value.

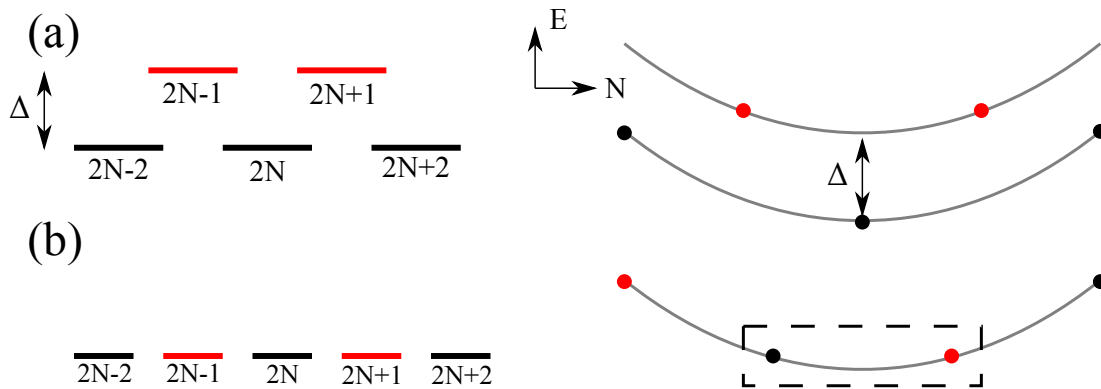


Figure 1.2: Energy spectrum of a superconductor as a function of the total number of electrons. States with an even (odd) number of electrons are marked black (red). The (right) left illustrations depict a situation with (non)zero charging energy E_c . (a) Without the existence of a MBS pair adjacent even and odd states differ at least by Δ in energy. (b) With a MBS pair present, the even-odd effect vanishes. Figure based on [26].

This situation is highlighted by a dashed box in Fig. 1.2 (b) on the right. Changing the parity of this ground state does not cost energy. Due to the presence of the charging energy it is energetically separated from all other states. In a low energy transport situation electrons will tunnel only through this highly nonlocal ground state formed by the two MBSs. This gave rise to talk of “teleportation” in this context since the process is phase coherent and the electron travels through this state from one end of the wire to the other by delocalization and not as a local quantity. The maximal conductance in this situation is $G = e^2/h$ at $T = 0$ because this teleportation through the ground state is the only open channel if the charging energy dominates and separates higher states involving Cooper pair creation. In the case of vanishing E_c (situation Fig. 1.2 (b) left) another channel is open. A normal electron can create a Cooper-pair in the wire by the reflection of a hole at the interface. This is called a local Andreev reflection and causes a maximal conductance of $2e^2/h$ in the $E_c = 0$ limit. We will get back to these processes and their contribution to the total conduction in detail during the derivation of a master equation approach in Sec. 2.2. Next we introduce our central study object of this first part of the thesis.

2 The Majorana single-charge transistor

With the Majorana single-charge transistor (MSCT) we investigate a model which extends a previously studied transport setup from Ref. [25] by the explicit inclusion of a bulk superconductor which can exchange Cooper-pairs with a TS wire placed between metallic leads and hosting MBS at its ends. The exchange is possible through a thin normal conducting barrier creating a Josephson contact. This coupling introduces the additional parameter E_J to the model from [25], representing the maximal Josephson energy of the junction. A schematic illustration of the complete setup is given in Fig. 2.1 and we will explain all remaining details below.

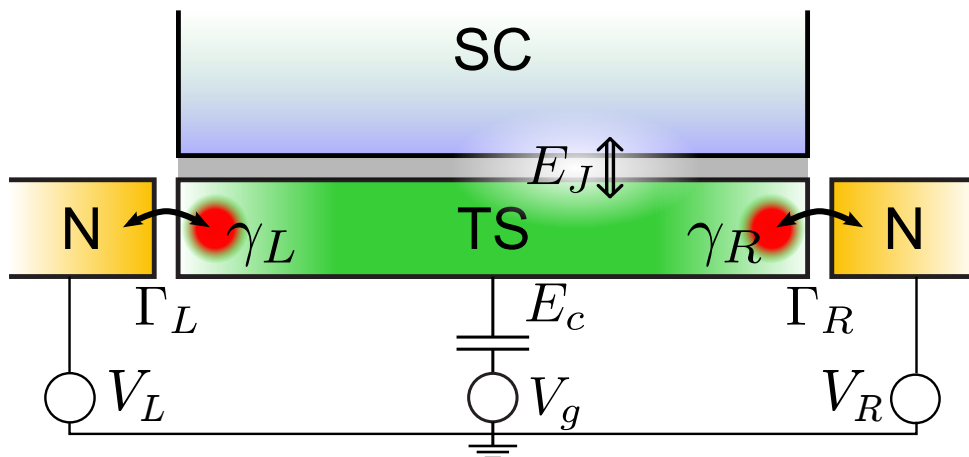


Figure 2.1: Majorana single-charge transistor: A topological superconductor (TS) wire hosting two MBS ($\gamma_{L/R}$) tunnel coupled ($\Gamma_{L/R}$) to normal metal leads (N) and Josephson coupled (E_J) to another bulk superconductor (SC). Capacitive charging effects are encoded by E_c and can be tuned by a gate voltage parameter $n_g \propto V_g$.

The MSCT device from Fig. 2.1 is a typical transport setup. We have a central region involving dominant interactions to study (tunable to some extent by gate parameters) and place it in between two normal conducting (metallic) leads separated by tunnel junctions. By applying a bias voltage $V = V_L - V_R$ to the leads, they will act as source and drain for electrons tunneling through the junctions and the central region. This nonequilibrium transport situation then allows for the study of quantities like the current as function of the bias voltage $I(V)$ or the differential conductance dI/dV in different parameter regimes. Both will show unique fingerprints of the physics within the central region and lead to a characterization of the MSCT within a wide range of its parameter space.

2.1 The MSCT Hamiltonian

For our proposed setup the theoretical description starts from the MSCT Hamiltonian consisting of three parts

$$H = H_c + H_t + H_l, \quad (2.1)$$

with H_c modeling the central region, H_t the tunneling and H_l the left and right ($j = L/R$) metallic leads. The central part is a TS wire hosting a single unpaired MBS ($\gamma_{L/R}$) near each end based on the argumentation in Sec. 1.2.1 and 1.2.2. Additionally the TS wire is explicitly Josephson coupled to another bulk superconductor (substrate) [27, 33]. The maximal Josephson energy of this junction is E_J and depends on the phase difference between the TS phase χ and the fixed bulk SC phase ϕ_S . Experimentally the Cooper-pair transfer via this Josephson junction is controllable by modifying E_J with a small magnetic field parallel to the junction. The coupling to the superconducting substrate plays the role of a controllable grounding of the TS wire. If the Cooper-pair exchange via this Josephson junction is small compared to the tunneling rates Γ_α , the Coulomb interaction within the wire becomes important. Like previously discussed in Sec. 1.2.3 we include it via a charging energy E_c . This also breaks the ground state degeneracy of a perfectly grounded TS wire with MBS. If the charging energy dominates all energy scales of the system we are in the Coulomb blockade (CB) regime and transport can become impossible. With the TS phase χ conjugate to \hat{N} , where $[\chi, \hat{N}] = i$ and $e^{-i\chi}$ ($e^{+i\chi}$) lowering (raising) N by one, H_c is an extension of Eq. (1.13) from Sec. 1.2.3:

$$H_c = E_c(2\hat{N} + \hat{n}_d - n_g)^2 - E_J \cos(\chi - \phi_S). \quad (2.2)$$

The length of the TS wire is assumed sufficiently long to exclude a direct tunnel coupling between γ_L and γ_R , corresponding to an overlap and decreasing the nonlocality of the d state. However, note that E_c introduces a dynamical coupling between the two Majoranas. We focus on the most interesting case of a large proximity gap $\Delta_{\text{TS}} > \max(E_c, \Gamma, T)$, where charge transport involves MBSs and the contribution of quasi-particles above the gap can be neglected. The lead part H_l is

$$H_l = \sum_{jk} \epsilon_{jk} c_{jk}^\dagger c_{jk}, \quad \epsilon_{jk} = \epsilon_k + \mu_j, \quad (2.3)$$

with electrons in lead j corresponding to free fermions with chemical potential² $\mu_j = \mu_j(V)$, dispersion relation ϵ_k and (effectively spinless [25]) fermionic operators $c_{j,k}$ for momentum k . H_l is treated within the usual wide-band approximation³ and the bias voltage is $eV = \mu_L - \mu_R$. Taking into account charge conservation and expressing the Majoranas in terms of the nonlocal d fermion, the tunnel Hamiltonian reads [25]

$$H_t = \sum_j \lambda_j c_j^\dagger \eta_j + \text{H.c.}, \quad \eta_j = \frac{1}{\sqrt{2}}(d + s_j e^{-i\chi} d^\dagger), \quad (2.4)$$

where $c_j = \sum_k c_{j,k}$, $s_{L/R} = \pm 1$ and $\lambda_{L,R}$ denotes the respective tunnel matrix elements [11]. Tunneling from the TS to lead j thus proceeds either by destroying the d state

²Measured with respect to the chemical potential $\mu_s = 0$ of the TS condensate.

³It is straightforward to go beyond this approximation by allowing for energy-dependent $\Gamma_j(\epsilon)$ in the equations below.

without changing N (“normal” tunneling - later also called channel “ a ”) or by occupying the d state and simultaneously splitting a Cooper-pair (“anomalous” tunneling - later also called channel “ b ”), plus the conjugate processes.

During the following derivations we use the hybridization scales $\Gamma_j = 2\pi\nu_j|\lambda_j|^2$, where ν_j is the density of states in lead j at the Fermi level. Experimentally, the Γ_j (and n_g) can be changed via gate voltages [13]. Realistic parameter estimations for an experimental realization of an MSCT setup can be found in [13] since they deal with the same components but a different setup.

We will now start to analyze the transport properties of the MSCT from a master equation approach.

2.2 Master equation approach

For finite temperature and the time between tunneling events being the largest time scale in the system ($\Gamma_L + \Gamma_R = \Gamma \ll T = 1/\beta$) the occupation probabilities P_Q of a wire charge state $|Q\rangle \equiv |N, n_d\rangle$ in the presence of the leads are accessible after solving a master equation. For simplicity we have set $E_J = 0$ here⁴ and defined $Q = 2N + n_d$. We are only interested in a stationary state solution ($\dot{P}_Q = 0$) and not in the time evolution. This defines the master equation for the occupation probabilities

$$\dot{P}_Q = \sum_{Q' \neq Q} [W_{Q' \rightarrow Q} P_{Q'} - W_{Q \rightarrow Q'} P_Q] = 0 \quad ; \quad \sum_Q P_Q = 1 . \quad (2.5)$$

The transition rates $W_{Q \rightarrow Q'}$ are a summation of all rates contributing to a transition from $|Q\rangle$ to $|Q'\rangle$ up to a maximal order taken into account

$$W_{Q \rightarrow Q \pm 1} = \sum_{j=L/R} \Gamma_{j, Q \rightarrow Q \pm 1}^{(\text{SEQ})} \quad ; \quad W_{Q \rightarrow Q \pm 2} = \Gamma_{LR, Q \rightarrow Q \pm 2}^{(\text{AR})} + \sum_{j=L/R} \Gamma_{jj, Q \rightarrow Q \pm 2}^{(\text{AR})} . \quad (2.6)$$

Schematically Fig. 2.2 shows all transitions possible in our expansion. Next, we will first present a systematic second-order T -matrix expansion in $\Gamma_{L,R}$ to derive the sequential tunneling rates $\Gamma_{j, Q \rightarrow Q \pm 1}^{(\text{SEQ})}$ and local and nonlocal cotunneling rates associated with Andreev reflection processes $\Gamma_{jj', Q \rightarrow Q \pm 2}^{(\text{AR})}$. (A detailed description of the processes is given during their derivation.)

Afterwards we define the exact relations for the currents through the MSCT. The master equation (2.5) represents a net charge flow analysis between different wire charge states, leading to a stationary distribution. Once the distribution is known a similar net flow analysis between the leads, based on the known occupation probabilities, provides the currents in the system. Finally we provide numerical and analytical strategies to solve the master equation.

⁴Additional rates (not specified here) involving Cooper-pair transfer between the TS and the bulk superconductor must be included for finite E_J .

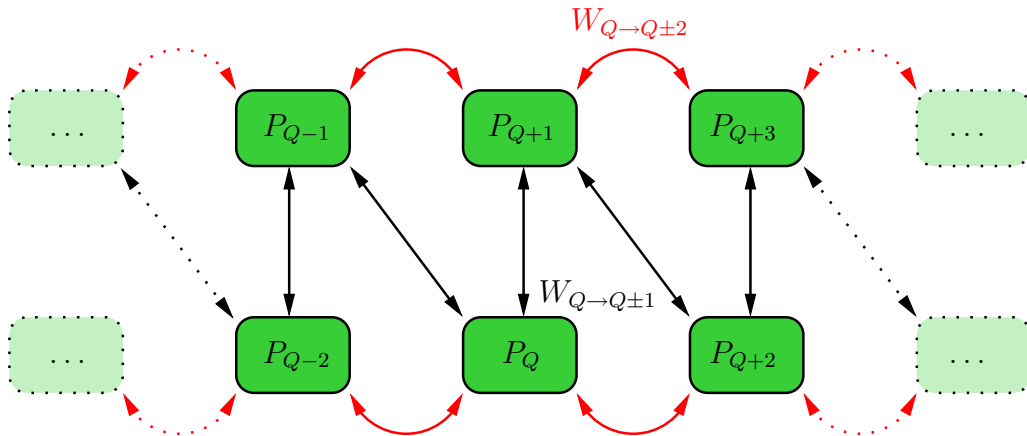


Figure 2.2: Schematic illustration of the infinite set of states involved in the master equation (labeled by their occupation probabilities $P_Q \equiv P_{n_d}(N)$) and all possible transition rates taken into account. The upper and lower states have different parity.

2.2.1 Rate derivation up to second order from golden rule

We consider the weak tunneling regime with Γ being the smallest energy in the system and treat H_t as a perturbation. We work in a charge basis and the dot is described by a nonequilibrium ($V \neq 0$) distribution function $P_Q \equiv P_{n_d}(N; t)$ that gives the probability to find the dot in the instantaneous charge state $|Q\rangle \equiv |n_d, N\rangle$, where $n_d \in \{0, 1\}$ and $N \in \mathbb{N}_0$ are eigenvalues of \hat{n}_d and \hat{N} , respectively. Transition rates between various dot states can be calculated from Fermi's golden rule using a T -matrix expansion [34] in H_t :

$$T = H_t + H_t G(E_i) T, \quad G(E_i) = \frac{1}{E_i - H_0 + i0}, \quad H_0 = H_c + H_{leads}, \quad (2.7)$$

where E_i is the energy of a given initial state of the decoupled 'dot plus leads' system.

Sequential tunneling

To lowest order in H_t , the transition rate between an initial $|i\rangle$ and a final $|f\rangle$ state is

$$\Gamma_{fi}^{(1)} = \frac{2\pi}{\hbar} |\langle f | H_t | i \rangle|^2 \delta(E_i - E_f). \quad (2.8)$$

According to Eq. (2.4), there are two types of tunneling processes between the dot and the leads in the lowest order:

- (a) not involving the condensate, $|0, N\rangle \leftrightarrow |1, N\rangle$
- (b) involving the condensate, $|0, N\rangle \leftrightarrow |1, N-1\rangle$.

Below we refer to these processes as channel *a* ('normal') and *b* ('anomalous'), respectively. Note that in the deep CB regime, these channels become basically decoupled for half-integer n_g , which leads to the unitary conductance value e^2/h instead of $2e^2/h$ [26]. This

regime corresponds to the energy situation depicted in Fig. 1.2, bottom right. For large enough E_c only the two states marked with the dashed box are accessible by the system. Regarding for example the right state, marked black, the two channels correspond to transitions either to the adjacent left or right red state. While for the left transition no energy must be paid, the transition to the right state costs energy and gets suppressed and finally blocked in the deep CB regime.

Throughout the thesis we define the Fermi- and the Bose-distribution without chemical potentials

$$n_F(\epsilon) = \frac{1}{e^{\beta\epsilon} + 1} \quad ; \quad n_B(\epsilon) = \frac{1}{e^{\beta\epsilon} - 1} , \quad (2.9)$$

to facilitate calculations when using symmetry relations like

$$n_F(\epsilon) = 1 - n_F(-\epsilon) \quad ; \quad 1 + n_B(\epsilon) = -n_B(-\epsilon) . \quad (2.10)$$

Assuming that the dot is initially in the state $|n_d, N\rangle$, the rates $\Gamma_{j,\alpha}^{(\text{SEQ},+)}(n_d, N)$ for tunneling through channel $\alpha = a/b$ from lead $j = L/R$ onto the dot are given by:

$$\Gamma_{j,a}^{(\text{SEQ},+)}(n_d, N) = \pi |\lambda_j|^2 \sum_k n_F(\epsilon_k) \delta(E_1(N) - (E_0(N) + \epsilon_{jk})) \delta_{n_d,0} , \quad (2.11)$$

$$\Gamma_{j,b}^{(\text{SEQ},+)}(n_d, N) = \pi |\lambda_j|^2 \sum_k n_F(\epsilon_k) \delta(E_0(N+1) - (E_1(N) + \epsilon_{jk})) \delta_{n_d,1} , \quad (2.12)$$

where $E_{n_d}(N)$ are charging-energy eigenvalues of H_c for $E_J = 0$:

$$E_{n_d}(N) = E_c (2N + n_d - n_g)^2 . \quad (2.13)$$

In the wide-band approximation, summation over k yields:

$$\begin{aligned} \sum_k n_F(\epsilon_k) \delta(\epsilon_{jk} - \epsilon_\alpha^+(N)) &= \int d\xi \sum_k \delta(\xi - \epsilon_k) n_F(\xi) \delta(\xi + \mu_j - \epsilon_\alpha^+(N)) \\ &\approx \nu_j n_F [\epsilon_\alpha^+(N) - \mu_j] , \end{aligned} \quad (2.14)$$

where $\nu_j = \sum_k \delta(\epsilon_k)$ is the density of states in each lead, and

$$\epsilon_\alpha^+(N) = \begin{cases} E_1(N) - E_0(N), & \text{for } \alpha = a \\ E_0(N+1) - E_1(N), & \text{for } \alpha = b \end{cases} \quad (2.15)$$

is a single-charge excitation energy in the channel α . As a result, one obtains:

$$\Gamma_{j,\alpha}^{(\text{SEQ},+)}(n_d, N) = \frac{\Gamma_j}{2} n_F [\epsilon_\alpha^+(N) - \mu_j] (\delta_{\alpha,a} \delta_{n_d,0} + \delta_{\alpha,b} \delta_{n_d,1}) , \quad (2.16)$$

where Γ_j is the previously defined hybridization. Similarly, defining

$$\epsilon_\alpha^-(N) = \begin{cases} E_1(N) - E_0(N), & \text{for } \alpha = a \\ E_0(N) - E_1(N-1), & \text{for } \alpha = b \end{cases} \quad (2.17)$$

the rates $\Gamma_{j,\alpha}^{(\text{SEQ},-)}(n_d, N)$ for tunneling out of the dot into lead $j = L/R$ are given by

$$\Gamma_{j,a}^{(\text{SEQ},-)}(n_d, N) = \pi |\lambda_j|^2 \sum_k [1 - n_F(\epsilon_k)] \delta(E_1(N) - (E_0(N) + \epsilon_{jk})) \delta_{n_d,1}, \quad (2.18)$$

$$\Gamma_{j,b}^{(\text{SEQ},-)}(n_d, N) = \pi |\lambda_j|^2 \sum_k [1 - n_F(\epsilon_k)] \delta(E_0(N) - (E_1(N-1) + \epsilon_{jk})) \delta_{n_d,0}. \quad (2.19)$$

In the wide-band limit this is equivalent to:

$$\Gamma_{j,\alpha}^{(\text{SEQ},-)}(n_d, N) = \frac{\Gamma_j}{2} (1 - n_F[\epsilon_\alpha^-(N) - \mu_j]) (\delta_{\alpha,a} \delta_{n_d,1} + \delta_{\alpha,b} \delta_{n_d,0}). \quad (2.20)$$

At sufficiently low temperature and bias voltage, quantum coherent processes will dominate⁵, so we also need the tunneling rates of the next order:

Cotunneling

To second order in H_t , the transition rate between initial $|i\rangle$ and final $|f\rangle$ states is given by [see Eq. (2.7)]

$$\Gamma_{fi}^{(2)} = \frac{2\pi}{\hbar} |\langle f | H_t G(E_i) H_t | i \rangle|^2 \delta(E_i - E_f), \quad G(E_i) = \frac{1}{E_i - H_0 + i0}. \quad (2.21)$$

Explicitly, one finds:

$$H_t G(E_i) H_t \propto \sum_{j,j'=L,R} \left[\left(c_j^\dagger d + s_{j'} e^{+i\chi} d c_{j'} \right) G(E_i) \left(d^\dagger c_j + s_j e^{-i\chi} c_j^\dagger d^\dagger \right) \right. \\ \left. + \left(d^\dagger c_{j'} + s_{j'} e^{-i\chi} c_{j'}^\dagger d^\dagger \right) G(E_i) \left(c_j^\dagger d + s_j e^{+i\chi} d c_j \right) \right]. \quad (2.22)$$

Note that these two terms operate in the mutually orthogonal Fock subspaces corresponding to $n_d = 0$ and $n_d = 1$, respectively. In Eq. (2.22), one can distinguish the following processes which may contribute to the current:

(i) *elastic cotunneling* of an electron from lead j to the opposite lead $(-j)$ through channel

$$(a) : \begin{cases} c_{-j}^\dagger d G(E_i) d^\dagger c_j & (n_d = 0) \\ d^\dagger c_j G(E_i) c_{-j}^\dagger d & (n_d = 1) \end{cases}, \quad (b) : \begin{cases} -e^{+i\chi} d c_j G(E_i) e^{-i\chi} c_{-j}^\dagger d^\dagger & (n_d = 0) \\ -e^{-i\chi} c_{-j}^\dagger d^\dagger G(E_i) e^{+i\chi} d c_j & (n_d = 1) \end{cases}; \quad (2.23)$$

In this context, ‘‘elastic’’ reflects the fact that the dot state is not changed after this process and no energy has been transferred to the dot. In contrast to this,

(ii) *inelastic cotunneling* involves two electrons from leads j and j' by creating (‘gluing’) or destroying (‘splitting’) one Cooper-pair in the final state. This will change the dot

⁵cf. conductance in the Coulomb blockade valleys of Fig. 3.2.

state and thus transfers energy to/from it which gives rise to the term “inelastic”.

$$\text{'split':} \begin{cases} c_{j'}^\dagger d G(E_i) e^{-i\chi} c_j^\dagger d^\dagger & (n_d = 0) \\ e^{-i\chi} c_{j'}^\dagger d^\dagger G(E_i) c_j^\dagger d & (n_d = 1) \end{cases}, \quad \text{'glue':} \begin{cases} e^{+i\chi} d c_{j'} G(E_i) d^\dagger c_j & (n_d = 0) \\ d^\dagger c_{j'} G(E_i) e^{+i\chi} d c_j & (n_d = 1) \end{cases}. \quad (2.24)$$

Additionally, note that the cases $j' = j$ and $j' = -j$ correspond to the processes of local and crossed Andreev reflection, respectively. (Both transport a charge of $2e$ across an interface between a superconductor and a normal metal, i.e. they convert between a normal and a supercurrent.)

Elastic cotunneling rates

For the dot in the initial state $|n_d, N\rangle$, the rates $\Gamma_j^{(\text{EC})}(n_d, N)$ for elastic cotunneling from lead j to the opposite lead ($-j$) are given by a superposition of the a - and b -channel contributions [see Eq. (2.23)]:

$$\Gamma_j^{(\text{EC})}(0, N) = \frac{\pi |\lambda_L \lambda_R|^2}{2} \sum_i \left| \langle f | c_{-j}^\dagger d G(E_i) d^\dagger c_j - e^{+i\chi} d c_j G(E_i) e^{-i\chi} c_{-j}^\dagger d^\dagger | i \rangle \right|^2 w_i \delta(E_i - E_f), \quad (2.25)$$

$$\Gamma_j^{(\text{EC})}(1, N) = \frac{\pi |\lambda_L \lambda_R|^2}{2} \sum_i \left| \langle f | d^\dagger c_j G(E_i) c_{-j}^\dagger d - e^{-i\chi} c_{-j}^\dagger d^\dagger G(E_i) e^{+i\chi} d c_j | i \rangle \right|^2 w_i \delta(E_i - E_f), \quad (2.26)$$

where the sum runs over all states in the (decoupled) leads, each weighted by a thermal distribution function w_i . Explicitly, one finds:

$$\begin{aligned} \Gamma_j^{(\text{EC})}(0, N) &= \frac{\pi |\lambda_L \lambda_R|^2}{2} \sum_{k, k'} n_F(\epsilon_k) [1 - n_F(\epsilon_{k'})] \delta(\epsilon_{jk} - \epsilon_{-j, k'}) \quad (2.27) \\ &\times \left| \frac{1}{\epsilon_{jk} - \epsilon_a^+(N) + i0} + \frac{1}{\epsilon_b^-(N) - \epsilon_{-j, k'} + i0} \right|^2 \\ &= \frac{\Gamma_L \Gamma_R}{4} \int \frac{d\epsilon}{2\pi} n_F(\epsilon - \mu_j) n_F(\mu_{-j} - \epsilon) \left| \frac{1}{\epsilon - \epsilon_a^+(N) + i0} - \frac{1}{\epsilon - \epsilon_b^-(N) - i0} \right|^2 \\ \Gamma_j^{(\text{EC})}(1, N) &= \frac{\Gamma_L \Gamma_R}{4} \int \frac{d\epsilon}{2\pi} n_F(\epsilon - \mu_j) n_F(\mu_{-j} - \epsilon) \left| \frac{1}{\epsilon - \epsilon_b^+(N) + i0} - \frac{1}{\epsilon - \epsilon_a^-(N) - i0} \right|^2, \end{aligned}$$

with $\epsilon_a^\pm(N)$ given by Eq. (2.15) and $\epsilon_b^\pm(N)$ by Eq. (2.17).

Inelastic cotunneling rates (Andreev reflection processes)

Assuming the dot in initial state $|n_d, N\rangle$, we introduce inelastic cotunneling rates $\Gamma_{j', j}^{(\text{AR}, \pm)}(n_d, N)$ for the processes which involve electrons from lead(s) j and j' and result

in a creation/annihilation of one Cooper-pair [see Eq. (2.24)]. One finds for $n_d = 0$:

$$\begin{aligned}
\Gamma_{j',j}^{(\text{AR},-)}(0, N) &= \frac{\pi |\lambda_j \lambda_{j'}|^2}{2} \sum_i w_i \delta(E_i - E_f) \\
&\quad \times \left| \langle f | c_{j'}^\dagger d G(E_i) e^{-i\chi} c_j^\dagger d^\dagger + (1 - \delta_{j',j}) s_{jj'} c_{j'}^\dagger d G(E_i) e^{-i\chi} c_j^\dagger d^\dagger | i \rangle \right|^2 \\
&= \frac{\pi |\lambda_j \lambda_{j'}|^2}{2} \sum_{k,k'} \frac{1 + \delta_{j',-j}}{2} [1 - n_F(\epsilon_k)] [1 - n_F(\epsilon_{k'})] \\
&\quad \times \delta(E_0(N) - E_0(N-1) - \epsilon_{jk} - \epsilon_{j',k'}) \\
&\quad \times \left| \frac{1}{\epsilon_b^-(N) - \epsilon_{jk} + i0} - \frac{s_{jj'}}{\epsilon_b^-(N) - \epsilon_{j',k'} + i0} \right|^2 \\
&= \rho_{jj'} \frac{\Gamma_j \Gamma_{j'}}{4} \int \frac{d\epsilon d\epsilon'}{2\pi} \delta(\epsilon + \epsilon' - \Delta_0^-(N)) n_F[-(\epsilon - \mu_j)] n_F[-(\epsilon' - \mu_{j'})] \\
&\quad \times \left| \frac{1}{\epsilon - \epsilon_b^-(N) - i0} - \frac{s_{jj'}}{\epsilon' - \epsilon_b^-(N) - i0} \right|^2, \tag{2.28}
\end{aligned}$$

where $s_{jj'} = s_j s_{j'}$, $\rho_{jj'} = (1 + \delta_{j',-j})/2$ and [see also Eq. (2.13)]

$$\Delta_{n_d}^\pm(N) = \pm(E_{n_d}(N \pm 1) - E_{n_d}(N)). \tag{2.29}$$

Note that for $j' = j$ (local Andreev reflection) the two fractions in Eq. (2.28) come from the superposition of the two scattering amplitudes, $c_{jk}^\dagger G(E_i) c_{j'k'}^\dagger + c_{j'k'}^\dagger G(E_i) c_{jk}^\dagger$, corresponding to different orderings in the emission of lead electrons with energies ϵ_{jk} and $\epsilon_{j,k'}$, while the factor $\rho_{jj} = 1/2$ is included to avoid double counting in the sum over initial states of the lead. Also note that for $j' = j$ the terms with $\epsilon_{jk} = \epsilon_{j,k'}$, which are not allowed by the Pauli exclusion principle, automatically do not contribute to the cotunneling rate (2.28). Similarly, one finds:

$$\begin{aligned}
\Gamma_{j',j}^{(\text{AR},+)}(0, N) &= \frac{\pi |\lambda_j \lambda_{j'}|^2}{2} \sum_i w_i \delta(E_i - E_f) \\
&\quad \times \left| \langle f | e^{+i\chi} d c_{j'} G(E_i) d^\dagger c_j + (1 - \delta_{j',j}) s_{jj'} e^{+i\chi} d c_j G(E_i) d^\dagger c_{j'} | i \rangle \right|^2 \\
&= \frac{\pi |\lambda_j \lambda_{j'}|^2}{2} \rho_{jj'} \sum_{k,k'} n_F(\epsilon_k) n_F(\epsilon_{k'}) \delta(E_0(N) - E_0(N+1) + \epsilon_{jk} + \epsilon_{j',k'}) \\
&\quad \times \left| \frac{1}{\epsilon_{jk} - \epsilon_a^+(N) + i0} - \frac{s_{jj'}}{\epsilon_{j',k'} - \epsilon_a^+(N) + i0} \right|^2 \\
&= \rho_{jj'} \frac{\Gamma_j \Gamma_{j'}}{4} \int \frac{d\epsilon d\epsilon'}{2\pi} \delta(\epsilon + \epsilon' - \Delta_0^+(N)) n_F[(\epsilon - \mu_j)] n_F[(\epsilon' - \mu_{j'})] \\
&\quad \times \left| \frac{1}{\epsilon - \epsilon_a^+(N) + i0} - \frac{s_{jj'}}{\epsilon' - \epsilon_a^+(N) + i0} \right|^2. \tag{2.30}
\end{aligned}$$

The corresponding rates for $n_d = 1$ are given by:

$$\begin{aligned}
 \Gamma_{j',j}^{(\text{AR},-)}(1, N) &= \frac{\pi |\lambda_j \lambda_{j'}|^2}{2} \sum_i w_i \delta(E_i - E_f) \\
 &\quad \times \left| \langle f | e^{-i\chi} c_{j'}^\dagger d^\dagger G(E_i) c_j^\dagger d + (1 - \delta_{j',j}) s_{jj'} e^{-i\chi} c_{j'}^\dagger d^\dagger G(E_i) c_j^\dagger d | i \rangle \right|^2 \\
 &= \rho_{jj'} \frac{\Gamma_j \Gamma_{j'}}{4} \int \frac{d\epsilon d\epsilon'}{2\pi} \delta(\epsilon + \epsilon' - \Delta_1^-(N)) n_F[-(\epsilon - \mu_j)] n_F[-(\epsilon' - \mu_{j'})] \\
 &\quad \times \left| \frac{1}{\epsilon - \epsilon_a^-(N) - i0} - \frac{s_{jj'}}{\epsilon' - \epsilon_a^-(N) - i0} \right|^2, \tag{2.31}
 \end{aligned}$$

$$\begin{aligned}
 \Gamma_{j',j}^{(\text{AR},+)}(1, N) &= \frac{\pi |\lambda_j \lambda_{j'}|^2}{2} \sum_i w_i \delta(E_i - E_f) \\
 &\quad \times \left| \langle f | d^\dagger c_{j'} G(E_i) e^{+i\chi} d c_j + (1 - \delta_{j',j}) s_{jj'} d^\dagger c_j G(E_i) e^{+i\chi} d c_{j'} | i \rangle \right|^2 \\
 &= \rho_{jj'} \frac{\Gamma_j \Gamma_{j'}}{4} \int \frac{d\epsilon d\epsilon'}{2\pi} \delta(\epsilon + \epsilon' - \Delta_1^+(N)) n_F[(\epsilon - \mu_j)] n_F[(\epsilon' - \mu_{j'})] \\
 &\quad \times \left| \frac{1}{\epsilon - \epsilon_b^+(N) + i0} - \frac{s_{jj'}}{\epsilon' - \epsilon_b^+(N) + i0} \right|^2. \tag{2.32}
 \end{aligned}$$

2.2.2 Compact rate expressions

During the derivation of the tunneling rates we emphasized the involved channels a and b . Additionally we always distinguished between charge stored as Cooper-pairs and the parity of the wire, defined by the charge state of the nonlocal fermionic level formed from the MBS. One basic assumption of our setup is that the superconducting gap is the highest energy scale in the system and therefore no single fermionic levels above the gap are involved. This allows to always reconstruct the charge state of the nonlocal d level from the knowledge of the island's total charge number $Q = 2N + n_d$. For a unified description of all processes included in our master equation approach we will now express all rates in terms of $Q \in \mathbb{N}_0$, introducing electrostatic level energies E_Q and transition energies $\epsilon_{Q \rightarrow Q'}$

$$E_Q = E_c(Q - n_g)^2 \quad ; \quad \epsilon_{(Q \rightarrow Q')} = \text{sgn}(Q' - Q)(E_{Q'} - E_Q) . \quad (2.33)$$

Within this notation, sequential tunneling yields the rate

$$\Gamma_{j,Q \rightarrow Q \pm 1}^{(\text{SEQ})} = \frac{\Gamma_j}{2} n_F(\pm(\epsilon_{(Q \rightarrow Q \pm 1)} - \mu_j)) \quad (2.34)$$

for one particle tunneling into (out of) the TS from (to) lead $j = L, R$. Next, elastic cotunneling transfers a particle from lead j to the opposite lead $-j$ with virtual excitation of the TS states $Q \pm 1$. The elastic cotunneling rate is

$$\begin{aligned} \Gamma_{j,Q}^{(\text{EC})} &= \frac{\Gamma_L \Gamma_R}{8\pi} \int d\epsilon n_F[+(\epsilon - \mu_j)] n_F[-(\epsilon - \mu_{-j})] \\ &\times \left| \frac{1}{\epsilon - \epsilon_{(Q \rightarrow Q+1)} + i0} - \frac{1}{\epsilon - \epsilon_{(Q \rightarrow Q-1)} - i0} \right|^2 , \end{aligned} \quad (2.35)$$

where the two terms come from the interference of normal and anomalous tunneling (Former channel a and b). We note in passing that for large Δ_{TS} , inelastic cotunneling does not contribute at all, while the conventional elastic cotunneling rate due to quasi-particle states above the gap (and without MBSs) would be much smaller, $\Gamma^{(\text{EC})} \propto \Gamma_L \Gamma_R / \Delta_{\text{TS}}$ [35]. To the same order in $\Gamma_{L,R}$, we also have local (and crossed) AR processes, where an electron and a hole from the same (different) lead(s) are combined to form a Cooper-pair, $Q \rightarrow Q + 2$; the reverse process describes Cooper-pair splitting, $Q \rightarrow Q - 2$. Some algebra yields the unified picture for the AR rates:

$$\begin{aligned} \Gamma_{j,j',Q \rightarrow Q \pm 2}^{(\text{AR})} &= \frac{1 + \delta_{j,-j'}}{2} \frac{\Gamma_j \Gamma_{j'}}{8\pi} \int d\epsilon \int d\epsilon' \delta(\epsilon + \epsilon' - \epsilon_{(Q \rightarrow Q \pm 2)}) \\ &\times n_F(\pm(\epsilon - \mu_j)) n_F(\pm(\epsilon' - \mu_{j'})) \left| \frac{1}{\epsilon - \epsilon_{(Q \rightarrow Q \pm 1)} \pm i0} - \frac{s_j s_{j'}}{\epsilon' - \epsilon_{(Q \rightarrow Q \pm 1)} \pm i0} \right|^2 , \end{aligned} \quad (2.36)$$

where $j = j'$ ($j \neq j'$) corresponds to local (crossed) AR. The $i0$ terms indicate that a regularization of the integrals in Eq. (2.35) and Eq. (2.36) is necessary. Following the regularization scheme from Refs. [36, 37] the correct cotunneling rates correspond to keeping only the principal values of the integrals involved. The detailed regularization procedure and its motivation is presented in Appendix A. Next, we derive the expressions needed to obtain the current from the master equation.

2.2.3 Expectation value of the current

The solution of our master equation represents a stationary state of the system, which is completely determined by the knowledge of all occupation probabilities P_Q . Together with the level dependent net flow rates J_Q through the MSCT from the left to the right lead, the weighted average

$$\langle J \rangle = \sum_Q J_Q P_Q, \quad (2.37)$$

gives the total current through the system. The net flow rates follow directly from the tunneling rates and allow for a separation of the total current into contributions from the different tunneling processes involved.

Local and symmetrized current

We only treat the limit $E_J = 0$ with our master equation where the dot is not grounded and current conservation $I = I_L = -I_R$ always holds. Nevertheless, given the normalized solution P_Q of Eq. (2.5), we define a symmetrized steady-state current

$$I = \frac{I_L - I_R}{2} = \frac{e}{\hbar} \sum_{j=L/R} \frac{s_j}{2} \sum_Q J_{j,Q} P_Q \quad ; \quad s_{L/R} = \pm 1, \quad (2.38)$$

to emphasize lead dependencies since we plan to extend the master equation for $E_J > 0$ in the future. This would also allow to study nonlocal conductance effects. The local current for given Q is composed of the following contributions

$$J_{j,Q} = J_{j,Q}^{(\text{SEQ})} + J_{j,Q}^{(\text{EC})} + J_{j,Q}^{(\text{AR})} + J_{j,Q}^{(\text{CAR})}. \quad (2.39)$$

The local current from cross Andreev reflection (CAR) processes will give no contribution to the symmetrized current because the rates are symmetric, $\Gamma_{RL}^{(\text{AR})} = \Gamma_{LR}^{(\text{AR})}$, and cancel out in Eq. (2.38). But they must be included in I_j via

$$J_{j,Q}^{(\text{CAR})} = \Gamma_{j,-j,Q \rightarrow Q+2}^{(\text{AR})} - \Gamma_{j,-j,Q \rightarrow Q-2}^{(\text{AR})} \quad (2.40)$$

to obtain the current conservation $I_L + I_R = 0$. The sequential tunneling contribution is

$$J_{j,Q}^{(\text{SEQ})} = \left[\Gamma_{j,Q \rightarrow Q+1}^{(\text{SEQ})} - \Gamma_{j,Q \rightarrow Q-1}^{(\text{SEQ})} \right]. \quad (2.41)$$

Elastic cotunneling for tunneling from lead j to $-j$ is encoded in the rates $\Gamma_{j,Q}^{(\text{EC})}$ with

$$J_{j,Q}^{(\text{EC})} = \Gamma_{j,Q}^{(\text{EC})} - \Gamma_{-j,Q}^{(\text{EC})}, \quad (2.42)$$

while inelastic Andreev cotunneling yields

$$J_{j,Q}^{(\text{AR})} = 2 \left(\Gamma_{j,j,Q \rightarrow Q+2}^{(\text{AR})} - \Gamma_{j,j,Q \rightarrow Q-2}^{(\text{AR})} \right). \quad (2.43)$$

The prefactor stems from the fact that the processes involved always transfer two electrons at once from/to the leads. We have now defined everything needed to set up the master equation and compute the current from its solution. Next, we present how to solve it numerically.

2.3 Numerical solution of the master equation

Setting up the master equation for a finite number of levels

The master equation for the MSCT represent an infinite⁶ system of coupled equations, defined by Eq. (2.5). After limiting Q to a finite range we get a finite dimensional matrix-vector equation. A minimal example involving only three states is shown below

$$W\vec{P} = 0 \quad ; \quad \vec{P} = (P_{Q-1}, P_Q, P_{Q+1})^T \quad (2.44)$$

$$W = \begin{pmatrix} -(W_{Q-1 \rightarrow Q} + W_{Q-1 \rightarrow Q+1}) & W_{Q \rightarrow Q-1} & W_{Q+1 \rightarrow Q-1} \\ W_{Q-1 \rightarrow Q} & -(W_{Q \rightarrow Q-1} + W_{Q \rightarrow Q+1}) & W_{Q+1 \rightarrow Q} \\ W_{Q-1 \rightarrow Q+1} & W_{Q \rightarrow Q+1} & -(W_{Q+1 \rightarrow Q} + W_{Q+1 \rightarrow Q-1}) \end{pmatrix}.$$

The choice of $Q_{min/max}$ depends on the choice of n_g and must be checked. This can be done after solving the system by inspecting the resulting P_Q , e.g. see Fig. 2.3. The important criterion is, that the occupation probability of the energetically lowest and highest levels involved must decay to zero due to physics and not due to the limitation to a finite set of $|Q\rangle$ states. This can be always achieved for the interacting case $E_c \neq 0$. For the data shown in Sec. 3 we used 26 level which was always sufficient.

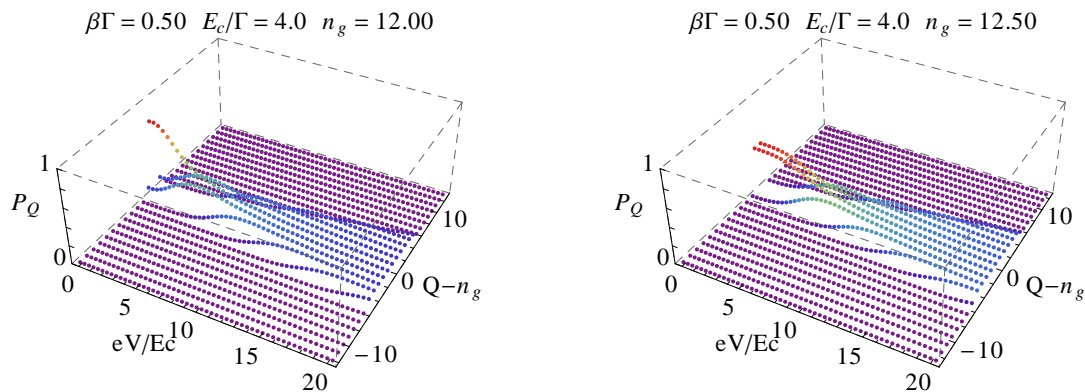


Figure 2.3: Example solution for P_Q from the MSCT master equation as a function of voltage and $Q - n_g$. The left plot shows an integer choice of n_g : Only a single level has a significant occupation probability at $eV = 0$ in the case of $(\Gamma, 1/\beta) \ll E_C$. The right plot for a half integer choice of n_g shows the reduction of P_Q to two equally probable significant level at zero voltage for $(\Gamma, 1/\beta) \ll E_C$. All other parameters are shown above the distributions. Increasing the total energy in the system by applying a bias voltage broadens the distribution as expected.

For $E_c = 0$ all levels have the same energy and therefore the same probability $P_Q = 1/(Q_{max} - Q_{min} + 1)$, but this is no problem, since in this case also all rates lose

⁶The total number of charge states within the wire is finite but in the order of 10^{23} and compared to the number of relevant states treated as not fixed.

their Q -dependence⁷ and a summation over all Q states is not necessary to compute the currents (see also Eq. (2.37) with $J_Q \rightarrow J$).

Singular value decomposition

Investigating Eq. (2.44) we directly see that we have to solve an eigenvalue equation and only might get a solution if there exists exactly one nontrivial eigenvector for the eigenvalue zero. Accordingly, W is singular and puts $\dim(\vec{P}) - 1$ constraints on the solution of Eq. (2.44). Uniqueness of \vec{P} is only reached by an additional constraint - the normalization condition $\sum_Q P_Q = 1$ with all $P_Q \geq 0$. (Including the normalization condition directly in Eq. (2.44) would be another way to tackle the problem but one still has to check for all $P_Q \geq 0$.) Due to numerical stability we will solve the problem using a singular value decomposition (SVD) [38].

In general W has not to be quadratic for a SVD to work but in our case it always is. Starting from Eq. (2.44) the SVD decomposes W in a product of three matrices

$$W = \Lambda \Sigma \Pi^\dagger \quad ; \quad \Lambda \Lambda^\dagger = \Pi \Pi^\dagger = 1 \quad ; \quad \Sigma_{ij} = \xi_i \delta_{ij} \quad , \quad (2.45)$$

with Λ, Π being unitary, and Σ only containing the so called singular values on its diagonal. Picking one singular value ξ_i , the following holds

$$W \vec{P} = \xi_i \vec{L} \quad ; \quad W^\dagger \vec{L} = \xi_i \vec{P} \quad , \quad (2.46)$$

with \vec{L} and \vec{P} being the left-singular and right-singular vectors for ξ_i . They can be read off from the corresponding columns of Λ and Π . As mentioned before, a unique nontrivial solution \vec{P} of Eq. (2.44) can only exist if W has exactly one singular value $\xi_i = 0$ which corresponds to the fact that the $Q_{max} - Q_{min} + 1$ equations from (2.5) are coupled in a way, that one of them is redundant.

Applying this to our problem, we first have to find the \vec{P} which corresponds to $\xi_i = 0$. If we have found it, we ensure, that all elements of \vec{P} have the same sign, and therefore can be normalized to probabilities using the normalization condition $\sum_Q P_Q = 1$ and $P_Q \geq 0$. If this normalization and interpretation as probabilities cannot be achieved due to numerical instability, the corresponding data point is thrown away.

2.4 Analytical solutions of the master equation

Before we present numerical results obtained from our master equation, we will focus now on some limits where an analytical solution of the master equation is possible. We will first analyze the limit $E_c = 0$. As already mentioned, in that limit the rates become Q independent and the master equation trivial. Consequently also the currents J_Q become level independent and directly yield the total current. Afterwards, we will focus on the linear conductance at zero bias voltage. In a deep CB limit the charging energy is the dominant energy scale. This limits the number of accessible charge states to one or two, dependent on the choice of the gate voltage parameter n_g (integer or half integer). Again the master equation becomes trivial and allows for an analytical solution. See also Fig. 2.3.

⁷ $E_c = 0$ implies $E_Q - E_{Q'} = 0$. All states are energetically equal. See also left side of Fig. 1.2 (b).

2.4.1 Current through the grounded wire

Without a regularization the cotunneling rates become divergent under peak conditions at finite temperatures, e.g. for zero bias voltage and half integer n_g . For $E_c = E_J = 0$ the system is analytically solvable and we will now compare our regularized expressions with the exact result from [25]. Since all rates become Q -independent in this limit we have to reintroduce the \pm sign next to the rate type to distinguish between charge creation or annihilation on the dot.

Assuming symmetric conditions, $\Gamma_L = \Gamma_R = \Gamma/2$ and $\mu_{L/R} = \pm eV/2$, the sequential rates are reduced to the simple expression

$$\Gamma_j^{(\text{SEQ},\pm)} = \frac{\Gamma}{4} n_F[\mp \mu_j] . \quad (2.47)$$

From Eq. (2.38) and Eq. (2.41) we get

$$\begin{aligned} I^{(\text{SEQ})} &= \frac{e}{2\hbar} ((\Gamma_L^{(\text{SEQ},+)} - \Gamma_L^{(\text{SEQ},-)}) - (\Gamma_R^{(\text{SEQ},+)} - \Gamma_R^{(\text{SEQ},-)})) \\ &= \frac{e\Gamma}{4\hbar} (n_F[-eV/2] - n_F[eV/2]) = \frac{e\Gamma}{4\hbar} \tanh \left[\frac{\beta eV}{4} \right] . \end{aligned} \quad (2.48)$$

According to Eq. (A.4) from the appendix, the elastic rates require to set $s = -1$ in Eq. (A.13) which directly sets these rates and the corresponding current $I^{(\text{EC})}$ to zero. The same is true for the crossed Andreev process and the associated current. For the local Andreev process we get

$$\begin{aligned} \Gamma_{j,j,Q \rightarrow Q \pm 2}^{(\text{AR})} \Big|_{E_c=0} &= \frac{\Gamma_j^2}{16\pi} \left(K_{reg} \Big|_{\alpha=\pm; \mu_1=\mu_2=\mu_j; \epsilon_{(a)}=\epsilon_{(b)}=\epsilon_{(c)}=0; s=1} \right) \\ &= \left(\frac{\Gamma_j}{2\pi} \right)^2 \alpha \beta n_B(-2\alpha \mu_j) \text{Im} \left(\psi_1 \left[\frac{1}{2} - i \frac{\alpha \beta}{2\pi} \mu_j \right] \right) , \end{aligned} \quad (2.49)$$

with the definition of $\text{Im} \psi_1$ from Eq. (A.11). The following symmetry relations hold

$$\Gamma_{R,R,Q \rightarrow Q+2}^{(\text{AR})} \Big|_{E_c=0} = - \Gamma_{L,L,Q \rightarrow Q-2}^{(\text{AR})} \Big|_{E_c=0} \quad ; \quad \Gamma_{R,R,Q \rightarrow Q-2}^{(\text{AR})} \Big|_{E_c=0} = - \Gamma_{L,L,Q \rightarrow Q+2}^{(\text{AR})} \Big|_{E_c=0} ,$$

and lead to a vanishing current contribution from the local Andreev processes

$$\begin{aligned} J_Q^{(\text{AR})} \Big|_{E_c=0} &= \left[(\Gamma_{L,L,Q \rightarrow Q+2}^{(\text{AR})} - \Gamma_{L,L,Q \rightarrow Q-2}^{(\text{AR})}) - (\Gamma_{R,R,Q \rightarrow Q+2}^{(\text{AR})} - \Gamma_{R,R,Q \rightarrow Q-2}^{(\text{AR})}) \right] \Big|_{E_c=0} \\ &= \left[(\Gamma_{L,L,Q \rightarrow Q+2}^{(\text{AR})} - \Gamma_{L,L,Q \rightarrow Q-2}^{(\text{AR})}) + (\Gamma_{L,L,Q \rightarrow Q-2}^{(\text{AR})} - \Gamma_{L,L,Q \rightarrow Q+2}^{(\text{AR})}) \right] \Big|_{E_c=0} = 0 . \end{aligned} \quad (2.50)$$

In total we only get a contribution from the sequential rate in the limit $E_c = 0$.

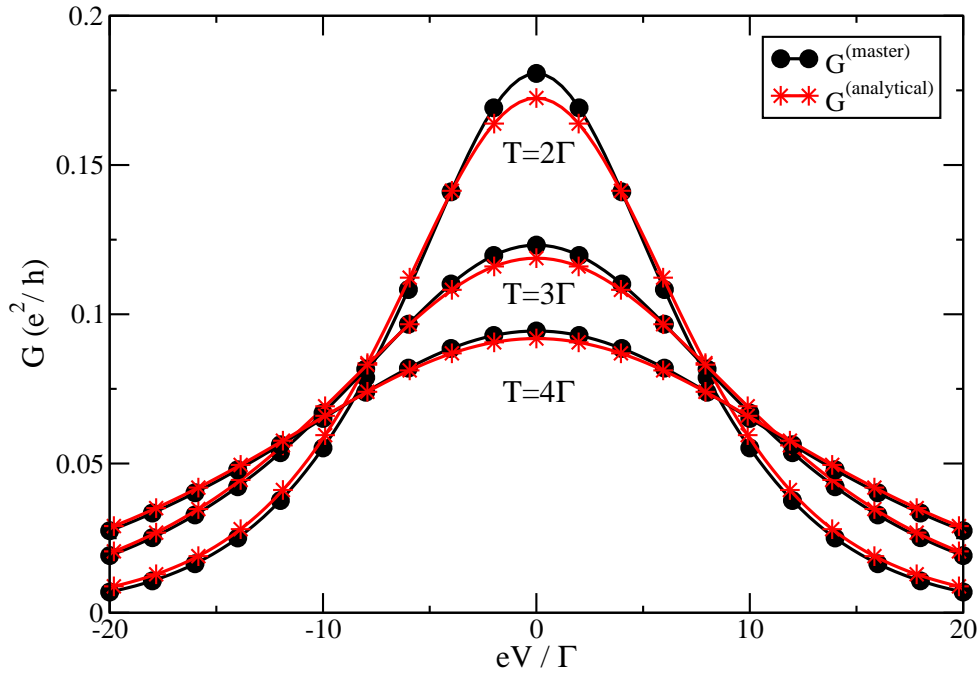


Figure 2.4: Exact differential conductance from Eq. (2.76) (black lines with dots) for different temperatures $T \in \{2, 3, 4\}\Gamma$ and $E_c = E_J = 0$, compared to the result from the master equation with regularized rates for the same parameters. Due to $E_c = 0$, the dependence on the gate voltage parameter $n_g \propto V_g/\Gamma$ drops out. As expected, the master equation becomes quantitatively a better approximation with increasing temperature.

Next, we compare this current with the exact analytical result from [25], which is the $E_c = E_J = 0$ limit of Eq. (2.76), presented later.

$$\begin{aligned}
 I^{(\text{exact})} &= \frac{e\Gamma}{2\hbar} \int_{-\infty}^{+\infty} d\epsilon \left(\frac{F(\epsilon - eV/2) - F(\epsilon + eV/2)}{2} \frac{-\Gamma/2}{\epsilon^2 + (\Gamma/2)^2} \right) \\
 &= \frac{e\Gamma}{4\hbar} \int_{-\infty}^{+\infty} d\epsilon (n_F(\epsilon - eV/2) - n_F(\epsilon + eV/2)) \frac{\Gamma/2}{\pi(\epsilon^2 + (\Gamma/2)^2)} \\
 &\approx \frac{e\Gamma}{4\hbar} \tanh\left(\frac{\beta eV}{4}\right) = I^{(\text{SEQ})}.
 \end{aligned} \tag{2.51}$$

For the last approximation we used a Lorentzian representation of the delta distribution

$$\lim_{\xi \rightarrow 0} \frac{\xi}{\pi(\epsilon^2 + \xi^2)} = \delta(\epsilon), \tag{2.52}$$

which is justified in the limit $\Gamma \ll 1$ that coincides with the regime, where the master equation holds. The quality of this approximation is demonstrated in the Fig. 2.4, depicting the analytical differential conductance and data from our master equation for different temperatures. As expected, deviations between the master equation and the exact solution vanish in the limit $T/\Gamma \rightarrow \infty$. Nevertheless, already for $T/\Gamma = 2$ the master equation is a very good approximation.

2.4.2 Linear conductance from analytics

We consider again a symmetric system, $\Gamma_L = \Gamma_R = \Gamma/2$ and $\mu_L = -\mu_R = eV/2 \rightarrow 0$ and define a dimensionless linear conductance g by

$$G(E_c, \beta, n_g) = \frac{e^2}{h} g(E_c, \beta, n_g) . \quad (2.53)$$

The only free parameter beside E_c , β and n_g is the hybridization Γ . For the linear conductance, we actually need the rates only at $V = 0$, since the P_Q are needed only in equilibrium. Regarding J_Q , the leading coefficient

$$\mathcal{G}_Q = \lim_{V \rightarrow 0} \frac{2\pi}{eV} J_Q \quad (2.54)$$

must be computed and g in Eq. (2.53) then follows with knowledge of the charge state distribution P_Q in the same fashion like the current before

$$g = \langle \mathcal{G}_Q \rangle_Q = \sum_Q \mathcal{G}_Q P_Q . \quad (2.55)$$

Equilibrium rates

Here we determine the $\mu_\alpha = 0$ rates entering the equilibrium master equation. The sequential tunneling rate (2.34) and Eq. (2.6) yield

$$W_{Q \rightarrow Q \pm 1} = \frac{\Gamma}{2} n_F(\pm \epsilon_{(Q \pm 1)}) . \quad (2.56)$$

Inelastic cotunneling rates are reduced to

$$\begin{aligned} W_{Q \rightarrow Q \pm 2} &= \frac{(\Gamma/2)^2}{8\pi} \int d\epsilon n_F(\pm(\epsilon)) n_F(\pm(\epsilon_{(Q \pm 2)} - \epsilon)) \\ &\times \sum_{s=\pm} \left| \frac{1}{\epsilon - \epsilon_{(Q \pm 1)} \pm i0} - \frac{s}{\epsilon_{(Q \pm 2)} - \epsilon_{(Q \pm 1)} - \epsilon \pm i0} \right|^2 . \end{aligned} \quad (2.57)$$

Level dependent conductances

For convenience we first introduce the negative derivative of the Fermi distribution, which will become a delta distribution in the limit $T \rightarrow 0$ ($\beta \rightarrow \infty$)

$$\delta_\beta(\epsilon) \equiv -\partial_\epsilon n_F(\epsilon) \equiv \frac{\beta}{4 \cosh^2\left(\frac{\beta\epsilon}{2}\right)} \equiv \beta n_F(\epsilon) n_F(-\epsilon) . \quad (2.58)$$

From Eq. (2.54) and with the level dependent current definitions from Sec. 2.2.3, we obtain the sequential contribution

$$\begin{aligned} \mathcal{G}_Q^{(\text{SEQ})} &= \lim_{eV \rightarrow 0} \frac{2\pi}{eV} J_Q^{(\text{SEQ})} \\ &= \lim_{eV \rightarrow 0} \frac{\pi}{eV} \left(\Gamma_{L,Q \rightarrow Q+1}^{(\text{SEQ})} - \Gamma_{L,Q \rightarrow Q-1}^{(\text{SEQ})} - \Gamma_{R,Q \rightarrow Q+1}^{(\text{SEQ})} + \Gamma_{R,Q \rightarrow Q-1}^{(\text{SEQ})} \right) \\ &= \frac{\pi}{4} \Gamma (\delta_\beta(\epsilon_{Q+1}) + \delta_\beta(\epsilon_{Q-1})) . \end{aligned} \quad (2.59)$$

For the last identity we used the auxiliary relation

$$\begin{aligned} & \lim_{eV \rightarrow 0} \frac{n_F[\epsilon_{Q+1} - \frac{eV}{2}] - n_F[-(\epsilon_{Q-1} - \frac{eV}{2})] - n_F[\epsilon_{Q+1} + \frac{eV}{2}] + n_F[-(\epsilon_{Q-1} + \frac{eV}{2})]}{eV} \\ &= -\partial_{\epsilon_{Q+1}} n_F[\epsilon_{Q+1}] - \partial_{\epsilon_{Q-1}} n_F[-\epsilon_{Q-1}] = \delta_\beta(\epsilon_{Q+1}) + \delta_\beta(\epsilon_{Q-1}), \end{aligned} \quad (2.60)$$

and the definition of $\delta_\beta(\epsilon)$ from Eq. (2.58). The elastic cotunneling contribution is given by

$$\begin{aligned} \mathcal{G}_Q^{(\text{EC})} &= \lim_{eV \rightarrow 0} \frac{2\pi}{eV} J_Q^{(\text{EC})} = \lim_{eV \rightarrow 0} \frac{2\pi}{eV} \left(\Gamma_{L,Q}^{(\text{EC})} - \Gamma_{R,Q}^{(\text{EC})} \right) \\ &= \frac{\Gamma^2}{16} \int d\epsilon \delta_\beta(\epsilon) \left| \frac{1}{\epsilon - \epsilon_{(Q+1)} + i0} - \frac{1}{\epsilon - \epsilon_{(Q-1)} - i0} \right|^2, \end{aligned} \quad (2.61)$$

again using an auxiliary relation

$$\begin{aligned} & \lim_{eV \rightarrow 0} \frac{n_F[\epsilon - \frac{eV}{2}] n_F[-(\epsilon + \frac{eV}{2})] - n_F[\epsilon + \frac{eV}{2}] n_F[-(\epsilon - \frac{eV}{2})]}{eV} \\ &= \lim_{eV \rightarrow 0} \frac{n_F[\epsilon - \frac{eV}{2}] - n_F[\epsilon + \frac{eV}{2}]}{eV} = -\partial_\epsilon n_F(\epsilon) = \delta_\beta(\epsilon). \end{aligned} \quad (2.62)$$

Similar ideas, the symmetry $\delta_\beta(\epsilon) = \delta_\beta(-\epsilon)$ and a more lengthy calculation finally lead to the inelastic cotunneling contribution

$$\begin{aligned} \mathcal{G}_Q^{(\text{AR})} &= \frac{\Gamma^2}{32} \sum_{\pm} \left(\pm \int d\epsilon \left\{ [\delta_\beta(\epsilon) n_F(\pm(\epsilon_{Q\pm 2} - \epsilon)) + n_F(\pm\epsilon) \delta_\beta(\epsilon_{Q+2} - \epsilon)] \right. \right. \\ &\quad \left. \left. \times \left| \frac{1}{\epsilon - \epsilon_{Q\pm 1} \pm i0} + \frac{1}{\epsilon - (\epsilon_{Q\pm 2} - \epsilon_{Q\pm 1}) \pm i0} \right|^2 \right\} \right). \end{aligned} \quad (2.63)$$

In the master equation, defined by Eq. (2.5), the overall prefactor Γ cancels out, i.e., the distribution function P_Q is determined only by E_c/Γ , n_g and $\beta\Gamma$ (universality). Remember that $n_g \propto V_g/\Gamma$ holds. The same is now found for the conductance coefficients \mathcal{G}_Q , and thus universality is valid for the conductance, $g = g(E_c/\Gamma, \beta\Gamma, n_g)$.

2.4.3 Low temperature strong Coulomb blockade limit

Below we study sequential tunneling and cotunneling processes and the linear conductance in the strong Coulomb blockade (CB) regime $\Gamma \ll 1/\beta \ll E_c$ at low temperature. We approximate the Fermi function with the Heaviside function θ , and introduce consistently its derivative, the delta distribution $\delta(\epsilon)$, as low temperature limit of $\delta_\beta(\epsilon)$:

$$\lim_{\beta \rightarrow \infty} n_F(\epsilon) = \theta(-\epsilon) \quad ; \quad \lim_{\beta \rightarrow \infty} \delta_\beta(\epsilon) = \delta(\epsilon) = -\partial_\epsilon \theta(-\epsilon). \quad (2.64)$$

The equilibrium rates entering the master equation are further simplified in this limit

$$W_{Q \rightarrow Q \pm 1} \approx \frac{\Gamma}{2} \theta(\mp \epsilon_{(Q \pm 1)}) \quad ; \quad (2.65)$$

$$W_{Q \rightarrow Q \pm 2} \approx \frac{(\Gamma/2)^2}{8\pi} \int d\epsilon \theta(\mp(\epsilon)) \theta(\mp(\epsilon_{(Q \pm 2)} - \epsilon)) \\ \times \sum_{s=\pm} \left| \frac{1}{\epsilon - \epsilon_{(Q \pm 1)} \pm i0} - \frac{s}{\epsilon_{(Q \pm 2)} - \epsilon_{(Q \pm 1)} - \epsilon \pm i0} \right|^2. \quad (2.66)$$

The conductance matrix elements for $\beta \rightarrow \infty$ are

$$\mathcal{G}_Q^{(\text{SEQ})} \approx \frac{\pi}{4} \Gamma (\delta(\epsilon_{Q+1}) + \delta(\epsilon_{Q-1})) \quad , \quad (2.67)$$

$$\mathcal{G}_Q^{(\text{EC})} \approx \frac{\Gamma^2}{16} \int d\epsilon \delta(\epsilon) \left| \frac{1}{\epsilon - \epsilon_{(Q+1)} + i0} - \frac{1}{\epsilon - \epsilon_{(Q-1)} - i0} \right|^2 = \frac{\Gamma^2}{16} \left| \frac{1}{\epsilon_{(Q+1)} - i0} - \frac{1}{\epsilon_{(Q-1)} + i0} \right|^2 \quad ,$$

$$\mathcal{G}_Q^{(\text{AR})} \approx \frac{\Gamma^2}{32} \sum_{\pm} \left(\pm \int d\epsilon \left\{ [\delta(\epsilon) n_F(\pm(\epsilon_{Q \pm 2} - \epsilon)) + n_F(\pm\epsilon) \delta(\epsilon_{Q \pm 2} - \epsilon)] \right. \right. \\ \left. \left. \times \left| \frac{1}{\epsilon - \epsilon_{Q \pm 1} \pm i0} + \frac{1}{\epsilon - (\epsilon_{Q \pm 2} - \epsilon_{Q \pm 1}) \pm i0} \right|^2 \right\} \right) \approx 0 \quad .$$

For the last low temperature approximation we used the fact, that

$$\delta(\epsilon) n_F(\pm(\epsilon_{Q \pm 2} - \epsilon)) + n_F(\pm\epsilon) \delta(\epsilon_{Q \pm 2} - \epsilon) = n_F(\pm(\epsilon_{Q \pm 2})) (\delta(\epsilon) + \delta(\epsilon_{Q \pm 2} - \epsilon)) \quad (2.68)$$

holds and the \pm prefactor in the summation then extinguishes the whole AR conductance. Next, we focus on the two scenarios of integer and half-integer gate potential n_g , corresponding to a valley and peak situation in a Coulomb oscillation plot (see also Fig. 3.2).

CB valley conductance

First consider an 'even' valley, $n_g = 2\ell$ with $\ell \in \mathbb{N}_0$. The charging energy (2.33) selects the only possible state $N = \ell$ and $n_d = 0$, i.e., $P_Q = \delta_{Q,n_g}$ solves the master equation:

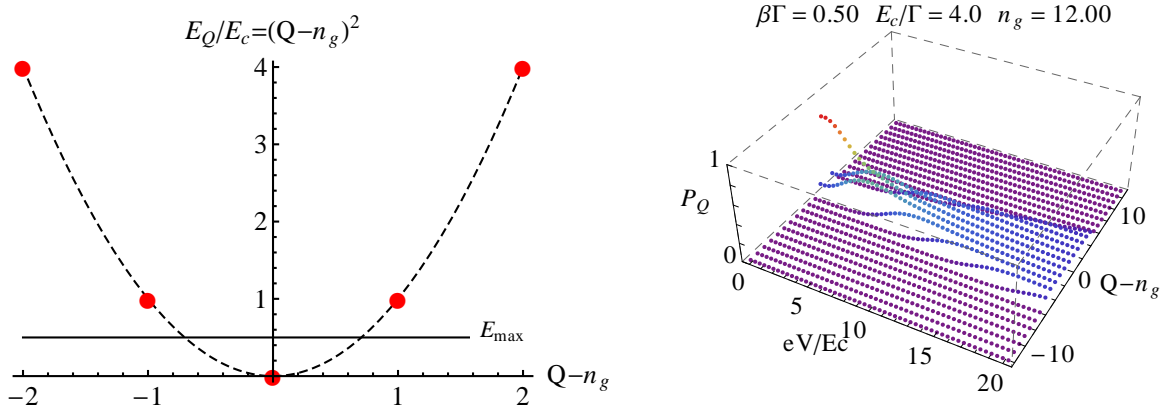


Figure 2.5: Left: Charging energy E_Q as function of $Q - n_g$ in the situation of an integer n_g . The solid black line represents a low energy situation of the system ($eV = 0, T < E_c$). Only the state P_{n_g} has a finite occupation probability. Right: Numerical solution of the master equation in the same parameter limit. For $eV = 0$ only the state $|Q = n_g\rangle$ has a significant occupation probability.

The corresponding transition energy $\epsilon_{Q\pm 1} = E_c$ implies that $\mathcal{G}_Q^{(\text{SEQ})}$ is always exponentially small, cf. Eq. (2.67) and $\delta_\beta(E_c) = 0$ holds for $E_c \neq 0$ in the limit $\beta \rightarrow \infty$. Only $\mathcal{G}_Q^{(\text{EC})}$ remains and by introducing small gate charge fluctuations ($n_g \rightarrow n_g - \delta$; $|\delta| \ll 1$) we get an analytical expression for the valley conductance, valid in a small region around the valley center where it is also safe to put $i0 = 0$ without any regularization procedure

$$\epsilon_{Q\pm 1}|_{Q=n_g} = \pm E_c(1 \pm 2\delta) \quad ; \quad \mathcal{G}_{n_g}^{(\text{EC})} \approx \left(\frac{\Gamma}{4E_c}\right)^2 \left(\frac{1}{1+2\delta} - \frac{1}{1-2\delta}\right)^2. \quad (2.69)$$

We have only one finite weight for $Q = n_g$, i.e. $P_Q = \delta_{Q,n_g}$. Therefore the valley conductance is always

$$G_{\text{valley}} = \frac{e^2}{h} \left(\frac{\Gamma}{2E_c}\right)^2 \frac{1}{(1-4\delta^2)^2}. \quad (2.70)$$

Since experiments so far were conducted in the regime $T > \Gamma$ [13], let us specify next the line shape near a conductance peak.

CB peak conductance

For a conductance peak and $E_c \gg \Gamma$, we need to keep two states (two-state approximation). For $n_g = 2\ell + 1/2 - \delta$ (again allowing for small fluctuations $|\delta| \ll 1$), we have $P_{n_g \mp 1/2} = \frac{1}{2}$ and thus the transition energies

$$\begin{cases} Q = n_g - 1/2 : & \epsilon_{Q-1} = 2E_c(\delta - 1) \quad ; \quad \epsilon_{Q+1} = 2E_c\delta \\ Q = n_g + 1/2 : & \epsilon_{Q+1} = 2E_c(\delta + 1) \quad ; \quad \epsilon_{Q-1} = 2E_c\delta \end{cases} \quad (2.71)$$

A schematic illustration of the dispersion and a numerical example solution clarifies the situation:

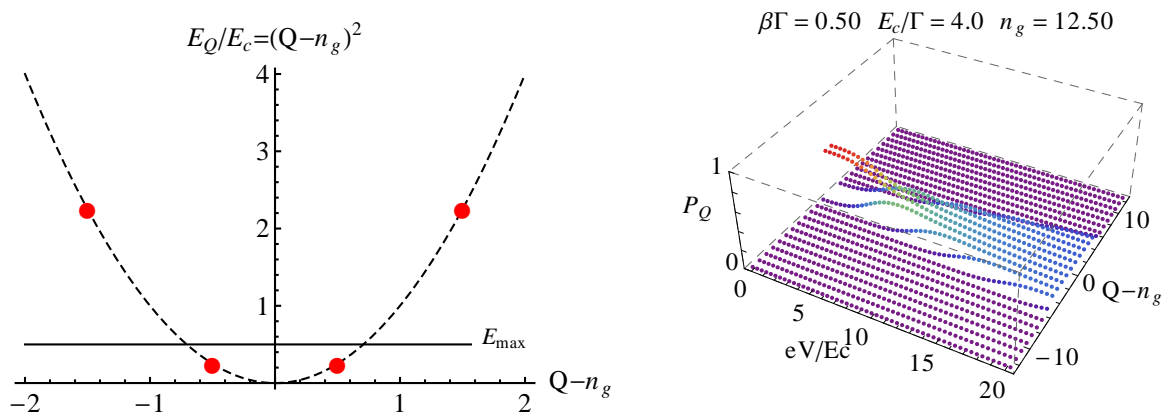


Figure 2.6: Left: Charging energy E_Q as function of $Q - n_g$ in the situation of half integer n_g . The solid black line represents a low energy situation of the system ($eV = 0, T < E_c$). Only the states $P_{n_g \mp 1/2}$ have a finite occupation probability. Right: Numerical solution of the master equation in the same parameter limit. For $eV = 0$ only the states $|Q = n_g \mp 1/2\rangle$ have a significant occupation probability.

Now inelastic cotunneling is negligible for $E_c \gg T$ since the symmetry of the transition energies involved just cancels the interference term in $\mathcal{G}_Q^{(\text{EC})}$ from Eq. (2.67). Only $\mathcal{G}_Q^{(\text{SEQ})}$ survives and for each Q involved the two δ_β -functions pick only the one transition without energy cost, cf. Eq. (2.71)

$$g^{(\text{SEQ})} \approx \frac{\pi}{4} \Gamma \sum_Q \frac{1}{2} (\delta_\beta(\epsilon_{Q+1}) \delta_{Q, n_g - 1/2} + \delta_\beta(\epsilon_{Q-1}) \delta_{Q, n_g + 1/2}) = \frac{\pi}{4} \Gamma (\delta_\beta(2E_c\delta)). \quad (2.72)$$

Inserting the definition of δ_β we get the analytical result for $G_{\text{peak}} = g^{(\text{SEQ})}(e^2/h)$ valid close around a peak

$$G_{\text{peak}} = \frac{e^2}{h} \frac{\pi \Gamma}{16} \frac{\beta}{\cosh^2(\delta \beta E_c)}. \quad (2.73)$$

We stress that the peak conductance [$G_{\text{peak}}(\delta = 0)$] is indeed halved compared to $E_c = 0$ [8]. (Decoupling of Q -summation, no factor 1/2 and all transition energies equal zero in Eq. (2.72)) Moreover, it exhibits both a thermal and an interaction-induced reduction.

2.5 Other methods used for comparison

Our master equation approach has two limitations. First, we need to have a finite temperature in the system to fulfill $\Gamma \ll 1/\beta$, second we neglected the Josephson coupling ($E_J = 0$). To get a full picture of our MSCT device we also compare with other methods in [39]. They are the result of a collaborative work and therefore only directly cited in this chapter. More details are given in the supplementary material of [39]. Relations between the different Keldysh Green's functions and the connection to the Meir-Wingreen formula are in detail discussed in the second part of this thesis in Sec. 8.2.

2.5.1 Exact expression for the current

Using nonequilibrium Green's function (GF) techniques [35, 34, 40], the current I_j flowing from lead j to the TS can be expressed in terms of the Keldysh GF

$$\check{G}_{\eta_j}(t, t') = -i \langle \mathcal{T}_C \eta_j(t) \eta_j(t') \rangle, \quad (2.74)$$

where \mathcal{T}_C denotes Keldysh time ordering and the pseudo-fermion η_j has been defined in Eq. (2.4). With the Fourier-transformed retarded, $G_{\eta_j}^R(\epsilon)$, and Keldysh, $G_{\eta_j}^K(\epsilon)$, components of \check{G}_{η_j} , we obtain

$$I_j = (e\Gamma_j/h) \int d\epsilon [F(\epsilon - \mu_j) \text{Im}G_{\eta_j}^R(\epsilon) + (i/2)G_{\eta_j}^K(\epsilon)], \quad (2.75)$$

where $F(\epsilon) = 1 - 2n_F(\epsilon) = \tanh(\epsilon/2T)$. Next we note that $G_{\eta_j}^K(t, t) = 0$ as a consequence of $\eta_j^\dagger \eta_j = \eta_j \eta_j^\dagger = 1/2$. Hence we find the exact result

$$I_j = \frac{e\Gamma_j}{h} \int d\epsilon F(\epsilon - \mu_j) \text{Im}G_{\eta_j}^R(\epsilon), \quad (2.76)$$

stating that the current can be computed from the spectral function $\propto \text{Im}G_{\eta_j}^R$. The well-known Meir-Wingreen formula for interacting quantum dots [41] has thereby been extended to the interacting Majorana wire; note that there are two spectral functions associated to the currents I_L and I_R . Current conservation here implies $I_L + I_R + I_S = 0$, with the supercurrent I_S flowing through the interface to the bulk superconductor. Below we define the conductance $G = dI/dV$ using the symmetrized current $I = (I_L - I_R)/2$. For $E_c = 0$, the pseudo-fermions η_j reduce to Majorana fermions γ_j , and the Lorentzian spectral function,

$$\mathcal{A}(\epsilon) = -2\text{Im}G_{\gamma_j}^R(\epsilon) = \frac{2\Gamma_j}{(\epsilon^2 + \Gamma_j^2)}, \quad (2.77)$$

implies resonant AR with $G = 2e^2/h$ [8, 9, 10]. For finite E_c , we shall present several complementary approximations in order to achieve a broad physical understanding of the MSCT transport properties. Eq. (2.76) should also be useful for numerically exact calculations, e.g., using the numerical or density-matrix renormalization group.

2.5.2 Equation-of-motion (EOM) approach

We constructed an EOM approach for $G_{\eta_j}^R$ to access the linear conductance near a peak. Within this method, we introduce the Nambu spinors $\Psi_d = (d, e^{-i\chi}d^\dagger)^T$ and the corresponding retarded GF, $G_{dd}^R = -i\Theta(t-t')\langle\{\Psi_d(t), \Psi_d^\dagger(t')\}\rangle$. The EOM for G_{dd}^R generates higher-order GFs of the type $\Gamma_{N^m dd}^R = -i\Theta(t-t')\langle\{\hat{N}^m(t)\Psi_d(t), \Psi_d^\dagger(t')\}\rangle$, which we truncate at the level $m = 2$ and solve in a self-consistent way - see supplementary material of [39]. The resulting GF G_{dd}^R then yields $G_{\eta_j}^R = \frac{1}{2}\text{Tr}[(1 + s_j\sigma_x)G_{dd}^R]$ with Pauli matrix σ_x . Finally, we obtain the conductance from Eq. (2.76). This approximation is valid by construction for $E_c \gtrsim \Gamma$, but the imposed self-consistency (supplementary material of [39]) allows us to extend it to $E_c < \Gamma$, where the resulting conductance (being determined by truncated fluctuations) gives a lower bound for the exact result.

2.5.3 Zero-bandwidth model (ZBWM)

In the Zero-bandwidth model (ZBWM) each lead is represented by just a single fermionic level and the number of Cooper-pairs on the wire is limited ($N < N_{\text{max}}$). The associated Hilbert space then has the finite dimension $8N_{\text{max}}$, which allows for a numerical calculation of the spectral density $\propto \text{Im}G_{\eta_j}^R(\epsilon)$ via its Lehmann representation, with poles phenomenologically broadened by Γ . A similar description has been pursued before for $E_c = E_J = 0$ in Ref. [42]. With this spectral function, again Eq. (2.76) yields the conductance within the ZBWM.

2.5.4 Weak coupling limit

For $E_c = 0$ and $E_J = 0$ the MSCT setup reduces to a resonant tunneling setup with only one degenerate level at zero energy coupled by the two channels a and b to the metallic leads and is exactly solvable. Due to the two channels the maximum conductance at $T = 0$ is $2e^2/h$ and starting from this exact solution one can perform a perturbative expansion in E_c like done in Ref. [25].

3 Results

3.1 Peak conductance halving

We focus on the symmetric problem defined by $\Gamma_\alpha = \frac{\Gamma}{2}$ and $\mu_L = -\mu_R = \frac{eV}{2}$ in all figures. Results for the peak conductance are shown in Fig. 3.1 below.

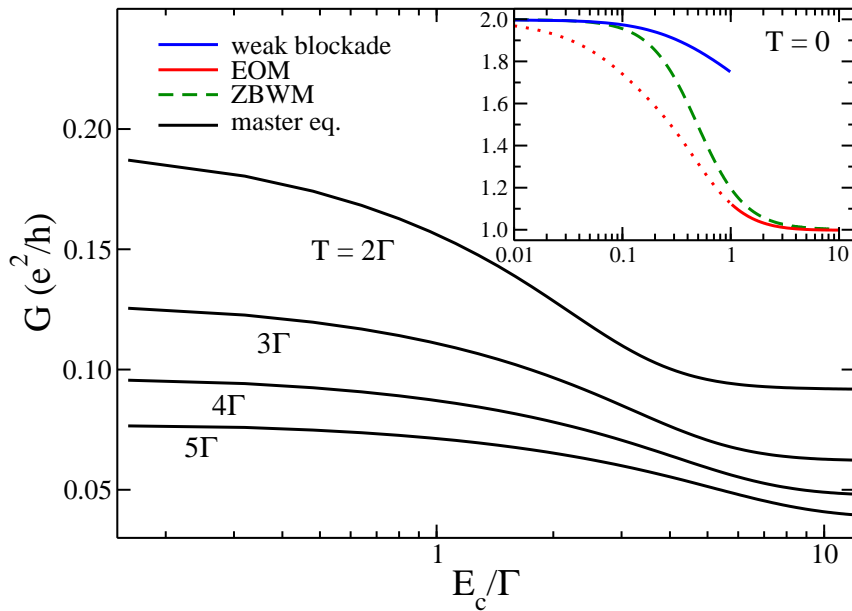


Figure 3.1: Peak conductance G vs E_c/Γ on a semi-logarithmic scale. Main panel: Results from the master equation for several temperatures $T > \Gamma$ and $E_J = 0$. Inset: Comparison of $T = 0$ results using perturbation theory in E_c/Γ [25] (blue solid curve), the EOM approach (red dotted-solid curve), and the ZBWM (black dashed curve). The shown EOM results are quantitatively valid only for $E_c \gtrsim \Gamma$ (solid part) but give a lower bound when $E_c \lesssim \Gamma$ (dotted part). Also here $E_J = 0$ since G only weakly depends on E_J for $E_J \lesssim E_c$.

The main panel of Fig. 3.1 is obtained from the master equation and confirms the universal halving of the peak conductance also holds at finite- T when E_c/Γ increases. It represents the crossover from resonant AR [8, 9, 10] to electron teleportation [26] and arises due to the increasing domination of the charging energy which leads to a blockade of one of the two possible transport channels (a or b). The effect is also observable in Fig. 3.2. For $T = 0$ (inset) the maximal conductance values in both regimes are realized and we obtain a decay from $G = 2e^2/h$ to $G = e^2/h$. The known small- E_c behavior [25] is nicely reproduced by the ZBWM calculation. In the opposite large- E_c limit, the EOM method is very accurate and Fig. 3.1 suggests that the simple ZBWM already captures the crossover surprisingly well.

3.2 Coulomb blockade

3.2.1 Coulomb oscillations

Let us address next the n_g -dependence of the linear ($V \rightarrow 0$) conductance, see Fig. 3.2 and also 3.5. In Fig. 3.2 both the master equation (main panel, finite T) and the ZBWM (inset, $T = 0$) reveal clear conductance oscillations in the MSCT for $E_c \gg \Gamma$, with peaks (valleys) for half-integer (integer) gate voltage parameter n_g .

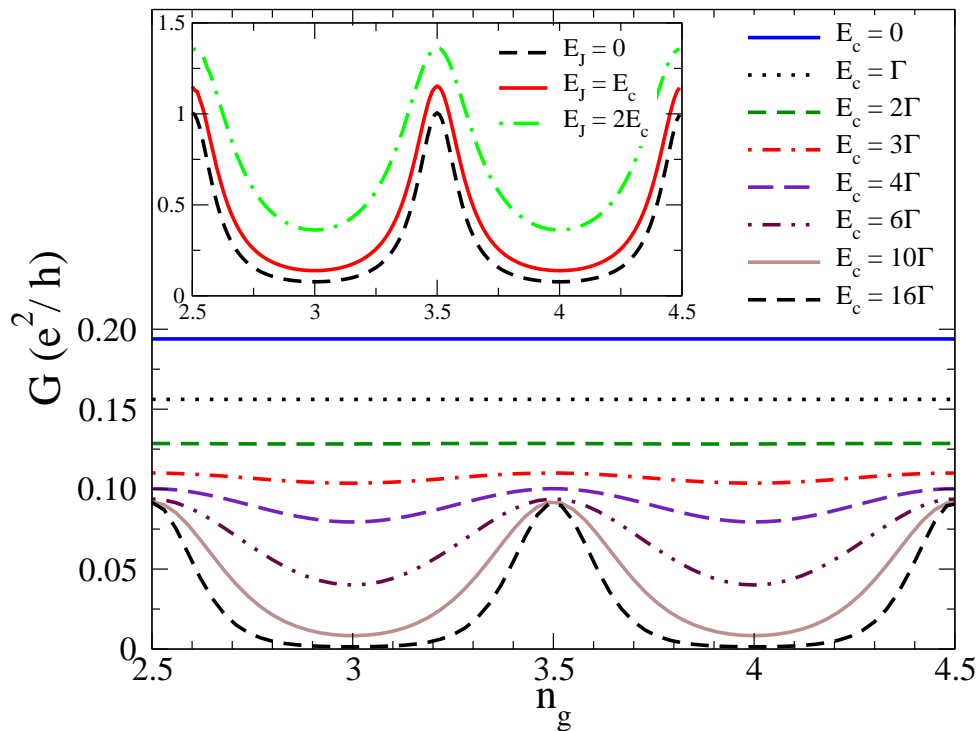


Figure 3.2: Coulomb oscillations in the MSCT. Main panel: Conductance G vs n_g from the master equation for $E_J = 0, T = 2\Gamma$ and several E_c . Inset: Same but from ZBWM for $T = 0, E_c = 5\Gamma$ and several E_J .

The main panel of Fig. 3.2 additionally depicts that the peak (valley) conductance is halved (strongly suppressed) when going from the noninteracting to the deep Coulomb blockade limit. The peaks are dominated by sequential contributions while the valleys are dominated by elastic cotunneling. The inset of Fig. 3.2 shows that G increases when the Josephson coupling E_J grows. One can understand this by noting that for $E_J \gg E_c$, one ultimately reaches the resonant AR limit of a grounded TS, with the n_g -independent $T = 0$ conductance $G = 2e^2/h$. If a Cooper-pair exchange via the Josephson junction with the SC substrate is always energetically favorable this limit corresponds to an almost “infinite” capacitance of the wire which sets its charging energy to zero and opens again both channels.

3.2.2 Finite-voltage sidebands

Next we discuss the differential conductance at finite bias voltage V . Master equation results for $T = 2\Gamma$ are shown in Fig. 3.3.

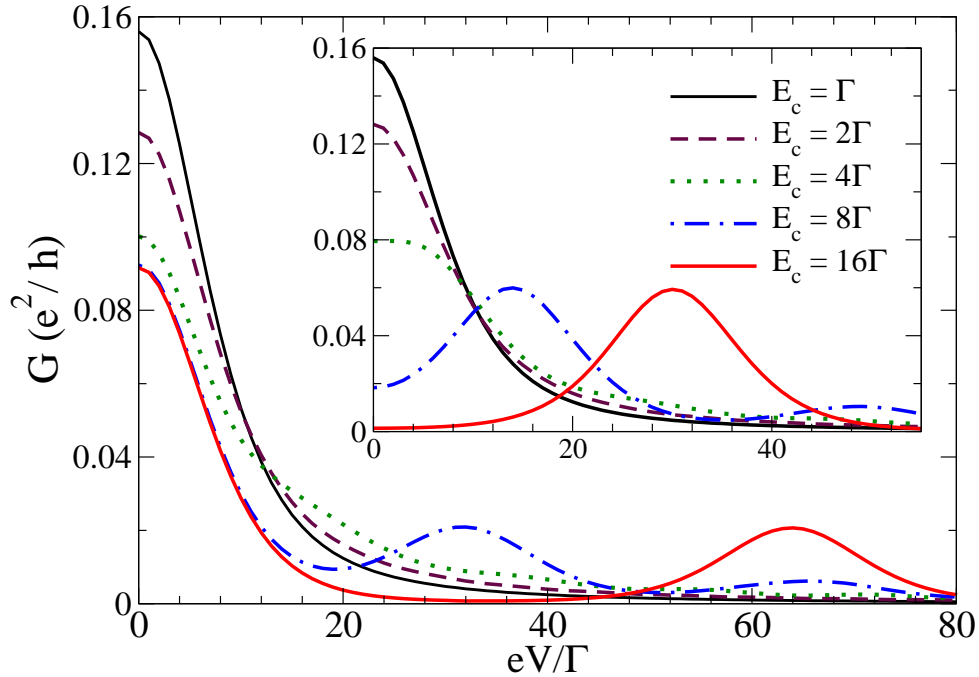


Figure 3.3: Differential conductance $G = dI/dV$ vs voltage V from the master equation for $T = 2\Gamma$, $E_J = 0$, and several E_c/Γ . The main panel (inset) is for half-integer (integer) n_g .

Starting with the main panel, we find sideband peaks when eV is equal to an integer multiple of $4E_c$. For these voltages, the chemical potentials $\mu_{L,R}$ are resonant with two (almost) degenerate higher-order charge states, implying additional sequential tunneling contributions beyond the resonant transition determining the linear conductance peak [Eq. (2.73)]. Note that the fluctuations in N needed to reach higher-order charge states can only be achieved through anomalous tunneling processes [see Eq. (2.4)]. Similar sideband peaks are also found for other n_g ; the integer- n_g valley case is shown in the inset of Fig. 3.3.

In Fig. 3.4 we show the evolution of the sideband peaks as E_J is changed, determined from the ZBWM at $T = 0$. For half-integer n_g , the sideband peak position observed in the main panel of Fig. 3.4 is well described by $eV \simeq 4E_c\sqrt{1 + (E_J/2E_c)^2}$, which comes from the Josephson coupling between the two relevant charge states. Since E_J can be tuned by applying a small magnetic field parallel to the junction between the TS and the bulk superconductor, an experimental observation of the sideband peak and its shift with magnetic field (cf. the expression for the peak position above) would provide clear evidence for the anomalous tunneling mechanism, and thereby for the presence of MBSs.

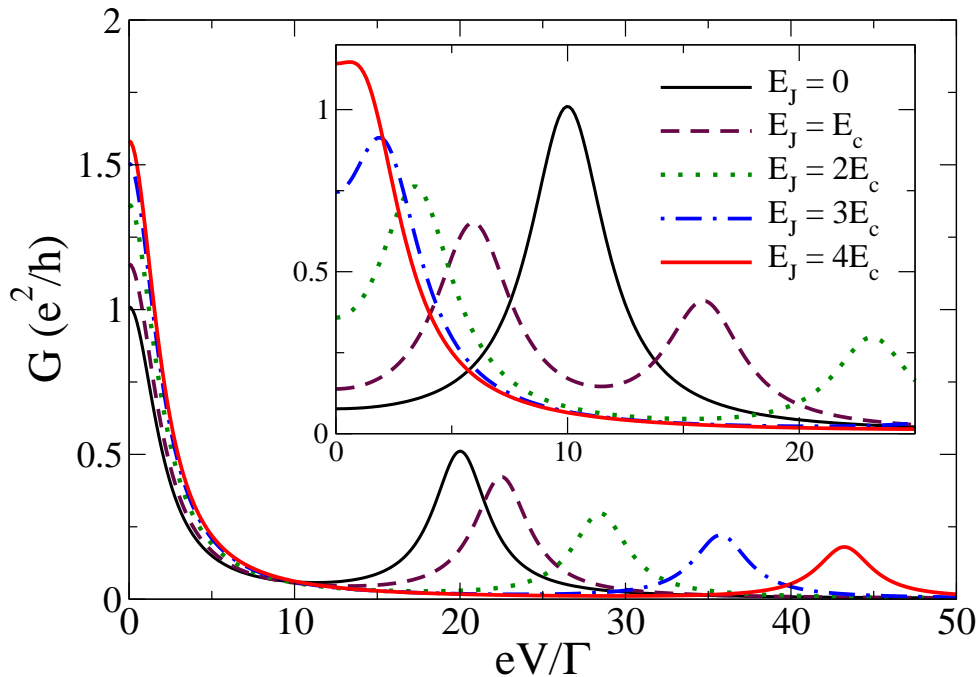


Figure 3.4: Same as Fig. 3.3 but from ZBWM for $T=0$, $E_c=5\Gamma$ and several E_J .

Coulomb diamonds

Figure 3.5 illustrates the differential conductance of the MSCT as function of the bias voltage V and the gate potential n_g . The differential conductance is color coded in units of e^2/h with the scale given for each plot individually. Except for the top two plots, the color codes coincide. The previously shown $dI/dV(eV)$ and $dI/dV(n_g)$ plots represent single vertical and horizontal cuts through the three dimensional plots from Fig. 3.5. The only difference is that eV is scaled now in units of the charging energy E_c . This pins the transitions between peaks and valleys also to the voltage axis and allows for a better analysis of the Coulomb diamond formation with increasing E_c . In the top left plot temperature alone is enough for the electrons to overcome the charging energy and enter the MSCT. Like also expected for the grounded situation $E_c = 0$, we observe one Lorentzian conductance peak without sidebands and independent of the gate potential. Already for a charging energy $E_c = 4\Gamma$ which is twice of the temperature in the system, a Coulomb blockade starts to build up. The blockaded conductance valleys and the conductance sidepeaks get further pronounced until for $E_c = 16\Gamma$ we have extremely sharp peak to valley transitions. Together with their gate potential dependence, these peaks form the typical Coulomb diamond structure, also observable in quantum dot systems whenever charging effects dominate the transport behavior.

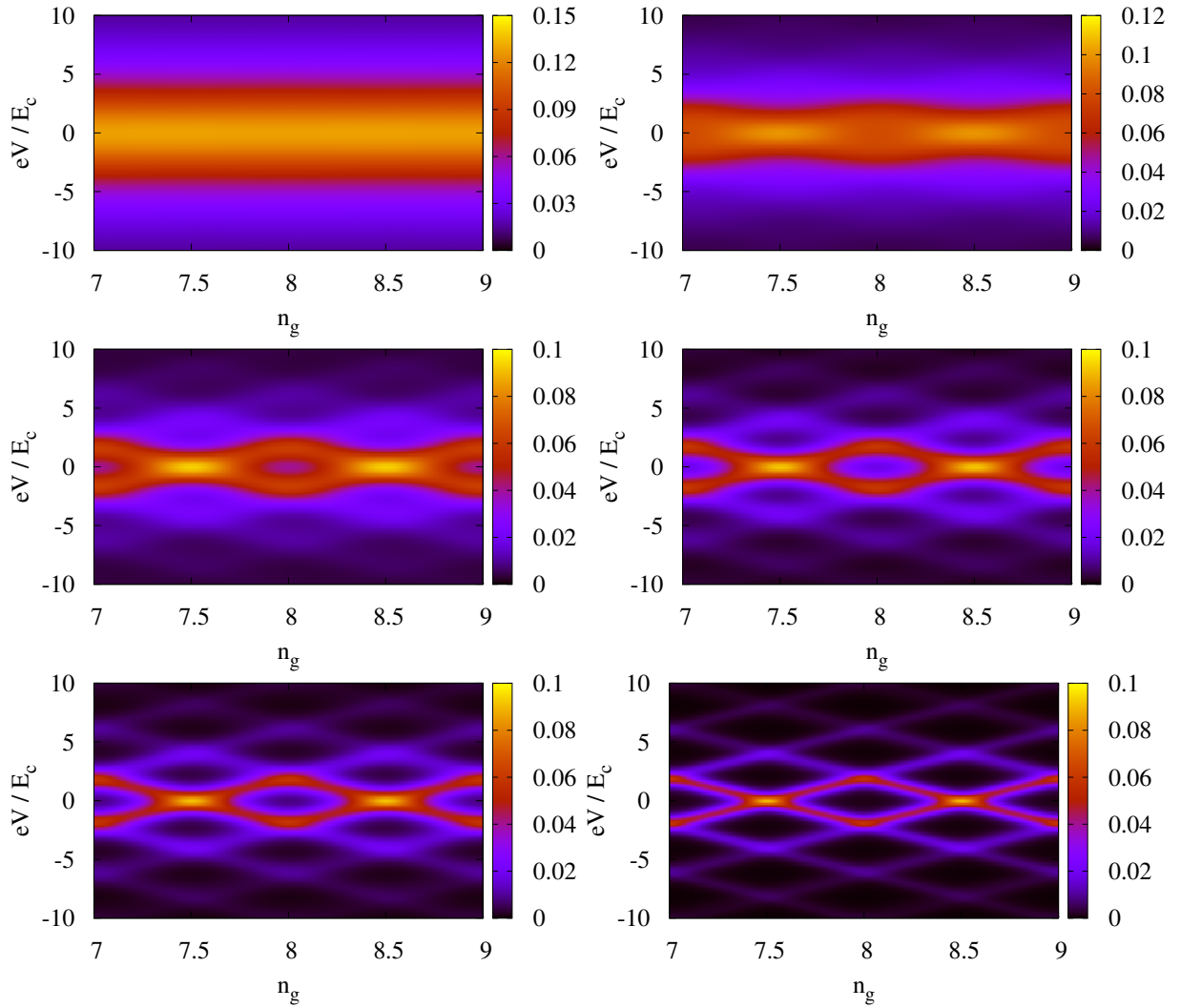


Figure 3.5: The typical diamond like structure of a Coulomb blockade builds up in the system when increasing the charging energy E_c . From left to right and then from top to bottom we have $E_c = \{2, 4, 6, 8, 10, 16\} \Gamma$. The colors encode the differential conductance dI/dV in units of e^2/h as a function of the gate potential n_g and the dimensionless bias voltage eV/Γ . All plots are at temperature $T = 2\Gamma$ and obtained from the master equation for $E_J = 0$.

4 Conclusions

In this first part of the thesis, we have studied the transport properties of an interacting Majorana single-charge transistor and provided a comprehensive picture in a wide parameter regime. From an experimental point of view, our results should also be directly relevant for extending existing work, see, e.g., Ref. [13], where conductance peaks for tunneling into Majorana wires were reported.

The inclusion of interactions in form of a charging energy together with the interplay of a normal and an anomalous (involving the condensate) tunneling channel predicts a sideband structure in the differential conductance.

When varying the gate voltage parameter n_g , we find Coulomb oscillations and have characterized the behavior of the peak and valley conductances in detail.

Building the MSCT as a spectroscopy setup and comparing the dI/dV signal with our predictions, Majorana fermions in this system could be identified by observing the sideband peaks in the nonlinear conductance and verifying their dependence on tunable system parameters. Also the crossover behavior of the Coulomb peak conductance with respect to the charging energy provides another identifying feature which is observable at zero as well as at finite temperature. Regarding our master equation approach in the limit of $E_J = 0$, current conservation prevents us from accessing intrinsic nonlocal features of the Majorana fermions involved. Consequently the next step would be the inclusion of the Josephson coupling in a perturbative way which corresponds to attaching a third lead within the master equation framework and yields access to nonlocal features which could strengthen a hypothesis of the presence of Majorana fermions in our MSCT setup, if our results could be experimentally reproduced.

Part II

Iterative Summation of Path-Integrals (ISPI) for nonequilibrium molecular quantum transport

5 Introduction

Understanding quantum transport in nanoscale electronic systems with vibrational or mechanical (“phonon”) degrees of freedom is of topical interest in several areas of physics, including molecular electronics [43, 44], inelastic tunneling spectroscopy [45], nanoelectromechanical systems [46, 47], break junctions [48], and suspended semiconductor or carbon-based nanostructures [49, 50, 51, 52]. The electron-phonon interaction allows to observe a rich variety of intriguing phenomena, such as negative differential conductance, the Franck-Condon blockade of transport, rectification, vibrational sidebands or step-like features in the current-voltage (IV) characteristics, and current-induced heating or cooling. Already the simplest nonequilibrium spinless “Anderson-Holstein” (AH) model [53, 54], where the nanostructure corresponds to just one spinless electronic level coupled to a single oscillator mode, captures much of this richness [55, 56]; for a review, see Ref. [45].

Analytical approaches allow us to understand the AH model in various corners of its parameter space, but no controlled approximation, let alone exact solution, connecting these corners seems in reach. One may expect that a unified picture is available from numerics. However, numerical renormalization group [57] or quantum Monte Carlo (QMC) calculations [58, 59] are usually restricted to equilibrium. For the nonequilibrium AH model, Han [60] employed an imaginary-time QMC approach followed by a double analytical continuation scheme; unfortunately, the latter step is plagued by instabilities [61]. A promising avenue for the AH model has recently been suggested by real-time path-integral QMC simulations [62, 63], where one directly computes the time-dependent current. Such calculations have to deal with the infamous dynamical sign problem at long times, but in several parameter regions, especially when a secondary phonon bath is present, the stationary steady-state regime can be reached.

In this second part of the thesis, we formulate and apply an alternative numerical approach, which in practice is useful unless both the temperature T and the bias voltage V are small. It is also based on a Keldysh path-integral formulation but does not involve stochastic sampling schemes and thus remains free from any sign problem. To that end, we extend the “iterative summation of path integrals” (ISPI) technique [64, 65] to the AH model. Technical aspects of the present approach, in particular our mapping to an effective three-state system via the “spin-1 Hirsch-Fye transformation” in Eq. (6.36), should also be of interest to QMC schemes [59]. In essence, the ISPI method exploits that time correlations of the auxiliary three-state Keldysh variable, which arise after functional integration over the phonon and the (dot and lead) fermion degrees of freedom, can be truncated beyond a certain memory time τ_c when either T or V is finite. Together with a convergence scheme designed to eliminate systematic errors due to the finiteness of τ_c , such calculations allow to obtain numerically exact results. The ISPI method has already been successfully applied to the spinful Anderson model [64, 66, 67], where instead of the phonon a local charging interaction is present and also to the magnetic Anderson model which consists of a spinful single-orbital quantum dot with an incorporated quantum mechanical spin-1/2 magnetic impurity [68].

While we focus on the simplest version of the AH model with a single unequilibrated⁸ phonon mode here, the conceptual generalization to include Coulomb interactions, more phonon modes, or several dot levels is straightforward. We benchmark our ISPI code against three different analytical approaches and then study the crossover between the respective regimes.

5.1 The spinless Anderson-Holstein model

A starting point in molecular electronics is the study of molecular transport junctions (MTJ). They are typical transistor setups where the central “active” region consists of a single molecule which is contacted by leads from two sides. In a nonequilibrium situation caused by an applied bias voltage V they act as electron source and drain and often also a third gate electrode is coupled capacitively to the molecule. The gate electrode allows for changing the energy of molecular states with respect to the leads and hence the interplay of the potentials of all three electrodes generates a characteristic bias current vs voltage signal $I(V)$. Dependent on the point of view or stage of development one can either see this signal as the desired characteristics of a miniaturized device or as the output signal from some type of molecular spectroscopy. Since the molecule itself possesses mechanical degrees of freedom and the whole setup might also be placed within some solvent, a general theoretical description is quite complex [45].

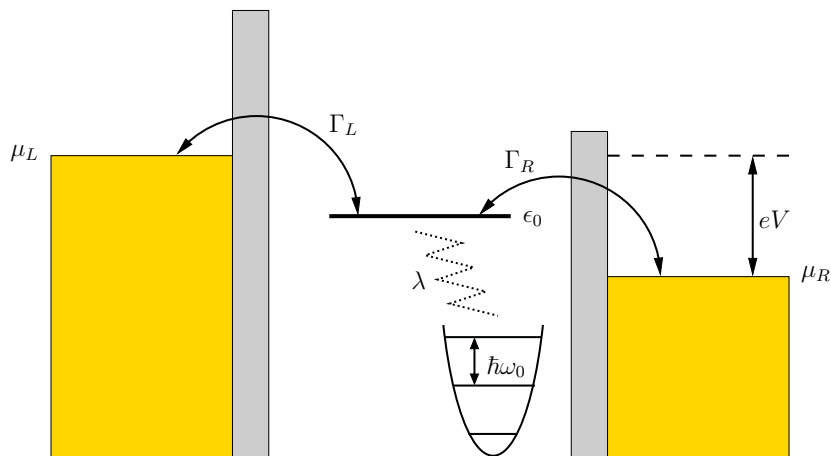


Figure 5.1: Schematic illustration of the spinless Anderson-Holstein model. The molecular dot (central region) consists of a single relevant electronic level of energy ϵ_0 and one phonon mode of frequency ω_0 coupled linearly to it with strength λ . The two metallic leads are at different chemical potentials $\mu_{L/R}$ due to an attached bias voltage $eV = \mu_L - \mu_R$. In the usual wide band approximation the tunneling between the leads and the molecular dot introduces the hybridization energy scales $\Gamma_{L/R}$.

⁸For an equilibrated mode, i.e., in the presence of a secondary phonon bath, both ISPI and other numerical schemes [56, 62, 63] simplify substantially.

By an appropriate parameter choice we can reduce or neglect much of the complexity of an MTJ without rendering the problem trivial and out of touch with reality. We don't include any surrounding solvent and assume a large energy spacing between molecular orbitals to describe the relevant electronic structure in terms of the highest occupied and lowest unoccupied molecular orbital, referred to as the HOMO and the LUMO. We model the LUMO by a single level of energy ϵ_0 . The charging energy of the molecule is assumed to be high enough so that we can set it at infinity and neglect spin and Coulomb interaction at all. Vibrational degrees of freedom are assumed to be dominated by a single resonant frequency ω_0 and included by a single harmonic phonon mode. The intermolecular electron phonon coupling is taken linear in the phonon coordinate and only couples to the one electronic level with strength λ . With all these assumptions made we end up at the spinless Anderson-Holstein (AH) model, schematically shown in Fig. 5.1 including all relevant parameters. Despite of all simplifications made, the remaining spinless AH model for a MTJ is far away from being simple and still provides much of its richness to explore.

Since the properties of the molecule are related to a level structure split into an electronic and a vibronic part, it is also common to speak of a quantum dot with a phonon coupled to it or a molecular quantum dot. We will use all expressions equivalently. If not stated explicitly otherwise, we set $\hbar = k_B = 1$ in all following derivations.

5.2 The Hamiltonian

We will split the Hamiltonian of the spinless AH in two parts $\hat{\mathcal{H}} = \hat{\mathcal{H}}_{mol} + \hat{\mathcal{H}}_{env}$, representing the isolated molecule and the environment. Using bosonic $\{\hat{b}^\dagger, \hat{b}\}$ (fermionic $\{\hat{d}^\dagger, \hat{d}\}$) creation and annihilation operators for the phonon mode (electronic dot level) we get

$$\hat{\mathcal{H}}_{mol} = \omega_0 \hat{b}^\dagger \hat{b} + (\epsilon_0 + \lambda \hat{Q}) \hat{d}^\dagger \hat{d} \quad ; \quad \hat{Q} = (\hat{b}^\dagger + \hat{b}) . \quad (5.1)$$

The electron-phonon coupling has strength λ and we already define the oscillators position operator Q for later reference. The coupling reflects the fact that adding an electron to the molecule modifies its charge distribution and therefore also the equilibrium distances between its nuclei which again affects its vibration [69]. Regarding the environmental part $\hat{\mathcal{H}}_{env}$ we introduce fermionic creation and annihilation operators $\{\hat{c}_{\mathbf{k}\alpha}^\dagger, \hat{c}_{\mathbf{k}\alpha}\}$ for electrons with momentum \mathbf{k} in the noninteracting lead $\alpha = L/R$ at chemical potential μ_α .

$$\hat{\mathcal{H}}_{env} = \sum_{\mathbf{k}, \alpha} \left(\epsilon_{\mathbf{k}} \hat{c}_{\mathbf{k}\alpha}^\dagger \hat{c}_{\mathbf{k}\alpha} - t_\alpha [\hat{c}_{\mathbf{k}\alpha}^\dagger \hat{d} + \hat{d}^\dagger \hat{c}_{\mathbf{k}\alpha}] \right) . \quad (5.2)$$

The chemical potential difference defines the bias voltage $eV = \mu_L - \mu_R$. The tunneling amplitudes are directly assumed to be real and momentum independent since we will use again the wide band approximation and they get absorbed in the hybridization⁹ energy scales $\Gamma_\alpha \equiv \pi \nu_\alpha(\epsilon_F) |t_\alpha|^2$. As usual this approximation assumes the local density of states ν_α to be constant around the Fermi energy ϵ_F . All relevant parameters of our system will be later scaled in units of the total hybridization energy $\Gamma = \Gamma_L + \Gamma_R$.

⁹Note that there is some freedom of choice in the definition of this scale and that we have defined it without the factor 2 present in the MSCT chapter. The main reason was to achieve a better comparability of expressions regarding existent results in different parameter limits of the AH model.

5.3 The current operator

As motivated before we are interested in the current-voltage characteristics of the AH model and want to extend the accessible parameter regime to close the gap between existing methods working well in different regimes. We start from the current operator and develop a scheme that allows for the numerical exact computation of its expectation value. As long as possible we stay at analytic expressions before we will switch to numerics. The derivation of the current operator for the AH model is the first step and we start from the total number operator \hat{N}_α in lead $\alpha = L/R$

$$\hat{N}_\alpha = \sum_{\mathbf{k}} \hat{c}_{\mathbf{k}\alpha}^\dagger \hat{c}_{\mathbf{k}\alpha} . \quad (5.3)$$

Its time evolution is governed by Heisenberg's equation of motion which only involves the tunneling part of the total AH Hamiltonian since all other parts commute

$$\dot{\hat{N}}_\alpha = \text{i}[\hat{\mathcal{H}}, \hat{N}_\alpha]_- = -\text{i} \sum_{\mathbf{k}, \mathbf{k}', \alpha'} t_{\alpha'} \left([\hat{c}_{\mathbf{k}'\alpha'}^\dagger \hat{d}, \hat{c}_{\mathbf{k}\alpha}^\dagger \hat{c}_{\mathbf{k}\alpha}] + [\hat{d}^\dagger \hat{c}_{\mathbf{k}'\alpha'}, \hat{c}_{\mathbf{k}\alpha}^\dagger \hat{c}_{\mathbf{k}\alpha}] \right) . \quad (5.4)$$

A further simplification originates from the usual fermionic anticommutation relations

$$\dot{\hat{N}}_\alpha = \text{i} \sum_{\mathbf{k}, \mathbf{k}', \alpha'} t_{\alpha'} \left(\hat{c}_{\mathbf{k}\alpha}^\dagger \underbrace{\{\hat{c}_{\mathbf{k}\alpha}, \hat{c}_{\mathbf{k}'\alpha'}^\dagger\}}_{\delta_{\alpha, \alpha'} \delta_{\mathbf{k}, \mathbf{k}'}} \hat{d} - \hat{d}^\dagger \underbrace{\{\hat{c}_{\mathbf{k}'\alpha'}, \hat{c}_{\mathbf{k}\alpha}^\dagger\}}_{\delta_{\alpha, \alpha'} \delta_{\mathbf{k}, \mathbf{k}'}} \hat{c}_{\mathbf{k}\alpha} \right) = \text{i} \sum_{\mathbf{k}} t_\alpha \left(\hat{c}_{\mathbf{k}\alpha}^\dagger \hat{d} - \hat{d}^\dagger \hat{c}_{\mathbf{k}\alpha} \right) .$$

Since $\dot{\hat{N}}_\alpha$ is the operator for the net rate of electrons tunneling into lead α , we directly get the current operator \hat{I}_α for the current flowing from lead α to the dot by multiplying $\dot{\hat{N}}_\alpha$ with the electron charge $-e$

$$\hat{I}_\alpha = -e \dot{\hat{N}}_\alpha . \quad (5.5)$$

Note that there is no truncation in the tunneling and processes of all orders are included within our method. Finally the operator for the symmetrized current $I = (I_L - I_R)/2$ is defined using the convention $\alpha = L/R = \pm$

$$\hat{I} = -\frac{\text{i}e}{2} \sum_{\mathbf{k}\alpha} \alpha t_\alpha \left(\hat{c}_{\mathbf{k}\alpha}^\dagger \hat{d} - \hat{d}^\dagger \hat{c}_{\mathbf{k}\alpha} \right) . \quad (5.6)$$

The challenge for the rest of this second part of the thesis is to compute the nonequilibrium expectation value of the symmetrized current. For this we need the Keldysh path-integral formalism which we will introduce and directly apply to our AH model in the next chapter. We will end up with a so called Keldysh generating function in a special form which allows for a numerically exact computation of the symmetrized current after adapting the ISPI scheme [64] to our problem in Sec. 9.

6 The Keldysh path-integral formalism

Many tools in statistical physics are only valid for systems in a thermodynamic equilibrium situations since they involve the following assumption: adiabatic modification of an equilibrium quantum state during its time evolution is reversible and always allows to restore an initial state of a system up to a global phase factor in the future. For a system entering a nonequilibrium situation during its time evolution this is not true anymore and a final state in the future is unknown. Nevertheless it is possible to get access to expectation values under nonequilibrium situations if one circumvents the necessity to know the state of a system in the future and only relies on the knowledge of a defined initial state in the past. The corresponding technique was developed by L.V. Keldysh in 1964 [70]. We will apply it together with the framework of real-time path integrals and recommend [40] as a very good introduction.

6.1 The Keldysh formalism

The AH Hamiltonian with all couplings and interactions present [Eqs. (5.1) and (5.2)] corresponds to a not exactly solvable system and at some point we will have to proceed numerically. The eigenstates are unknown and equivalently the corresponding nonequilibrium density operator $\tilde{\rho}$ is also not directly accessible. Nevertheless it exists and we can write down a formal definition of our desired expectation value

$$I(t_m) = \text{tr}[\tilde{\rho}(t_m)\hat{I}] . \quad (6.1)$$

The computation of this expectation value is equivalent to performing a measurement on the system and we explicitly assign a measurement time t_m to the resulting symmetrized current.

A way to reformulate Eq. (6.1) in terms of objects which are known or at least allow for good approximations was invented by Keldysh [70] in 1965. His idea is to take advantage of the determinism of the time evolution of a quantum state. Accessible initial conditions are gained from the equilibrium density matrix $\tilde{\rho}_0$ in a distant past, originating from a Hamiltonian where all “complicated” parts which render the system unsolvable are switched off. What follows is a forward and backward time evolution along the time contour \mathcal{C} shown in Fig. 6.1. At the beginning and the end of this time-evolution the “complicated” parts - namely the interactions - are adiabatically switched on and off again. The determinism of this time evolution loop together with the adiabatic switching guarantees to end up in the same quantum state but having passed the measurement time with the full interacting system.

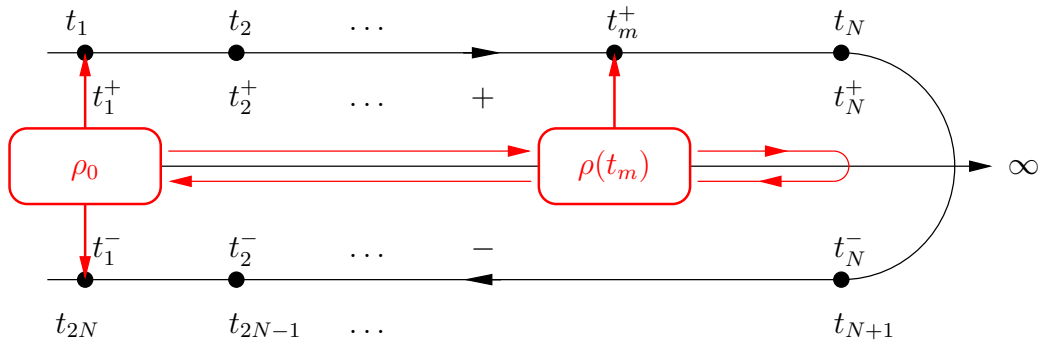


Figure 6.1: Black: Keldysh contour with discrete times labeled for later discretization in slices (t_1^\pm to t_N^\pm with boundary condition $t_N^+ = t_N^-$) respectively for a discretization along the contour (t_1 to t_{2N} with boundary condition $t_N = t_{N+1}$). Red: Forward and backward evolution of the density matrix. Arrow pointing to reference time.

The corresponding contour time evolution operator \mathcal{U}_C must equal unity and is defined by a contour ordered exponential where \mathcal{T}_C is the contour ordering operator. It results in (anti-) time-ordering for the (lower) upper branch of the contour, respectively.

$$\mathcal{U}_C = \mathcal{T}_C e^{-i \oint_C dt' \hat{\mathcal{H}}(t')} = \mathbb{1} . \quad (6.2)$$

A time evolution and thus the corresponding operator must behave transitive and we can split up the loop evolution at different points and rewrite it as products of evolution operators propagating a state from time t_1 to t_2 on the contour

$$\mathcal{U}(t_2, t_1) = \mathcal{T}_C e^{-i \int_{t_1}^{t_2} dt' \hat{\mathcal{H}}(t')} . \quad (6.3)$$

How useful this time evolution construction is, will turn out shortly after introducing explicitly times on the contour [cf. Fig. 6.1] and establishing the connection back to Eq. (6.1).

6.1.1 The initial equilibrium partition function

We have a composite system, consisting of coupled parts, each one of them individually representing a “free” purely fermionic or bosonic system with well known eigenstates. In the absence of tunnel- and electron-phonon-coupling the corresponding density operator $\tilde{\rho}_0$ factorizes with respect to each subsystem and together with its definition we also introduce the equilibrium partition function \mathcal{Z} . In contrast to [40] we do not define a normalized \mathcal{Z} and keep the equilibrium definition as long as there is no source term present

$$\tilde{\rho}_0 = \frac{\rho_0}{\mathcal{Z}} \quad ; \quad \mathcal{Z} = \text{tr}(\rho_0) \quad ; \quad \rho_0 = e^{-\beta_p \omega_0 \hat{b}^\dagger \hat{b} - \beta_d (\epsilon - \mu_d) \hat{d}^\dagger \hat{d} - \beta \sum_{\mathbf{k}\alpha} (\epsilon_{\mathbf{k}} - \mu_\alpha) \hat{c}_{\mathbf{k}\alpha}^\dagger \hat{c}_{\mathbf{k}\alpha}} . \quad (6.4)$$

Note that \mathcal{Z} is a time and interaction independent constant. In principle, $\tilde{\rho}_0$ allows for different (inverse) temperatures for phonon, dot and leads $(\beta_p, \beta_d, \beta)$, and for some chemical potential μ_d of the dot (such that it is initially depopulated or full). From now on, we take $\beta_p = \beta_d = \beta$ and set $\mu_d = 0$ but a generalization is straight forward.

6.1.2 The Keldysh generating function

Based on the above argumentation the initial and final state are physically identical and associated with the times $0 = t_1^\pm$. For convenience we also double the return time $t = t_N^\pm$ and define the corresponding periodic boundary condition $\mathcal{U}(t_N^-, t_N^+) = \mathbb{1}$ connecting the upper “+” branch and the lower “-” branch of the contour. Exploiting the invariance of the trace operation under cyclic permutation condenses the whole argumentation into Eq. (6.5) and we get $\text{tr}(\rho(t_m)) = \text{tr}(\rho_0)$ as it should be

$$\text{tr}(\rho(t_m)) = \text{tr} [\mathcal{U}(t_m, t_1^+) \rho_0 \mathcal{U}(t_1^-, t_N^-) \mathcal{U}(t_N^-, t_N^+) \mathcal{U}(t_N^+, t_m)] = \text{tr}(\mathcal{U}_C \rho_0) = \text{tr}(\rho_0) = \mathcal{Z} . \quad (6.5)$$

Placing now the operator \hat{I} only on the “+”-branch of the contour at $t' = t_m$ breaks the symmetry between the branches and allows for the computation of its expectation value. Formally this “placing” corresponds to multiplying $\rho(t_m)$ by $\hat{I}(t_m)/\mathcal{Z}$ within Eq. (6.5) which establishes the connection to Eq. (6.1). Alternatively placing half of it on the upper and half on the lower branch also works, as long as it still breaks the symmetry in the correct way. Equivalently, we will use the concept of a generating function for convenience. After adding a so called source term $i\eta \hat{I} \delta(t' - t_m)$ (respectively $i\eta \hat{I} \delta_{j,m}/\delta_t$ for the discrete path-integral used later) to the Hamiltonian within the definition of the contour evolution operator \mathcal{U}_C , the partition function becomes the so called generating function $\mathcal{Z}[\eta]$

$$\mathcal{U}_C \rightarrow \mathcal{U}_C[\eta] = \mathcal{T}_C e^{-i \int_C dt' \hat{\mathcal{H}}(t') + i\eta \hat{I} \delta(t' - t_m)} \quad ; \quad \mathcal{Z} \rightarrow \mathcal{Z}[\eta] = \text{tr}(\mathcal{U}_C[\eta] \rho_0) \neq \text{tr}(\rho_0) . \quad (6.6)$$

The name stems from the fact that performing a functional derivative of $\ln \mathcal{Z}[\eta]$ with respect to η generates the definition of the expectation value at a measurement time t_m from Eq. (6.1)

$$\left. \frac{\partial}{\partial \eta} \ln \mathcal{Z}[\eta] \right|_{\eta=0} = \frac{\text{tr}[\mathcal{U}(t_1^-, t_m) \hat{I} \mathcal{U}(t_m, t_1^+) \rho_0]}{\text{tr}[\mathcal{U}(t_1^-, t_m) \mathcal{U}(t_m, t_1^+) \rho_0]} = \frac{\text{tr}[\rho(t_m) \hat{I}]}{\mathcal{Z}} = I(t_m) . \quad (6.7)$$

The next step is to evaluate the time evolution of the AH model along the Keldysh contour. We will use a real-time coherent state path integral for this, which we introduce in the following.

6.2 The real-time coherent state path-integral

Evaluating the trace in the definition of the Keldysh generating function [Eq. (6.6)] includes the evaluation of the contour evolution operator $\mathcal{U}_C[\eta]$ on some complete set of states. Since the eigenstates of the full Hamiltonian $\hat{\mathcal{H}}$ are unknown, we have to expand the exponential into its series and then evaluate it on a known complete set of states forming a basis of the Hilbert space. It will turn out to be useful to use coherent states which we will now first introduce before getting back to the actual evaluation of the contour evolution operator and the introduction of bosonic and fermionic coherent state path-integrals. A very good introduction to the general ideas presented in this section can be found in [71].

6.2.1 Fermionic and bosonic coherent states

For the evaluation of normal ordered products of creation and annihilation operators it turns out to be very useful to choose a basis of coherent states. They are defined as eigenstates of the annihilation operator. In the case of bosons the eigenvalue is just a complex number and we get

$$\hat{b}|\phi\rangle = \phi|\phi\rangle \quad \xleftrightarrow{\text{d.c.}} \quad \langle\phi|\hat{b}^\dagger = \langle\phi|\phi^* . \quad (6.8)$$

The bosonic dual correspondence (d.c.) is achieved by normal Hermitian conjugation of the eigenvalue equation. Introducing a similar relation for fermions is possible, but due to the anticommutative fermionic algebra, the eigenvalues also have to anticommute and cannot be normal complex numbers. Using anticommuting Grassmann numbers $\psi, \bar{\psi}$ solves the problem and we get a similar relation

$$\hat{d}|\psi\rangle = \psi|\psi\rangle \quad \xleftrightarrow{\text{d.c.}} \quad \langle\psi|\hat{d}^\dagger = \langle\psi|\bar{\psi} . \quad (6.9)$$

Two different Grassmann numbers fulfill the following anticommutation relations

$$\psi_\alpha\psi_\beta + \psi_\beta\psi_\alpha = 0 \quad \Rightarrow \quad \psi_\alpha^2 = 0 . \quad (6.10)$$

A similar connection to the dual space like for bosons is obtained by defining a conjugation operation for Grassmann numbers as done in [71]. Since the definition of a conjugation involves an arbitrary mapping of generators of the Grassmann algebra to each other we assign a $(\bar{\cdot})$ to this operation and not the usual $(*)$. Consequently ψ and $\bar{\psi}$ have to be interpreted as independent quantities of the same type and Eq. (6.10) is the only existent anticommutation relation for all of them. The rules for Grassmann conjugation are similar to the ones for complex numbers

$$\bar{\bar{\psi}} = \psi \quad ; \quad \overline{\psi_n\psi_{n-1}\dots\psi_1} = \bar{\psi}_1\dots\bar{\psi}_{n-1}\bar{\psi}_n \quad ; \quad \overline{z\psi} = z^*\bar{\psi} \quad , \quad z \in \mathbb{C} . \quad (6.11)$$

We will also need to integrate over functions of Grassmann numbers but since their square equals zero only linear functions can be defined from them and there is no difference between Grassmann integration and Grassmann differentiation. The only rule to follow is that one always has to anticommute Grassmann variables directly next to the “integration operator” before performing the integration. Some examples are

$$\int d\xi_\alpha \xi_\beta = \delta_{\alpha,\beta} \quad \Rightarrow \quad \int d\xi 1 = 0 \quad ; \quad \int d\xi \bar{\xi} = 0 \quad (6.12)$$

$$\int d\xi \bar{\xi}\xi = - \int d\xi \xi\bar{\xi} = - \bar{\xi} .$$

The equations (6.12) also hold if one replaces all ξ by $\bar{\xi}$ and vice versa. All integrations performed later, can be reduced to these examples by applying Eq. (6.10). Finally we will end this section with a summary of all important coherent state relations later needed:

Bosons:	Fermions:
$[\hat{b}_\alpha, \hat{b}_\beta^\dagger]_- = \delta_{\alpha\beta}$	$[\hat{d}_\alpha, \hat{d}_\beta^\dagger]_+ = \delta_{\alpha\beta}$ (6.13)
$\langle \phi \phi' \rangle = e^{\sum_\alpha \phi_\alpha^* \phi'_\alpha}$	$\langle \psi \psi' \rangle = e^{\sum_\alpha \bar{\psi}_\alpha \psi'_\alpha}$ (6.14)
$\langle \phi A(\hat{b}_\alpha^\dagger, \hat{b}_\alpha) \phi' \rangle = e^{\sum_\alpha \phi_\alpha^* \phi'_\alpha} A(\phi_\alpha^*, \phi_\alpha)$	$\langle \psi A(\hat{d}_\alpha^\dagger, \hat{d}_\alpha) \psi' \rangle = e^{\sum_\alpha \bar{\psi}_\alpha \psi'_\alpha} A(\bar{\psi}_\alpha, \psi_\alpha)$ (6.15)
$d\mu(\phi) := \frac{1}{2\pi\mathbf{i}} \prod_\alpha d\phi_\alpha^* d\phi_\alpha$	$d\mu(\psi) := \prod_\alpha d\bar{\psi}_\alpha d\psi_\alpha$ (6.16)
$\mathbb{1} = \int d\mu(\phi) e^{-\sum_\alpha \phi_\alpha^* \phi_\alpha} \phi\rangle \langle \phi $	$\mathbb{1} = \int d\mu(\psi) e^{-\sum_\alpha \bar{\psi}_\alpha \psi_\alpha} \psi\rangle \langle \psi $ (6.17)
$\text{tr}(\hat{A}) = \int d\mu(\phi) e^{-\sum_\alpha \phi_\alpha^* \phi_\alpha} \langle \phi \hat{A} \phi \rangle$	$\text{tr}(\hat{A}) = \int d\mu(\psi) e^{-\sum_\alpha \bar{\psi}_\alpha \psi_\alpha} \langle \psi \hat{A} -\psi \rangle$ (6.18)

The resolution of unity and the trace operation with respect to fermionic coherent states involve the Grassmann integration and we emphasize the small differences like the prefactor of the measure or the antiperiodic boundary condition hidden in the trace definition which are likely to be overseen.

6.2.2 The Trotter Suzuki break-up

We assume that during a noninfinitesimal time interval $[t, t']$ our Hamiltonian $\hat{\mathcal{H}}$ is time-independent¹⁰ and decompose it in two noncommuting parts $\hat{\mathcal{H}}_0$ and $\hat{\mathcal{H}}_1$. Since the eigenstates of $\hat{\mathcal{H}}$ are unknown, we have to evaluate

$$\mathcal{U}(t', t) = e^{\mp \mathbf{i} \hat{\mathcal{H}}(t-t')} = e^{\mp \mathbf{i} (\hat{\mathcal{H}}_0 + \hat{\mathcal{H}}_1)(t-t')} \quad (6.19)$$

involving an expansion of the exponential and afterwards the evaluation of an infinite series containing recursive commutator relations of $\hat{\mathcal{H}}_0$ and $\hat{\mathcal{H}}_1$ with respect to some basis. This direct evaluation is impossible and since we intend to use a basis of coherent states, we have to get at least a normal ordered version of the time-evolution operator. In the following we will show how this is possible by decomposing the time evolution along the interval $[t, t']$ into a sequence of evaluable normal ordered short-time propagations.

¹⁰The switching between the full interacting and noninteracting system needed during the Keldysh time propagation will be done in between two short-time propagations of the system, each with duration δ_t . See also [40].

We start from the exact Trotter Suzuki decomposition [72] which is valid for any bounded¹¹ operators $\hat{\mathcal{H}}_0$ and $\hat{\mathcal{H}}_1$

$$e^{\mp i(t-t')(\hat{\mathcal{H}}_0+\hat{\mathcal{H}}_1)} = \lim_{N \rightarrow \infty} \left(e^{\mp i\delta_t \hat{\mathcal{H}}_0} e^{\mp i\delta_t \hat{\mathcal{H}}_1} \right)^N \quad ; \quad \delta_t = (t-t')/N . \quad (6.20)$$

Keeping in mind, that we later need to use numerics, we have to split up the time-evolution operator into a finite product of normally ordered short-time evolution operators \mathcal{U}_{δ_t} and thus have to fix N at some large number. As a consequence the relation is not exact anymore and we introduce the so-called Trotter error

$$\mathcal{U}_{(\pm\delta_t)} = e^{\mp i\delta_t \hat{\mathcal{H}}_0} e^{\mp i\delta_t \hat{\mathcal{H}}_1} = e^{\mp i\delta_t (\hat{\mathcal{H}}_0+\hat{\mathcal{H}}_1)} + \mathcal{O}(\delta_t^2) \quad ; \quad \delta_t \Gamma \ll 1 . \quad (6.21)$$

As shown in [73] this introduces an error in our observable which scales with $\mathcal{O}(\delta_t^2)$ and we will explain in Sec. 9.5 how it is possible to eliminate it from our results. Now we have introduced all tools needed to formally construct the real-time path integral representation of the Keldysh generating function in the next section. Afterwards we can start to explicitly evaluate all expressions for the AH model.

6.2.3 Generating function from real-time path-integral

We discretize the Keldysh contour into $(2N-1)$ segments introducing times t_1 up to t_{2N} around the contour [cf. Fig. 6.1]. By assigning $t_1 = t_{2N} = 0$ and $t_N = t_{N+1} = t$, the duration of each time interval in one of the branches of the contour is $\delta_t = t/(N-1)$

$$\mathcal{Z}[\eta] = \text{tr}(\mathcal{U}_C[\eta]\rho_0) = \text{tr} \left[\left(\prod_{j=2N-1}^{N+1} \mathcal{U}_{-\delta_t}[\eta] \right) \mathbb{1} \left(\prod_{j=N-1}^1 \mathcal{U}_{+\delta_t}[\eta] \right) \rho_0 \right] + \mathcal{O}(\delta_t^2) . \quad (6.22)$$

Now we insert $2N-1$ coherent state identities $\mathbb{1}_j$ at each time slice $j \in \{2N-1, \dots, 1\}$

$$\begin{aligned} \mathbb{1}_j &= \int \frac{d(\text{Re}\phi_j)d(\text{Im}\phi_j)}{\pi} \int d\bar{\psi}_j d\psi_j e^{-\phi_j^* \phi_j - \bar{\psi}_j \psi_j} \int \prod_{\mathbf{k}\alpha} \{d\bar{\Psi}_{\mathbf{k}\alpha,j} d\Psi_{\mathbf{k}\alpha,j}\} \\ &\times e^{-\sum_{\mathbf{k}\alpha} \bar{\Psi}_{\mathbf{k}\alpha,j} \Psi_{\mathbf{k}\alpha,j}} |\phi_j \psi_j \Psi_j\rangle \langle \phi_j \psi_j \Psi_j| \quad ; \quad |\Psi_j\rangle = \bigotimes_{\mathbf{k}\alpha} |\Psi_{\mathbf{k}\alpha,j}\rangle \end{aligned} \quad (6.23)$$

and also perform the trace over the same coherent state basis at time $2N$. The $\{|\phi_j\rangle\}$ span the phonon subspace, and accordingly $\{|\psi_j\rangle\}$ and $\{|\Psi_j\rangle\}$ span the subspaces of the dot and the leads. In total this will give $2N$ integrations over the complete Hilbert space of the AH model; each at a different time. We directly shorten the notation by introducing the path-integral measure [34] for the bosonic degrees of freedom

$$\mathcal{D}[\phi^*, \phi] = \prod_{j=1}^{2N} \frac{d(\text{Re}\phi_j)d(\text{Im}\phi_j)}{\pi} = \prod_{j=1}^{2N} \frac{d\phi_j^* d\phi_j}{2\pi\mathfrak{i}} \quad (6.24)$$

and a corresponding relation for the fermionic degrees of freedom

$$\mathcal{D}[\bar{\psi}, \psi] = \prod_{j=1}^{2N} d\bar{\psi}_j d\psi_j \quad ; \quad \mathcal{D}[\bar{\Psi}, \Psi] = \prod_{j=1}^{2N} \prod_{\mathbf{k}\alpha} d\bar{\Psi}_{\mathbf{k}\alpha,j} d\Psi_{\mathbf{k}\alpha,j} . \quad (6.25)$$

¹¹Since we are dealing with Hamiltonians this is always fulfilled.

With these definitions Eq. (6.22) transforms to a real-time path integral

$$\mathcal{Z}[\eta] = \int \mathcal{D}[\phi^*, \phi] \mathcal{D}[\bar{\psi}, \psi] \mathcal{D}[\bar{\Psi}, \Psi] e^{-\sum_{j=1}^{2N} |\phi_j|^2 + \bar{\psi}_j \psi_j + \sum_{\mathbf{k}\alpha} \bar{\Psi}_{\mathbf{k}\alpha, j} \Psi_{\mathbf{k}\alpha, j}} \prod_{j=1}^{2N} U_{j+1, j}} . \quad (6.26)$$

To establish the connection to the action of the system we now have to evaluate the matrix elements $U_{j+1, j}$ of the short-time evolution operator with respect to the coherent state basis. Two of them are special and represent the periodic/antiperiodic boundary conditions of the closed Keldysh loop evolution while the rest only differs in the direction of the time evolution

$$U_{j+1, j} \left\{ \begin{array}{ll} \langle \phi_1, \psi_1, \Psi_1 | \rho_0 | \phi_{2N}, -\psi_{2N}, -\Psi_{2N} \rangle & ; \quad j = 2N \\ \langle \phi_{j+1}, \psi_{j+1}, \Psi_{j+1} | e^{-i\delta_t \hat{\mathcal{H}}_0} e^{-i\delta_t \hat{\mathcal{H}}_1} | \phi_j, \psi_j, \Psi_j \rangle & ; \quad j \in \{1 \dots N-1\} \\ \langle \phi_{N+1}, \psi_{N+1}, \Psi_{N+1} | \mathbb{1} | \phi_N, \psi_N, \Psi_N \rangle & ; \quad j = N \\ \langle \phi_{j+1}, \psi_{j+1}, \Psi_{j+1} | e^{+i\delta_t \hat{\mathcal{H}}_0} e^{+i\delta_t \hat{\mathcal{H}}_1} | \phi_j, \psi_j, \Psi_j \rangle & ; \quad j \in \{N+1 \dots 2N-1\} \end{array} \right. . \quad (6.27)$$

By choosing N big enough, Eq. (6.21) is a controlled approximation. The systematic error introduced will be later extrapolated out. Next, we explicitly evaluate the short-time evolution operators from Eq. (6.27).

6.3 The AH short-time propagators

Before we proceed, let us shortly motivate our proceeding. In this section we are dealing with the evaluation of short-time propagators which will result in expressions being dependent on complex or Grassmann fields. Once we have them, we can assemble all parts according to Eq. (6.26) into one path-integral representing the whole generating function. The general form of that path-integral will involve an action S dependent on the fields involved

$$\mathcal{Z}[\eta] \propto \int \mathcal{D}[\phi^*, \phi] \mathcal{D}[\bar{\psi}, \psi] \mathcal{D}[\bar{\Psi}, \Psi] e^{iS[\phi^*, \phi, \bar{\psi}, \psi, \bar{\Psi}, \Psi]} . \quad (6.28)$$

For its evaluation we need to carry out all remaining field integrations. They are analytically solvable if the corresponding action is in leading order quadratic in its fields. The exact formulas are given later and we only keep in mind that the goal of this section is to get exponential expressions for the short-time propagators which are quadratic in all fields introduced so far.

We start by deriving auxiliary relations from Eq. (6.15) for evaluating the already quadratic propagator parts corresponding to “free” subsystems

$$\langle \phi' | e^{\zeta \hat{b}^\dagger \hat{b}} | \phi \rangle = e^{e^\zeta \phi'^* \phi} \quad ; \quad \langle \psi' | e^{\zeta \hat{d}^\dagger \hat{d}} | \pm \psi \rangle = e^{\pm e^\zeta \bar{\psi}' \psi} \quad ; \quad \langle \Psi'_{\mathbf{k}\alpha} | e^{\zeta \hat{c}_{\mathbf{k}\alpha}^\dagger \hat{c}_{\mathbf{k}\alpha}} | \pm \Psi_{\mathbf{k}\alpha} \rangle = e^{\pm e^\zeta \bar{\Psi}'_{\mathbf{k}\alpha} \Psi_{\mathbf{k}\alpha}} . \quad (6.29)$$

With (anti-)periodic boundary conditions for (fermions) bosons, using the initial distribution (6.4) and the auxiliary relation (6.29), the matrix element $U_{1,2N}$ directly follows from Eq. (6.27) as

$$U_{1,2N} = \exp \left\{ e^{-\beta\omega_0} \phi_1^* \phi_{2N} - e^{-\beta\epsilon_0} \bar{\psi}_1 \psi_{2N} - \sum_{\mathbf{k}\alpha} e^{-\beta(\epsilon_{\mathbf{k}} - \alpha V/2)} \bar{\Psi}_{\mathbf{k}\alpha,1} \Psi_{\mathbf{k}\alpha,2N} \right\}. \quad (6.30)$$

The matrix element connecting t_N and t_{N+1} [no dynamical evolution, cf. Eq. (6.27)] follows with Eq. (6.14)

$$U_{N+1,N} = e^{\phi_{N+1}^* \phi_N + \bar{\psi}_{N+1} \psi_N + \sum_{\mathbf{k}\alpha} \bar{\Psi}_{\mathbf{k}\alpha,N+1} \Psi_{\mathbf{k}\alpha,N}}. \quad (6.31)$$

By construction, the source term enters only in one¹² short-time propagator as additional term to the Hamiltonian and thus must be proportional to a discrete representation of the delta-distribution. For the present arbitrary decomposition $\hat{\mathcal{H}} = \hat{\mathcal{H}}_0 + \hat{\mathcal{H}}_1$, we choose

$$\hat{\mathcal{H}}_0 = \left(\epsilon_0 + \lambda(\hat{b}^\dagger + \hat{b}) \right) \hat{d}^\dagger \hat{d} + \sum_{\mathbf{k}\alpha} \epsilon_{\mathbf{k}} \hat{c}_{\mathbf{k}\alpha}^\dagger \hat{c}_{\mathbf{k}\alpha} \quad (6.32)$$

$$\hat{\mathcal{H}}_1[\eta] = \omega_0 \hat{b}^\dagger \hat{b} - \sum_{\mathbf{k}\alpha} t_\alpha \left[1 - \eta \frac{\alpha}{2} \frac{\delta_{j,m}}{\delta_t} \right] \hat{c}_{\mathbf{k}\alpha}^\dagger \hat{d} + t_\alpha \left[1 + \eta \frac{\alpha}{2} \frac{\delta_{j,m}}{\delta_t} \right] \hat{d}^\dagger \hat{c}_{\mathbf{k}\alpha}. \quad (6.33)$$

We insert again the coherent-state unity from (6.23) between the two factors of the short-time propagator which will allow for their evaluation (These intermediate fields do not get an extra time index, since they will not enter the final path-integral.)

$$U_{j+1,j} = \int \frac{d(\text{Re}\phi)d(\text{Im}\phi)}{\pi} e^{-|\phi|^2} \int d\bar{\psi}d\psi e^{-\bar{\psi}\psi} \int \prod_{\mathbf{k}\alpha} \{d\bar{\Psi}_{\mathbf{k}\alpha}d\Psi_{\mathbf{k}\alpha}\} e^{-\sum_{\mathbf{k}\alpha} \bar{\Psi}_{\mathbf{k}\alpha} \Psi_{\mathbf{k}\alpha}} \\ \times \langle \phi_{j+1} \psi_{j+1} \Psi_{j+1} | e^{\mp i\delta_t \hat{\mathcal{H}}_0} | \phi \psi \Psi \rangle \langle \phi \psi \Psi | e^{\mp i\delta_t \hat{\mathcal{H}}_1} | \phi_j \psi_j \Psi_j \rangle. \quad (6.34)$$

Let us first evaluate the second factor which is unproblematic since it does not contain the electron-phonon coupling¹³ and already has a quadratic field structure. Now we use again the auxiliary relations from Eq. (6.29) together with Eq. (6.15) and get

$$\langle \phi \psi \Psi | e^{\mp i\delta_t \hat{\mathcal{H}}_1} | \phi_j \psi_j \Psi_j \rangle \simeq e^{e^{\mp i\omega_0 \delta_t} \phi^* \phi_j} e^{\bar{\psi} \psi_j + \sum_{\mathbf{k}\alpha} \bar{\Psi}_{\mathbf{k}\alpha} \Psi_{\mathbf{k}\alpha,j} \pm i t_\alpha \delta_t \left[\left[1 - \eta \frac{\alpha}{2} \frac{\delta_{j,m}}{\delta_t} \right] \bar{\Psi}_{\mathbf{k}\alpha} \psi_j + \left[1 + \eta \frac{\alpha}{2} \frac{\delta_{j,m}}{\delta_t} \right] \bar{\psi} \Psi_{\mathbf{k}\alpha,j} \right]}. \quad (6.35)$$

Strictly speaking, the t_α terms are here only treated to lowest order, but we do not expect any problem since the discretization of the lead self-energy is known to be unproblematic

¹²As mentioned before it is also possible to place the source term equally weighted by 1/2 on the upper and lower branch. Due to the finite time discretization we now even have four possibilities. On both branches exist two short-time propagator involving the measurement-time ($t_m^\pm - \delta_t \rightarrow t_m^\pm$ and $t_m^\pm \rightarrow t_m^\pm + \delta_t$ in the contour sense). To rule out uncertainties one could use a source term weighted by 1/4 and include it in all four propagators involving the measurement time but we found out that there is no difference in the current and include only one source term in the propagation $t_m^\pm \rightarrow t_m^\pm + \delta_t$.

¹³It is also possible to proceed in another way at this point by performing a polaron transformation and later introduce auxiliary fields for the lead integrations. However we proceed differently to be closer to [64].

from earlier studies. In the other term, we first exploit that $\hat{n}_d = d^\dagger d = 0, 1$, i.e., we have the operator identity

$$e^{\mp i\delta_t(\epsilon_0 + \lambda[\hat{b}^\dagger + \hat{b}])d^\dagger d} = \mathbb{1} - \hat{n}_d + M\hat{n}_d e^{\mp i\delta_t\epsilon_0} e^{\mp i\delta_t\lambda\hat{b}^\dagger} e^{\mp i\delta_t\lambda\hat{b}} \quad (6.36)$$

with

$$M = e^{-\frac{1}{2}[\mp i\delta_t\lambda\hat{b}^\dagger, \mp i\delta_t\lambda\hat{b}]} = e^{-\lambda^2\delta_t^2/2} \quad (6.37)$$

where we switched to boson normally-ordered form (needed for computing the coherent-state expectation value) via Baker-Hausdorff

$$e^{\hat{A}+\hat{B}} = e^{\hat{A}} e^{\hat{B}} e^{-[\hat{A},\hat{B}]/2} \quad \text{if} \quad [\hat{A}, [\hat{A}, \hat{B}]] = [[\hat{A}, \hat{B}], \hat{B}] = 0. \quad (6.38)$$

The equation (6.36) is the crucial step to disentangle the boson and fermion fields by introducing a summation variable $S_{j+1} = 0, \pm 1$ picking up the resulting three terms in the matrix element. The $S_{j+1} = 0$ part corresponds to the empty dot, and $S_{j+1} = \pm 1$ to the occupied dot (the fact that one needs ± 1 instead of just $+1$ has technical reasons – maybe there is a way to avoid this). Physically, $|S_{j+1}| = 0, 1$ corresponds to the occupation of the dot level. Technically, S_{j+1} plays the role of a Hubbard-Stratonovich auxiliary field in this scheme (cf. ISPI method for the Anderson model [64])

$$\begin{aligned} & \langle \phi_{j+1}\psi_{j+1}\bar{\Psi}_{j+1} | e^{\mp i\delta_t\hat{\mathcal{H}}_0} | \phi\psi\Psi \rangle \\ &= e^{\phi_{j+1}^*\phi + \bar{\psi}_{j+1}\psi + \sum_{\mathbf{k}\alpha} e^{\mp i\epsilon_{\mathbf{k}}\delta_t}\bar{\Psi}_{\mathbf{k}\alpha,j+1}\Psi_{\mathbf{k}\alpha}} \left(\underbrace{1 - \bar{\psi}_{j+1}\psi}_{e^{-\bar{\psi}_{j+1}\psi}} + M\bar{\psi}_{j+1}\psi e^{\mp i\delta_t[\epsilon_0 + \lambda(\phi_{j+1}^* + \phi)]} \right) \\ &= e^{\phi_{j+1}^*\phi + \sum_{\mathbf{k}\alpha} e^{\mp i\epsilon_{\mathbf{k}}\delta_t}\bar{\Psi}_{\mathbf{k}\alpha,j+1}\Psi_{\mathbf{k}\alpha}} \left(1 + M \underbrace{(e^{+\bar{\psi}_{j+1}\psi}\bar{\psi}_{j+1}\psi)}_{\bar{\psi}_{j+1}\psi} e^{\mp i\delta_t[\epsilon_0 + \lambda(\phi_{j+1}^* + \phi)]} \right) \\ &= e^{\phi_{j+1}^*\phi + \sum_{\mathbf{k}\alpha} e^{\mp i\epsilon_{\mathbf{k}}\delta_t}\bar{\Psi}_{\mathbf{k}\alpha,j+1}\Psi_{\mathbf{k}\alpha}} \left(1 + M \underbrace{\frac{1}{2}(e^{+\bar{\psi}_{j+1}\psi} - e^{-\bar{\psi}_{j+1}\psi})}_{\bar{\psi}_{j+1}\psi} e^{\mp i\delta_t[\epsilon_0 + \lambda(\phi_{j+1}^* + \phi)]} \right) \\ &= e^{\phi_{j+1}^*\phi + \sum_{\mathbf{k}\alpha} e^{\mp i\epsilon_{\mathbf{k}}\delta_t}\bar{\Psi}_{\mathbf{k}\alpha,j+1}\Psi_{\mathbf{k}\alpha}} \sum_{S_{j+1}=0,\pm 1} A_{S_{j+1}} e^{S_{j+1}\bar{\psi}_{j+1}\psi \mp i\delta_t[\epsilon_0 + \lambda(\phi_{j+1}^* + \phi)] \cdot |S_{j+1}|}. \quad (6.39) \end{aligned}$$

Now Eq. (6.39) immediately yields the exact matrix element for the $\hat{\mathcal{H}}_0$ propagation in Eq. (6.34) with three auxiliary field values

$$A_{S_{j+1}} = (S_{j+1} \cdot M/2)^{|S_{j+1}|} \equiv \begin{cases} A_0 = +1 \\ A_{\pm 1} = \pm M/2. \end{cases} \quad (6.40)$$

Note the appearance of the S_{j+1} factor in the $\bar{\psi}_{j+1}\psi$ term from Eq. (6.39) – the propagation (and boson interaction) only happens when the dot is occupied. The dot fermion (even after integrating out the leads) and the boson are then effectively noninteracting, and we may integrate out all boson/fermion fields to get a path integral over the S_{j+1} fields. Before doing so, let us integrate over the intermediate fields $\phi, \psi, \Psi_{\mathbf{k}\alpha}$ in Eq. (6.34). Inserting Eq. (6.35) and Eq. (6.39) into (6.34), let us first collect the terms depending on $\bar{\Psi}_{\mathbf{k}\alpha}$ and $\Psi_{\mathbf{k}\alpha}$ (different $\mathbf{k}\alpha$ decouple, so it is enough to consider just one choice for the

moment – this is named Ψ during the integration steps and the index is restored in the end). Expanding the exponentials needs to be done for each one individually and due to the Grassmann algebra truncating at first order, we get

$$\begin{aligned}
& \int d\bar{\Psi}d\Psi(1 - \bar{\Psi}\Psi)(1 + e^{\mp i\epsilon_{\mathbf{k}}\delta_t}\bar{\Psi}_{j+1}\Psi) \left(1 + \bar{\Psi} \left(\Psi_j \pm i t_{\alpha}\delta_t \left[1 - \eta\frac{\alpha}{2}\frac{\delta_{j,m}}{\delta_t} \right] \psi_j \right) \right) \\
&= \int d\bar{\Psi}d\Psi \left(-\bar{\Psi}\Psi + e^{\mp i\epsilon_{\mathbf{k}}\delta_t}\bar{\Psi}_{j+1}\Psi\bar{\Psi} \left(\Psi_j \pm i t_{\alpha}\delta_t \left[1 - \eta\frac{\alpha}{2}\frac{\delta_{j,m}}{\delta_t} \right] \psi_j \right) \right) \\
&= 1 + e^{\mp i\epsilon_{\mathbf{k}}\delta_t}\bar{\Psi}_{j+1} \left(\Psi_j \pm i\delta_t t_{\alpha} \left[1 - \eta\frac{\alpha}{2}\frac{\delta_{j,m}}{\delta_t} \right] \psi_j \right) \\
&= \exp \left\{ e^{\mp i\epsilon_{\mathbf{k}}\delta_t}\bar{\Psi}_{\mathbf{k}\alpha,j+1} \left(\Psi_{\mathbf{k}\alpha,j} \pm i t_{\alpha}\delta_t \left[1 - \eta\frac{\alpha}{2}\frac{\delta_{j,m}}{\delta_t} \right] \psi_j \right) \right\}. \tag{6.41}
\end{aligned}$$

The integrations are done using the rules from Eq. (6.12) and carefully respecting the anticommutation relation from Eq. (6.10). Likewise, we carry out the intermediate ψ and $\bar{\psi}$ integrals, which produce the contribution to $U_{j+1,j}$

$$\begin{aligned}
& \int d\bar{\psi}d\psi (1 - \bar{\psi}\psi)(1 + S_{j+1}\bar{\psi}_{j+1}\psi) \left(1 + \bar{\psi} \left(\psi_j \pm i\delta_t \sum_{\mathbf{k}\alpha} t_{\alpha} \left[1 + \eta\frac{\alpha}{2}\frac{\delta_{j,m}}{\delta_t} \right] \Psi_{\mathbf{k}\alpha,j} \right) \right) \\
&= \int d\bar{\psi}d\psi \left(-\bar{\psi}\psi + S_{j+1}\bar{\psi}_{j+1}\psi\bar{\psi} \left(\psi_j \pm i\delta_t \sum_{\mathbf{k}\alpha} t_{\alpha} \left[1 + \eta\frac{\alpha}{2}\frac{\delta_{j,m}}{\delta_t} \right] \Psi_{\mathbf{k}\alpha,j} \right) \right) \\
&= \exp \left\{ S_{j+1}\bar{\psi}_{j+1} \left(\psi_j \pm i\delta_t \sum_{\mathbf{k}\alpha} t_{\alpha} \left[1 + \eta\frac{\alpha}{2}\frac{\delta_{j,m}}{\delta_t} \right] \Psi_{\mathbf{k}\alpha,j} \right) \right\}. \tag{6.42}
\end{aligned}$$

Finally, the boson integration over $\phi = u + iv$ is a complex Gaussian integral

$$\begin{aligned}
& \int \frac{du dv}{\pi} \exp \left\{ -u^2 - v^2 + (\phi_{j+1}^* \mp i\lambda\delta_t|S_{j+1}|)(u + iv) + e^{\mp i\omega_0\delta_t}(u - iv)\phi_j \right\} \\
&= \frac{1}{\pi} \left[\int du e^{-u^2 + (\phi_{j+1}^* \mp i\delta_t\lambda|S_{j+1}| + e^{\mp i\omega_0\delta_t}\phi_j)u} \right] \left[\int dv e^{-v^2 + i(\phi_{j+1}^* \mp i\delta_t\lambda|S_{j+1}| - e^{\mp i\omega_0\delta_t}\phi_j)v} \right] \\
&= \exp \left\{ \frac{1}{4} (\phi_{j+1}^* \mp i\delta_t\lambda|S_{j+1}| + e^{\mp i\omega_0\delta_t}\phi_j)^2 - \frac{1}{4} (\phi_{j+1}^* \mp i\delta_t\lambda|S_{j+1}| - e^{\mp i\omega_0\delta_t}\phi_j)^2 \right\} \\
&= \exp \left\{ e^{\mp i\omega_0\delta_t}(\phi_{j+1}^* \mp i\lambda\delta_t|S_{j+1}|)\phi_j \right\}. \tag{6.43}
\end{aligned}$$

One observes here the ‘backaction’ of the dot on the oscillator. For consistency with $\mathcal{O}(\delta_t^2) = 0$ we set $\delta_t e^{\mp i\epsilon_{\mathbf{k}}\delta_t} = \delta_t \mp i\epsilon_{\mathbf{k}}\delta_t^2 + \dots \rightarrow \delta_t$ in the tunneling contribution. The same argumentation holds for the $e^{\mp i\omega_0\delta_t}$ term in the formula below. Collecting all terms, we arrive at the short-time propagator [see Eq. 6.34]

$$\begin{aligned}
U_{j+1,j} &= \sum_{S_{j+1}=0,\pm 1} A_{S_{j+1}} e^{\mp i\delta_t|S_{j+1}|[\epsilon_0 + \lambda(\phi_{j+1}^* + e^{\mp i\omega_0\delta_t}\phi_j)]} e^{\mp i\omega_0\delta_t\phi_{j+1}\phi_j} \\
&\quad \times e^{S_{j+1}\bar{\psi}_{j+1}\psi_j} e^{\sum_{\mathbf{k}\alpha} e^{\mp i\epsilon_{\mathbf{k}}\delta_t}\bar{\Psi}_{\mathbf{k}\alpha,j+1}\Psi_{\mathbf{k}\alpha,j}} \\
&\quad \times e^{\pm i\delta_t \sum_{\mathbf{k}\alpha} t_{\alpha} \left(\left[1 - \eta\frac{\alpha}{2}\frac{\delta_{j,m}}{\delta_t} \right] e^{\mp i\epsilon_{\mathbf{k}}\delta_t}\bar{\Psi}_{\mathbf{k}\alpha,j+1}\psi_j + S_{j+1} \left[1 + \eta\frac{\alpha}{2}\frac{\delta_{j,m}}{\delta_t} \right] \bar{\psi}_{j+1}\Psi_{\mathbf{k}\alpha,j} \right)}, \tag{6.44}
\end{aligned}$$

which now is quadratic in all of the original fields and in the next section we will introduce a compact matrix vector notation which allows us to integrate out all quadratic fields at once in a clear way and will only leave the summation over the auxiliary fields unsolved.

6.4 Gaussian integration and matrix notation

All boson and fermion integrations within $\mathcal{Z}[\eta]$ are reduced to $2N$ -dimensional Gaussian integrals, i.e., can be carried out analytically. Their solution will be given by the general formula from [34], after rewriting $\mathcal{Z}[\eta]$ in an appropriate form

$$\int \mathcal{D}[\xi^\dagger, \xi] e^{-\xi^\dagger G^{-1} \xi + \eta^\dagger \xi + \xi^\dagger \eta'} = (\det G)^\zeta e^{\eta^\dagger G \eta'} \quad ; \quad \zeta = \begin{cases} +1 & \text{bosons} \\ -1 & \text{fermions} \end{cases} . \quad (6.45)$$

The usage of η' instead of η is crucial and reflects the fact that for the complex bosonic integration the fields η and η' may be chosen independent of each other. The adjunction symbol \dagger is well defined and refers to Grassmann conjugation in the case of fermions. For the correct path-integral “measures” see Eqs. (6.24) and (6.25). The matrix G in Eq. (6.45) has in our case dimension $2N \times 2N$ and will correspond to discrete matrix representations of the inverse Green’s function (GF) of the “free” subsystems involved¹⁴. They are defined below, following the conventions from [40] and involving periodic boundary conditions (indices are defined modulo $2N$):

$$(\mathfrak{i}G)_{i,j}^{-1} = \delta_{i,j} - \delta_{i-1,j}(U)_{j+1,j} \quad ; \quad i, j \in \{1, \dots, 2N\} \quad ; \quad 0 \equiv 2N . \quad (6.46)$$

The contour dependent time direction is encoded by introducing the branch-operator σ

$$\sigma_i = \begin{cases} +1 & ; \quad i \in \{2, \dots, N\} \\ 0 & ; \quad i \in \{1, N+1\} \\ -1 & ; \quad i \in \{N+2, \dots, 2N\} \end{cases} . \quad (6.47)$$

For one mode with wave-vector \mathbf{k} in lead α we get the associated fermionic inverse GF $(\mathfrak{i}G_{\mathbf{k}\alpha})^{-1}$ by defining

$$(U_{\mathbf{k}\alpha})_{j+1,j} = \begin{cases} \rho_{\mathbf{k}\alpha} = +e^{-\beta(\epsilon_{\mathbf{k}} - \alpha V/2)} & ; \quad j = N \\ e^{-\mathfrak{i}\sigma_{j+1}\delta_t \epsilon_{\mathbf{k}}} & ; \quad j \in \{1, 2N-1\} \end{cases} . \quad (6.48)$$

For the bosonic phonon the difference in statistics enters by the leading sign of ρ_b and we get the inverse phonon GF $(\mathfrak{i}G_b)^{-1}$ using the definitions

$$(U_b)_{j+1,j} = \begin{cases} \rho_b = -e^{-\beta\omega_0} & ; \quad j = N \\ e^{-\mathfrak{i}\sigma_{j+1}\delta_t \omega_0} & ; \quad j \in \{1, 2N-1\} \end{cases} . \quad (6.49)$$

Due to the introduction of the auxiliary spin fields S_j and the effective decoupling of the dot degrees from the phonon degrees there is no inverse GF of the free dot left. Instead we get an object with a similar structure but dependent on these auxiliary fields which we will call $(\mathfrak{i}G_S[\vec{S}])^{-1}$. It is defined from

$$(U_S)_{j+1,j} = \begin{cases} \rho_d = +e^{-\beta\epsilon_0} & ; \quad j = N \\ S_{j+1} & ; \quad j \in \{1, 2N-1\} \end{cases} . \quad (6.50)$$

¹⁴Except for the dot part where an object with similar structure is defined. The “short-time propagators” involved are the spins themselves and they also become zero.

Since we also have to respect the Keldysh boundary conditions, $S_{N+1} = S_1 = 0$ is set, and inserting Eq. (6.44) in Eq. (6.26) introduces a summation over all $S_{j+1} \in \mathbb{S}_{j+1}$. Thus we define the $2N$ -dimensional configuration ‘‘vector’’ (tupel) \vec{S} , respecting the Keldysh boundary conditions. We define it from the Cartesian product of the spin sets at each discrete time

$$\vec{S} = (S_1, \dots, S_{2N}) \in \mathbb{S}^{2N} := \prod_{i=1}^{2N} \mathbb{S}_i \quad ; \quad \mathbb{S}_i := \begin{cases} \{0, \pm 1\} & ; \quad i \notin \{1, N+1\} \\ \{0\} & ; \quad i \in \{1, N+1\} \end{cases} . \quad (6.51)$$

With these definitions and $2N$ dimensional vectors ϕ containing the fields ϕ_j , and likewise for the fermionic fields we get the generating function in a more compact form

$$\begin{aligned} \mathcal{Z}[\eta] &= \sum_{\vec{S} \in \mathbb{S}^{2N}} \prod_{j=1}^{2N} \{A_{S_{j+1}} e^{[-i\delta_t \epsilon_0 \sigma_{j+1} |S_{j+1}|]}\} \\ &\times \int \mathcal{D}[\phi^*, \phi] e^{-\phi^{*,T} (\mathfrak{i}G_b)^{-1} \phi - i\delta_t \lambda \sum_j \sigma_{j+1} |S_{j+1}| (\phi_{j+1}^* + \phi_j)} \int \mathcal{D}[\bar{\psi}, \psi] e^{-\bar{\psi}^T (\mathfrak{i}G_S[\vec{S}])^{-1} \psi} \\ &\times \int \mathcal{D}[\bar{\Psi}, \Psi] e^{\sum_{\mathbf{k}\alpha} -\bar{\Psi}_{\mathbf{k}\alpha}^T (\mathfrak{i}G_{\mathbf{k}\alpha})^{-1} \Psi_{\mathbf{k}\alpha} + i\delta_t t_\alpha \sum_j \sigma_{j+1} \left(\left[1 - \eta \frac{\alpha}{2} \frac{\delta_{j,m}}{\delta_t} \right] \bar{\Psi}_{\mathbf{k}\alpha, j+1} \psi_j + S_{j+1} \left[1 + \eta \frac{\alpha}{2} \frac{\delta_{j,m}}{\delta_t} \right] \bar{\psi}_{j+1} \Psi_{\mathbf{k}\alpha, j} \right)} . \end{aligned} \quad (6.52)$$

Up to now we only rewrote the ‘‘free’’ parts, the next step is to also rewrite the tunneling and source part using the same field vectors. Therefore we represent the branch-operator σ_j and the spins S_j as diagonal operators

$$(\sigma)_{i,j} = \sigma_i \delta_{i,j} \quad ; \quad (S)_{i,j} = S_i \delta_{i,j} . \quad (6.53)$$

Furthermore we need the measurement time projector Δ^m and the shift operator R

$$(\Delta^m)_{i,j} = \frac{\delta_{i,m}}{\delta_t} \delta_{i,j} \quad ; \quad (R)_{i,j} = \delta_{i,j+1} . \quad (6.54)$$

Now we can perform the Gaussian integrations by the application of Eq. (6.45). Again ignoring \vec{S} -independent constant prefactors and exploiting the fact that $|S_j| = S_j^2$ holds, the boson field integration produces the factor

$$\begin{aligned} &\int \mathcal{D}[\phi^*, \phi] e^{-\phi^{*,T} (\mathfrak{i}G_b)^{-1} \phi - i\delta_t \lambda \sum_j \sigma_{j+1} |S_{j+1}| (\phi_{j+1}^* + \phi_j)} \\ &= \int \mathcal{D}[\phi^*, \phi] e^{-\phi^{*,T} (\mathfrak{i}G_b)^{-1} \phi + (-i\delta_t \lambda \vec{\mathbb{1}}^T S^2 \sigma R) \phi + \phi^{*,T} (-i\delta_t \lambda S^2 \sigma R \vec{\mathbb{1}})} \\ &= \exp \left\{ -\lambda^2 \delta_t^2 \vec{\mathbb{1}}^T S^2 \sigma R (\mathfrak{i}G_b) S^2 \sigma R \vec{\mathbb{1}} \right\} \det(\mathfrak{i}G_b) = \exp \left\{ \vec{\mathbb{1}}^T S^2 \underbrace{(-\lambda^2 \delta_t^2) \sigma R (\mathfrak{i}G_b) \sigma S^2 \vec{\mathbb{1}}}_{\Lambda_{j,j'} = \sigma_j (\mathfrak{i}G_b)_{j-1,j'} \sigma_{j'}} \right\} , \end{aligned} \quad (6.55)$$

introducing the $2N \times 2N$ matrix $\Lambda_{j,j'} = \sigma_j (\mathfrak{i}G_b)_{j-1,j'} \sigma_{j'}$ and the $2N$ -vector $\vec{\mathbb{1}} = (\dots, 1, 1, \dots)^T$. The last identity in Eq. (6.55) follows from the fact that both σ and R are diagonal. Note that $\Lambda_{j+1,j'} \propto e^{\pm i\omega_0(t_j - t_{j'})}$ is highly oscillatory, especially with increasing correlation time. We can rewrite the first factor of Eq. (6.52) together with the result Eq. (6.55) from the phonon integration defining the diagonal matrix B

$$\begin{aligned}
 & \prod_{i=1}^{2N} \{ A_{S_{i+1}} e^{-i\delta_t \epsilon_0 \sigma_{i+1} |S_{i+1}|} \} e^{\sum_{j,j'=1}^{2N} |S_j| \Lambda_{jj'} |S_{j'}|} \\
 & = \prod_{i=1}^{2N} \underbrace{\left(\frac{S_i}{2} e^{-i\delta_t \epsilon_0 \sigma_i} \right)^{|S_i|}}_{(B_0[\vec{S}])_{i,i}} \underbrace{\left(M e^{\sum_{j=1}^{2N} \Lambda_{ij} |S_j|} \right)^{|S_i|}}_{(B_\lambda[\vec{S}])_{i,i}} = \det(B_0[\vec{S}]) \det(B_\lambda[\vec{S}]) =: \det(B[\vec{S}]) .
 \end{aligned} \tag{6.56}$$

We end up with Eq. (6.52) in a compact form only dependent on fermionic fields:

$$\begin{aligned}
 \mathcal{Z}[\eta] = & \sum_{\vec{S} \in \mathbb{S}^{2N}} \det(B[\vec{S}]) \int \mathcal{D}[\bar{\psi}, \psi] e^{-\bar{\psi}^T (iG_S[\vec{S}])^{-1} \psi} \int \mathcal{D}[\bar{\Psi}, \Psi] \exp \left\{ - \sum_{\mathbf{k}\alpha} \bar{\Psi}_{\mathbf{k}\alpha}^T (iG_{\mathbf{k}\alpha})^{-1} \Psi_{\mathbf{k}\alpha} \right. \\
 & \left. + \{ (-i\delta_t t_\alpha) (\bar{\Psi}_{\mathbf{k}\alpha}^T \sigma R [\mathbb{1} - \frac{\eta\alpha}{2} \Delta^m] \psi) \} + \{ (-i\delta_t t_\alpha) (\bar{\psi}^T S \sigma R [\mathbb{1} + \frac{\eta\alpha}{2} \Delta^m] \Psi_{\mathbf{k}\alpha}) \} \right\} .
 \end{aligned}$$

All integrations left, are integrations over Grassmann-field-vectors, and the complete action is quadratic in these fields. Therefore we can introduce combined field-vectors for the lead and dot degree of freedoms

$$\bar{\zeta} = (\bar{\psi}, \dots, \bar{\Psi}_{\mathbf{k}\alpha}, \dots) \quad ; \quad \zeta = (\psi, \dots, \Psi_{\mathbf{k}\alpha}, \dots)^T . \tag{6.57}$$

With respect to these fields the total action $S[\bar{\zeta}, \zeta] = i\bar{\zeta} \Phi \zeta$ is quadratic and defined from

$$\Phi[\vec{S}] = \left(\begin{array}{c|ccc} (iG_S[\vec{S}])^{-1} & & \dots & -i\delta_t t_\alpha S \sigma R [\mathbb{1} + \frac{\eta\alpha}{2} \Delta^m] & \dots \\ \vdots & & & & \\ -i\delta_t t_\alpha \sigma R [\mathbb{1} - \frac{\eta\alpha}{2} \Delta^m] & & \ddots & (iG_{\mathbf{k}\alpha})^{-1} & \\ \vdots & & & & \ddots \end{array} \right) . \tag{6.58}$$

We are left with a single Gaussian integration, leading to an almost final analytical result

$$\mathcal{Z}[\eta] = \sum_{\vec{S} \in \mathbb{S}^{2N}} \det B[\vec{S}] \int \mathcal{D}[\bar{\zeta}, \zeta] e^{iS[\bar{\zeta}, \zeta]} = \sum_{\vec{S} \in \mathbb{S}^{2N}} \det B[\vec{S}] \cdot \det(\Phi[\vec{S}]) . \tag{6.59}$$

A Schur decomposition of Φ now separates the contribution from the lead action

$$\det(\Phi) = \det \begin{pmatrix} \Phi_a & \Phi_b \\ \Phi_c & \Phi_d \end{pmatrix} = \det(\Phi_d) \cdot \det(\Phi_a - \Phi_b \cdot \Phi_d^{-1} \cdot \Phi_c) . \tag{6.60}$$

The advantage of this transformation is that η -independent scalar factors and terms in $\mathcal{O}(\eta^2)$ can be omitted in $\mathcal{Z}[\eta]$ since they drop out during the functional derivative in (6.7). Thus we divide by $\det(\Phi_d)$ and reduce the dimensionality of our problem

$$\mathcal{Z}[\eta] = \sum_{\vec{S} \in \mathbb{S}^{2N}} \det B[\vec{S}] \frac{\det(\Phi[\vec{S}])}{\det \Phi_d} := \sum_{\vec{S} \in \mathbb{S}^{2N}} \det B[\vec{S}] (i\mathcal{G}[\vec{S}])^{-1} . \tag{6.61}$$

The reduction corresponds to the encoding of the leads influence on the dot within its own Hilbert space in form of an self-energy. Note that a similar transformation holds in the $\lambda = 0$ case and directly corresponds to the exact solvable Dyson equation [34] of that problem. For the exact mapping, see Eqs. (8.4) and (8.5) presented later

$$\begin{aligned} (\mathbf{i}G[\vec{S}])^{-1} &= \det \left\{ (\mathbf{i}G_S[\vec{S}])^{-1} + \sum_{\alpha} \delta_t^2 \left(S \sigma R \left[\mathbb{1} + \frac{\eta_{\alpha}}{2} \Delta^m \right] X_{\alpha} \sigma R \left[\mathbb{1} - \frac{\eta_{\alpha}}{2} \Delta^m \right] \right) \right\} \\ &= \det \left\{ (\mathbf{i}G_S[\vec{S}])^{-1} + \delta_t^2 S \sigma R \left[X^{(+)} \sigma R + \frac{\eta}{2} \left(\Delta^m X^{(-)} \sigma R - X^{(-)} \sigma R \Delta^m \right) \right] \right\}. \end{aligned}$$

Note that there is still a summation over all momenta hidden in the definition of $X^{(\pm)}$

$$X^{(\pm)} = \sum_{\alpha} \alpha^{\frac{1\pm 1}{2}} X_{\alpha} \quad ; \quad X_{\alpha} = \sum_{\mathbf{k}} t_{\alpha}^2 \mathbf{i}G_{\mathbf{k}\alpha}. \quad (6.62)$$

In chapter 7 we will show how to get convergent expressions for this infinite summation and therefore we treat $X^{(\pm)}$ as a well known object from now on. The influence of the leads to the dot still enters after this separation as a self-energy contribution $\Sigma[\vec{S}, \eta] = \Sigma^{(+)}[\vec{S}] + \eta \Sigma^{(-)}[\vec{S}]$ in the dot space

$$\Sigma^{(+)}[\vec{S}] := -\mathbf{i} \delta_t^2 S \sigma R X^{(+)} \sigma R =: S \Sigma_0^{(+)} \quad (6.63)$$

$$\Sigma^{(-)}[\vec{S}] := -\mathbf{i} \delta_t^2 S \sigma R \frac{1}{2} \left(\Delta^m X^{(-)} \sigma R - X^{(-)} \sigma R \Delta^m \right) =: S \Sigma_0^{(-)}. \quad (6.64)$$

Note, that $\Sigma_0^{(+)}$ is the lead induced self-energy of the remaining resonant level model, when the phonon is decoupled. We will explicitly establish this connection in chapter 8. We also define the spin-independent self-energy $\Sigma_0[\eta] = \Sigma_0^{(+)} + \eta \Sigma_0^{(-)}$ including the source term and split $(\mathbf{i}G_S)^{-1}$ in a constant and a \vec{S} -dependent part

$$(\mathbf{i}G_S[\vec{S}])^{-1} = \underbrace{\begin{pmatrix} 1 & & & & e^{-\beta\epsilon_0} \\ & \ddots & & & \\ & & 1 & & \\ \hline & & -1 & 1 & \\ & & & & \ddots \\ & & & & & 1 \end{pmatrix}}_{(\mathbf{i}G_S)_{stat}^{-1}} - \underbrace{\begin{pmatrix} 0 & & & & & \\ S_2 & \ddots & & & & \\ & \ddots & \ddots & & & \\ \hline & & & \ddots & & \\ & & & & \ddots & \\ & & & & & \ddots \\ & & & & & & S_{2N} & 0 \end{pmatrix}}_{(\mathbf{i}G_S)_{dyn}^{-1}[\vec{S}] = S R}. \quad (6.65)$$

This structure will simplify the numerical implementation and emphasizes the row-wise spin dependence within Eq. (6.66).

The final result for our AH model is a finite spin summation over determinants of row-wise spin-dependent matrices which has the appropriate form for solving it with the ISPI algorithm from [64]

$$\begin{aligned}
 \mathcal{Z}[\eta] &= \sum_{\vec{S} \in \mathbb{S}^{2N}} \det B[\vec{S}] \det \left\{ (\mathfrak{i}G_S[\vec{S}])^{-1} + \mathfrak{i} \left(\Sigma^{(+)}[\vec{S}] + \eta \Sigma^{(-)}[\vec{S}] \right) \right\} \\
 &= \sum_{\vec{S} \in \mathbb{S}^{2N}} \det B[\vec{S}] \det \left\{ (\mathfrak{i}G_S)_{stat}^{-1} - S[\vec{S}] (R - \mathfrak{i}\Sigma_0[\eta]) \right\} \\
 &:= \sum_{\vec{S} \in \mathbb{S}^{2N}} \det \left\{ B[\vec{S}] (\mathfrak{i}\mathcal{G}[\vec{S}])^{-1} \right\} . \tag{6.66}
 \end{aligned}$$

Before we develop the algorithm to solve Eq. (6.66) in chapter 9 we will first perform the momentum summation hidden in the definition of X_α and also establish the exact connection to the resonant level model which remains from the AH model if the phonon is detached ($\lambda = 0$).

7 Fourier transformation of the free lead GF

In this section we present different ways how to treat the momentum summation involved in the definition of X_α , cf. Eq. (6.62). The main contribution to the lead self-energy comes from X_α and its definition includes a Fourier transformation of a Fermi-function from energy to time space with respect to integer multiples of a “minimal” correlation time δ_t . Since these integer multiples also involve a zero correlation time, we will get convergence problems at this equal time correlator, depending on how we model the leads density of states. In the following we present all details and also show how to circumvent the convergence problems by the introduction of a cut-off.

7.1 General expression in continuum limit

In order to calculate the correlation matrix X_α defined in Eq. (6.62), we need the free Green’s function $G_{\mathbf{k}\alpha}$ for lead α at fixed momentum \mathbf{k} . It is defined by its inverse from Eq. (6.48). For the example $N = 3$, we get the following matrix structure:

$$G_{\mathbf{k}\alpha} = \frac{i}{1 + \rho_{\mathbf{k}\alpha}} \begin{pmatrix} -1 & \rho_{\mathbf{k}\alpha} e^{+i\epsilon_k \delta_t} & \rho_{\mathbf{k}\alpha} e^{+2i\epsilon_k \delta_t} & \rho_{\mathbf{k}\alpha} e^{+2i\epsilon_k \delta_t} & \rho_{\mathbf{k}\alpha} e^{+i\epsilon_k \delta_t} & \rho_{\mathbf{k}\alpha} \\ -e^{-i\epsilon_k \delta_t} & -1 & \rho_{\mathbf{k}\alpha} e^{+i\epsilon_k \delta_t} & \rho_{\mathbf{k}\alpha} e^{+i\epsilon_k \delta_t} & \rho_{\mathbf{k}\alpha} & \rho_{\mathbf{k}\alpha} e^{-i\epsilon_k \delta_t} \\ -e^{-2i\epsilon_k \delta_t} & -e^{-i\epsilon_k \delta_t} & -1 & \rho_{\mathbf{k}\alpha} & \rho_{\mathbf{k}\alpha} e^{-i\epsilon_k \delta_t} & \rho_{\mathbf{k}\alpha} e^{-2i\epsilon_k \delta_t} \\ \hline -e^{-2i\epsilon_k \delta_t} & -e^{-i\epsilon_k \delta_t} & -1 & -1 & \rho_{\mathbf{k}\alpha} e^{-i\epsilon_k \delta_t} & \rho_{\mathbf{k}\alpha} e^{-2i\epsilon_k \delta_t} \\ -e^{-i\epsilon_k \delta_t} & -1 & -e^{+i\epsilon_k \delta_t} & -e^{+i\epsilon_k \delta_t} & -1 & \rho_{\mathbf{k}\alpha} e^{-i\epsilon_k \delta_t} \\ -1 & -e^{+i\epsilon_k \delta_t} & -e^{+2i\epsilon_k \delta_t} & -e^{+2i\epsilon_k \delta_t} & -e^{+i\epsilon_k \delta_t} & -1 \end{pmatrix}.$$

To perform the momentum summation, we first rewrite $G_{\mathbf{k}\alpha}$ using an index notation. We will introduce separate indices for real-times and for the Keldysh branch. Real-time indices i, j are running from 1 to N and Keldysh indices σ, σ' over \pm (See also Fig. 6.1). Within the discretized real-time we introduce a correlation-time-operator $\Delta T_{i,j} = \delta_t(i-j)$. Fermi-functions are recovered from the equilibrium distributions $\rho_{\mathbf{k}\alpha}$ by the relations

$$\frac{\rho_{\mathbf{k}\alpha}}{1 + \rho_{\mathbf{k}\alpha}} = n_F(\epsilon_{\mathbf{k}\alpha}) \quad ; \quad \frac{1}{1 + \rho_{\mathbf{k}\alpha}} = n_F(-\epsilon_{\mathbf{k}\alpha}) \quad ; \quad \epsilon_{\mathbf{k}\alpha} = \epsilon_{\mathbf{k}} - \mu_\alpha. \quad (7.1)$$

The Keldysh contour ordering can be compactly encoded in a time space operator $C_{i,j}$ with 2×2 Keldysh substructure

$$C_{i,j} = \theta(i-j) \begin{pmatrix} +1 & -1 \\ +1 & -1 \end{pmatrix} + \theta(j-i) \begin{pmatrix} -1 & -1 \\ +1 & +1 \end{pmatrix} + \delta_{i,j} \begin{pmatrix} +1 & -1 \\ +1 & +1 \end{pmatrix} \quad ; \quad \theta(0) = 0. \quad (7.2)$$

Based on the definitions above X_α takes a compact form, valid for arbitrary N

$$(X_\alpha)_{i,j}^{\sigma,\sigma'} = \sum_{\mathbf{k}} t_\alpha^2 C_{i,j}^{\sigma,\sigma'} n_F[-C_{i,j}^{\sigma,\sigma'}(\epsilon_{\mathbf{k}} - \mu_\alpha)] e^{-i\epsilon_{\mathbf{k}} \Delta T_{i,j}}. \quad (7.3)$$

To perform the momentum summation in the leads we first take the continuum limit

$$(X_\alpha)_{i,j}^{\sigma,\sigma'} = C_{i,j}^{\sigma,\sigma'} t_\alpha^2 \int_{-\infty}^{+\infty} d\epsilon \nu_\alpha(\epsilon) n_F[-C_{i,j}^{\sigma,\sigma'}(\epsilon - \mu_\alpha)] e^{-i\epsilon\Delta T_{i,j}} \quad (7.4)$$

by introducing the side-dependent density of states $\nu_\alpha(\epsilon)$. The next step is to model the density of states by some function to get a convergent expression. For keeping the notation compact we drop the time and Keldysh indices in the next sections and only focus on the convergence of the integral involved.

7.2 Flat infinite band limit

The simplest band model for the leads is the assumption of an infinite band with a constant density of states, named flat and wide band approximation in the following. In this model one fixes the density of states at its value at the Fermi-energy $\nu_\alpha(\epsilon_F)$ and introduces the hybridization energy Γ_α as universal energy scale

$$\int d\epsilon \nu_\alpha(\epsilon) \approx \frac{2\Gamma_\alpha}{|t_\alpha|^2} \int \frac{d\epsilon}{2\pi} \quad ; \quad \Gamma_\alpha = \pi\nu_\alpha(\epsilon_F)|t_\alpha|^2. \quad (7.5)$$

The justification of this approximation is based on the idea that all relevant processes only involve states around the Fermi-energy and that the continuum of states in the leads around the Fermi-energy is assumed to be locally homogeneous. Under these assumptions, the integral (7.4) is transformed to

$$X_\alpha = \Gamma_\alpha C \int_{-\infty}^{+\infty} \frac{d\epsilon}{\pi} \frac{e^{-i\epsilon\Delta T}}{e^{-\beta C(\epsilon - \mu_\alpha)} + 1} \quad ; \quad |C| = 1 \quad ; \quad \Delta T = \delta_t \mathbb{Z}. \quad (7.6)$$

Exploiting the fact that $|C| = 1$ holds, substituting $z := \beta(\epsilon - \mu_\alpha)C$ and after defining

$$\xi = \frac{\Gamma_\alpha C}{\pi\beta} e^{-i\mu_\alpha\Delta T} \quad ; \quad \vartheta = \frac{C\Delta T}{\beta} \in \mathbb{R}, \quad (7.7)$$

we have to solve the integral

$$X_\alpha = \Gamma_\alpha \frac{C}{\beta} \int_{-\infty}^{+\infty} dz \frac{e^{-i\Delta T(\frac{C}{\beta}z + \mu_\alpha)}}{e^{-z} + 1} = \xi \lim_{\eta \rightarrow 0^+} \int_{-\infty}^{+\infty} dz \frac{e^{-(\eta + i\vartheta)z}}{e^{-z} + 1}. \quad (7.8)$$

The solution, at least for $\Delta T \neq 0$, is provided by Eq. (3.311.9) from Gradshteyn & Ryzhik [74]:

$$X_\alpha = \lim_{\eta \rightarrow 0^+} \frac{\pi\xi}{\sin(\pi(\eta + \frac{C\Delta T}{\beta}))} = \frac{\Gamma_\alpha e^{-i\mu_\alpha\Delta T}}{i\beta \sinh(\frac{\pi}{\beta}\Delta T)}. \quad (7.9)$$

The case of matching times cannot be treated this way due to the singularity at $\Delta T = 0$. We solve this problem by the introduction of a finite bandwidth in the leads.

7.3 Flat finite band (hard cut-off)

The arising singularity in the flat wide band approximation is directly related to the (unphysical) assumption of an infinite band. By limiting the width of the band one gets an finite value for X_α at all correlation times and circumvents this problem. Nevertheless the exact value at matching times is directly related to the width and the shape of the band taken into account. In our work [75] we use a hard cut-off for limiting the flat band to the energy range $(\epsilon - \mu_\alpha) \in [-D, D]$. The corresponding definition for the density of states is

$$\nu_\alpha(\epsilon) = \nu_\alpha(\epsilon_F)\theta(-(\epsilon - \mu_\alpha - D))\theta(+(\epsilon - \mu_\alpha + D)) \quad ; \quad \theta(0) = 1 . \quad (7.10)$$

Note that D has to be chosen reasonable. It must be always the highest energy in the system and due to the fact that we are in principle dealing with an “free” object, the symmetry of a cut-off function should be aligned with the chemical potential μ_α . Following the notation in Eqs. (7.6) and (7.7) and introducing $\tilde{D} = \beta D$, we have to calculate

$$X_\alpha = \Gamma_\alpha C \int_{\mu_\alpha - D}^{\mu_\alpha + D} \frac{d\epsilon}{\pi} \frac{e^{-i\epsilon\Delta T}}{e^{-\beta C(\epsilon - \mu_\alpha)} + 1} = \xi \int_{-\tilde{D}}^{+\tilde{D}} dz \frac{e^{i\vartheta z}}{e^z + 1} . \quad (7.11)$$

The integral is solved by using the definition of the incomplete beta function

$$\mathfrak{B}[z, a, b] = \int_0^z u^{a-1}(1-u)^{b-1} du \quad (7.12)$$

and the the substitution $e^z = -u$:

$$\begin{aligned} X_\alpha &= -\xi \int_{-e^{-\tilde{D}}}^{-e^{+\tilde{D}}} \frac{e^{(i\vartheta-1)z}}{1-u} du \\ &= \xi(-1)^{i\vartheta} \int_{-e^{-\tilde{D}}}^{-e^{+\tilde{D}}} u^{i\vartheta-1}(1-u)^{-1} du \\ &= \xi(-1)^{i\vartheta} \left(\mathfrak{B}[-e^{+\tilde{D}}, i\vartheta, 0] - \mathfrak{B}[-e^{-\tilde{D}}, i\vartheta, 0] \right) . \end{aligned} \quad (7.13)$$

Applying now the relation $\mathfrak{B}[z, a, b] = \frac{z^a}{a} {}_2\mathfrak{F}_1[a, 1-b, a+1, z]$ between the incomplete beta function and the hypergeometric function ${}_2\mathfrak{F}_1$ together with the Pfaff transformation ${}_2\mathfrak{F}_1[a, b, c, z] = (1-z)^{c-a-b} {}_2\mathfrak{F}_1[c-a, c-b, c, z]$ we get the final expression used in the code:

$$X_\alpha = i \frac{\xi}{\vartheta} \left(e^{-i\tilde{D}\vartheta} {}_2\mathfrak{F}_1 \left[1, i\vartheta, 1 + i\vartheta, -e^{-\tilde{D}} \right] - e^{+i\tilde{D}\vartheta} {}_2\mathfrak{F}_1 \left[1, i\vartheta, 1 + i\vartheta, -e^{+\tilde{D}} \right] \right) . \quad (7.14)$$

In the case of matching times ($\Delta T = 0$), the integral reduces to

$$X_\alpha|_{\Delta T=0} = \frac{\Gamma_\alpha C}{\pi\beta} \int_{-\tilde{D}}^{+\tilde{D}} dz \frac{1}{e^z + 1} = \frac{\Gamma_\alpha C}{\pi\beta} \left[2\tilde{D} - \ln \left(\frac{1 + e^{+\tilde{D}}}{1 + e^{-\tilde{D}}} \right) \right] . \quad (7.15)$$

This is further simplified in the limit $\beta \rightarrow \infty$

$$\lim_{\beta \rightarrow \infty} X_\alpha|_{\Delta T=0} = \frac{2\Gamma_\alpha C D}{\pi} - \frac{\Gamma_\alpha C}{\pi} \underbrace{\lim_{\beta \rightarrow \infty} \frac{1}{\beta} \ln \left[\frac{1 + e^{+\beta D}}{1 + e^{-\beta D}} \right]}_{=D} = C \frac{\Gamma_\alpha}{\pi} D, \quad (7.16)$$

and shows the direct connection of the correlation at matching times with the width of the band taken into account and is consistent with setting $n_F(\epsilon) = \theta(-\epsilon)$ in Eq. (7.6).

7.4 Comparison of flat wide and flat finite band

Since Eq. (7.9) has a singularity at matching times ($\Delta T = 0$), we had to use a more realistic band model and introduced a cut-off. This resulted in the use of Eq. (7.14) for the computation of the matrix elements of X_α . Per construction we only need values of Eq. (7.14) at correlation times which are integer multiples of the fundamental time discretization length δ_t of the path-integral. The self-energy $\Sigma_0^{(+)}$ encodes the influence of the leads, is directly proportional to $X_L + X_R$ and exhibits best the effect of a cut-off.

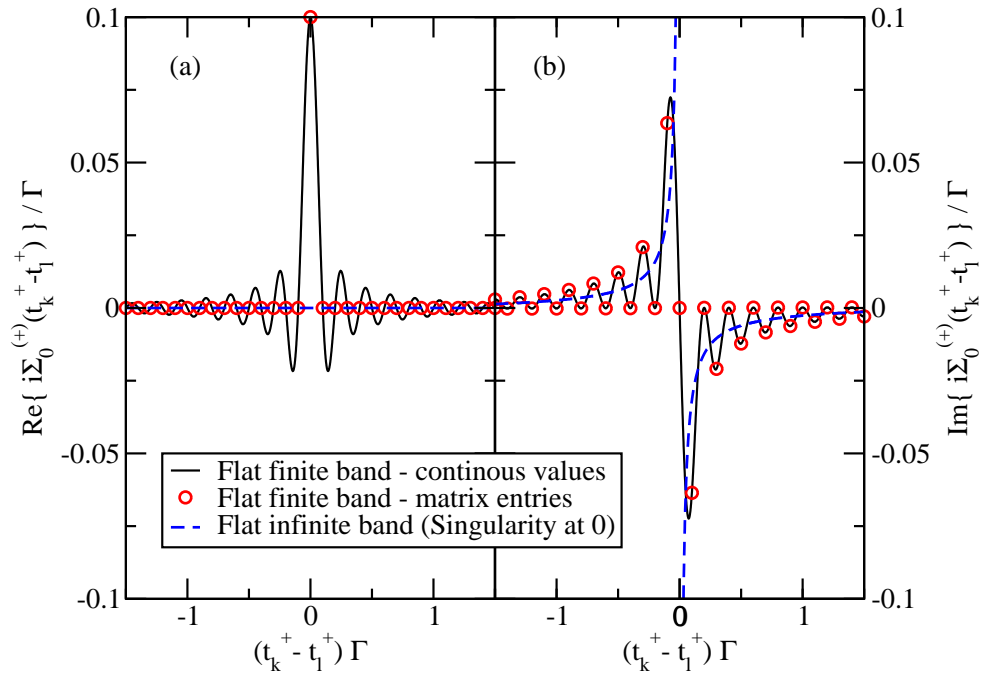


Figure 7.1: (a) Real and (b) imaginary part of $i\Sigma_0^{(+)}(t_i^+ - t_j^+)$. The parameters of this example are $\delta_t \Gamma = 0.1$; $\beta \Gamma = 5$; $eV = \Gamma$; $D = \frac{\pi}{\delta_t}$. The black lines are the continuous solutions from our flat finite band model (cf. Sec. 7.3). The red circles depict the values of the self-energy entering our matrix representation. The blue dashed line corresponds to the flat infinite band model, which is divergent for zero correlation time and not suitable for our numerics. (cf. Sec. 7.2)

Figure 7.1 above illustrates the real and the imaginary part of $i\Sigma_0^{(+)}(t_i^+ - t_j^+)$ as a function of the correlation time $t - t'$. The red points represent the values which enter the self-energy matrix we used in our ISPI code. They are based on Eq. (7.14). Ignoring the discretization and continuously evaluating the same formula leads to the black line. The dashed blue line is also a continuous evaluation, but based on Eq. (7.9). Note that for the real part the cut-off and the non-cut-off version have almost everywhere the same results, while for the imaginary part almost everywhere the non-cut-off result is an average of neighbored values of the cut-off result. We will now use different cut-off values and analyze their effect on the real and imaginary part of $i\Sigma_0^{(+)}(t_i^+ - t_j^+)$ separately to find the optimal cut-off value.

7.4.1 Finding the optimal cut-off

We found that a reduction in error for the extrapolated ISPI-current is achieved by using an optimal cut-off for each time-discretization. Optimal means that the cut-off choice is based on the fundamental relation between the minimal resolved difference in time δ_t and the corresponding maximal frequency ω_{max} taken into account within the leads

$$2\pi/\delta_t = \omega_{max} . \quad (7.17)$$

Setting this maximal frequency equal to the bandwidth $2D$ of the discrete Fourier-transformation used for the self-energy computation, we get the optimal cut-off frequency. Disadvantages of other choices are discussed further below

$$2D = \omega_{max} \Rightarrow D = \pi/\delta_t . \quad (7.18)$$

Effects on the imaginary part of the self-energy

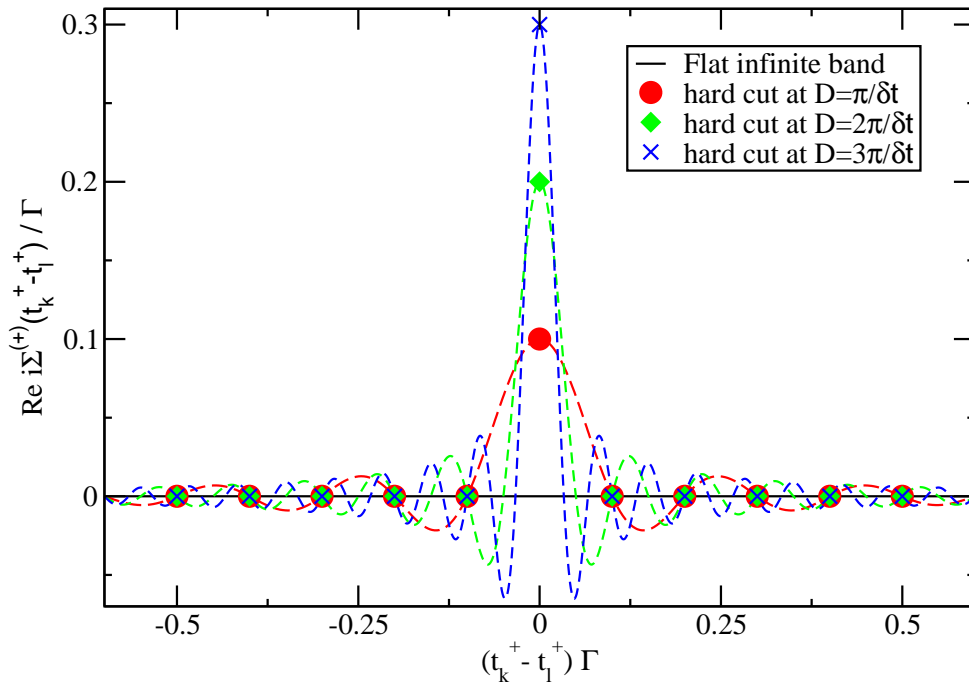


Figure 7.2: Real part of $i\Sigma^{+}(t_i^{+} - t_j^{+})$ for different cut-off frequencies and fixed $\delta_t\Gamma = 0.1$; $\beta\Gamma = 5$; $eV = \Gamma$. The colored points refer to the matrix elements of $i\Sigma^{+}$ while the same colored dashed lines refer to the continuous solution. The black line is the solution for the flat infinite band model. Note that integer multiples of $\frac{\pi}{\delta_t}$ chosen as cut-off frequency only affect the peak height at equal times and generate a singularity for $D \rightarrow \infty$.

Although usually one tries to choose a cut-off frequency as big as possible, this does not make any sense here. For the real part of $i\Sigma^{+}$ an increase of the cut-off frequency only affects the value at zero correlation time and decreases therefore the numerical stability, cf. Fig. 7.2.

Effects on the real part of the self-energy

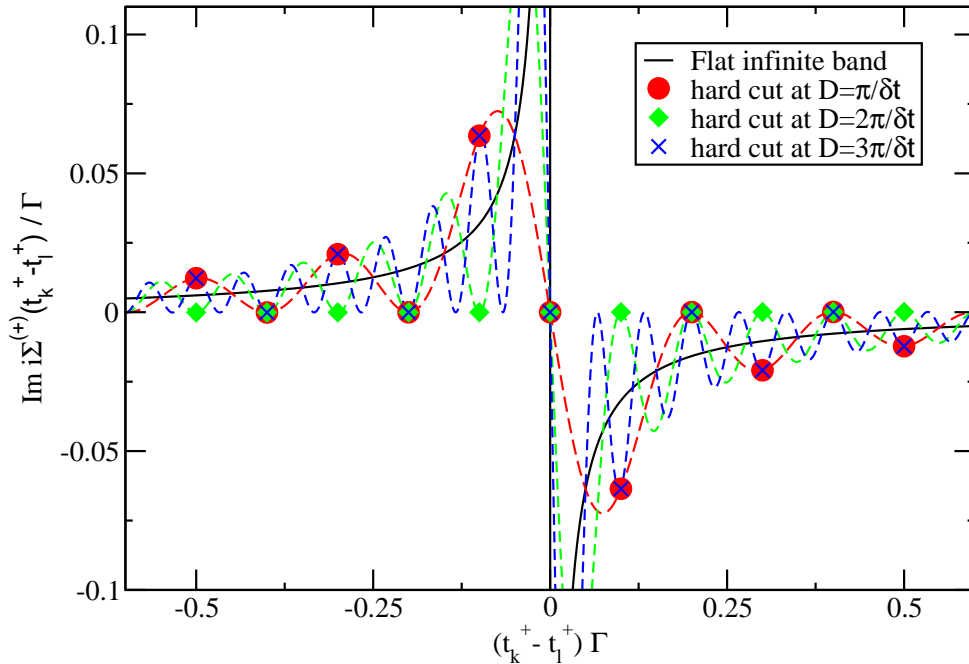


Figure 7.3: Imaginary part of $i\Sigma^{(+)}(t_i^+ - t_j^+)$ for different cut-off frequencies and fixed $\delta_t \Gamma = 0.1$; $\beta \Gamma = 5$; $eV = \Gamma$. The colored points refer to the matrix elements of $i\Sigma^{(+)}$ while the same colored dashed lines refer to the continuous solution. The black line is the solution for the flat infinite band model.

The effect on the imaginary part of $i\Sigma^{(+)}$ is seen in Fig. 7.3. Since only values marked with a symbol will enter the discretized version of $\Sigma^{(+)}$ we have to distinguish two cases. Firstly, odd multiples of $\frac{\pi}{\delta_t}$ just increase the oscillation frequency of the continuous solution without changing the discretized object itself. In this case, only the numerical precision of the discrete values is decreased by an increase of the cut-off. Secondly, even multiples of $\frac{\pi}{\delta_t}$ will set all entries in the imaginary part to zero and the resulting matrix is useless anyway. To conclude, the optimal solution is $D = \frac{\pi}{\delta_t}$. Without any relation between the cut-off and the time-discretization or by using noninteger multiples of π/δ_t we encountered the worst results. A starting point to further investigate the relations between an optimal cut-off and the current could be the Nyquist-Shannon sampling theorem, but this is beyond the scope of this work.

Due to the direct dependence of the cut-off on δ_t , an extrapolation $\delta_t \rightarrow 0$ directly implies an cut-off extrapolation $D \rightarrow \infty$. Therefore an extrapolated result does not have a cut-off in energy space and allows for a numerically exact result after an extrapolation. A similar argumentation also holds for our least dependence method. We assume convergence when the current is approximately stationary over an interval of different δ_t values. This directly implies a stationary current for an increasing cut-off and therefore it does not affect the result and is already big enough.

8 The resonant level model

A first check of the final form from Eq. (6.66) is to investigate its limit for $\lambda \rightarrow 0$ which corresponds to the resonant level (RL) model. There are two different motivations behind:

- (a) We want to recover the inverse GF of the “free” dot $[(G_d)^{-1}]$ from $[(G_S)^{-1}]$. This proofs that both encode the same information and nothing is omitted by our splitting procedure.
- (b) We want to check that our discrete expressions can be mapped to known continuous results for the RL model by performing a continuum limit.

As a byproduct we will get a discrete and the continuous analytic current-voltage relation.

8.1 Discrete solution for the RL model

Without the phonon attached, the Hamiltonian becomes quadratic in the fields and the Keldysh partition function is analytically solvable. This is equivalent to the fact that the corresponding Dyson equation [34], which treats the influence of the leads with respect to a “free” dot as self-energy, is also analytically solvable. Consequently we should be able to recover the inverse GF of the “free” dot from Eq. (6.66) in the limit $\lambda \rightarrow 0$ and get an analytic expression for the Keldysh generating function which is equivalent to known analytic expressions for the system’s symmetrized current. The free inverse GF $(iG_d)^{-1}$ of the dot is defined by inserting

$$(U_d)_{j+1,j} = \begin{cases} \rho_d = +e^{-\beta\epsilon_0} & ; \quad j = N \\ e^{-i\sigma_{j+1}\delta_t\epsilon_0} & ; \quad j \in \{1, 2N-1\} \end{cases} \quad (8.1)$$

for U in Eq. (6.46). Unlike in [64] the connection between $(i\mathcal{G})^{-1}$ and $(iG_d)^{-1}$ in this limit is not obvious. First we need to break down the determinant involved in Eq. (6.66) to a definition on the level of matrix elements. For a $2N \times 2N$ matrix Y its determinant can be defined by the Leibniz formula

$$\det(Y) = \sum_{\mathfrak{s} \in \mathfrak{S}_{2N}} \text{sgn}(\mathfrak{s}) \prod_{i=1}^{2N} (Y)_{i,\mathfrak{s}(i)} \quad (8.2)$$

with the sum running over all permutations \mathfrak{s} from the symmetric group \mathfrak{S}_{2N} of degree $2N$. Therefore the generating function \mathcal{Z} without phonon interaction is

$$\mathcal{Z}[\eta]|_{\lambda=0} = \sum_{\vec{S} \in \mathfrak{S}^{2N}} \det B_0[\vec{S}] \det \left\{ (iG_S)_{stat}^{-1} - S[\vec{S}] (R - i\Sigma_0[\eta]) \right\} \quad (8.3)$$

$$= \sum_{\mathfrak{s} \in \mathfrak{S}_{2N}} \text{sgn}(\mathfrak{s}) \prod_{i=1}^{2N} \sum_{S_i} (B_0)_{ii} [S_i] \left(\underbrace{((iG_S)_{stat}^{-1})_{i,\mathfrak{s}(i)}}_{\equiv F_a} - S_i \underbrace{(R - i\Sigma_0[\eta])_{i,\mathfrak{s}(i)}}_{\equiv F_b} \right). \quad (8.4)$$

Inserting the definition of $B_0[\vec{S}]$ leads to the auxiliary relation

$$\sum_{S_i} (B_0[\vec{S}])_{i,i} \{F_a - S_i F_b\} = \sum_{S_i} \left(\frac{S_i}{2} e^{-i\delta_t \epsilon_0 \sigma_i} \right)^{|S_i|} \{F_a - S_i F_b\} = F_a - \sigma_i^2 e^{-i\delta_t \epsilon_0 \sigma_i} F_b ,$$

with σ_i^2 fixing the Keldysh boundary conditions. Remembering that $\sigma_i^3 = \sigma_i$ holds and terms in $\mathcal{O}(\delta_t^2)$ are treated as zero we arrive at the final result for the RL model

$$\begin{aligned} \mathcal{Z}[\eta]|_{\lambda=0} &= \sum_{\mathfrak{s} \in \mathfrak{G}^{2N}} \text{sgn}(\mathfrak{s}) \prod_{i=1}^{2N} \left((iG_S)_{stat}^{-1} \right)_{i,\mathfrak{s}(i)} - \sigma_i^2 e^{-i\delta_t \epsilon_0 \sigma_i} \left(R - i\Sigma_0[\eta] \right)_{i,\mathfrak{s}(i)} \\ &= \sum_{\mathfrak{s} \in \mathfrak{G}^{2N}} \text{sgn}(\mathfrak{s}) \prod_{i=1}^{2N} \left((iG_d)_{i,\mathfrak{s}(i)}^{-1} + \sigma_i^2 e^{-i\delta_t \epsilon_0 \sigma_i} \underbrace{\left(i\Sigma_0[\eta] \right)_{i,\mathfrak{s}(i)}}_{\propto \sigma_i \delta_t^2} \right) \\ &= \det \{ (iG_d)^{-1} + i\Sigma_0[\eta] \} \equiv \det \{ G_d^{-1} - \Sigma_0[\eta] \} . \end{aligned} \quad (8.5)$$

The last identity in Eq. (8.5) holds since the current is invariant for $\mathcal{Z}[\eta]$ modulo any η -independent constant, cf. Eq. (6.7). The order δ_t^2 is again important here - the relations $\delta_t^2 \epsilon_0 \ll 1/\Gamma$; $\delta_t^2 \epsilon_{\mathbf{k}} \ll 1/\Gamma$ and $\delta_t^2 \omega_0 \ll 1/\Gamma$ have to be fulfilled and will become a restriction to the parameter space accessible with our method. Without a phonon involved, the generating function is directly dependent on the inverse GF G_d^{-1} of the “free” dot and the self-energy $\Sigma_0^{(+)}$ of the leads. We recover the standard result, that both are related by a Dyson equation for the total inverse GF of the RL model

$$G_0^{-1} = G_d^{-1} - \Sigma_0^{(+)} . \quad (8.6)$$

By this we have accomplished task (a) from the beginning of this chapter and for further reference we call the corresponding current $I_{\lambda=0} = \partial_\eta \mathcal{Z}[\eta]|_{\lambda=\eta=0}$, the “direct current”. The terminology refers to the fact that for $\lambda = 0$ Eq. (8.5) provides a direct way for getting numerically a current from the discrete inverse GFs without the need of an iteration. (We also used this expression to check our extrapolation schemes since it allows for arbitrary truncations of correlations, cf. chapter 9, without changing the runtime. Although Eq. (8.5) represents a quite compact expression, it is only exact in the limit ($N \rightarrow \infty$) which we will explore in the next section.

8.2 Continuous solution for the RL model

In the limit ($N \rightarrow \infty$) all fields become continuous functions of contour times and all matrices introduced so far will become operators acting on these fields. After introducing general relations and definitions we get back to the RL model, remaining from the AH model in the limit $\lambda = 0$, and will recover known analytic results¹⁵ including the exact current-voltage relation.

¹⁵They are identical with the relations from [64], except for a factor of two due to the spin.

8.2.1 Continuous time representation of GFs

Within the Keldysh formalism we have doubled all fields in time. Consequently, the general definition of a single particle GF is proportional to the expectation value of a contour ordered¹⁶ product of creation and annihilation operators $\{\xi^\dagger, \xi\}$ referring to different times $\{t_\mu, t'_\nu\}$ on the contour [40]

$$G^{\mu\nu}(t_\mu, t'_\nu) = -i \langle \mathcal{T}_C \{ \xi(t_\mu) \xi^\dagger(t'_\nu) \} \rangle . \quad (8.7)$$

The upper (lower) branch of the contour are labeled by “+” (“−”) which allows for four different combinations of the time arguments $\{t_\mu, t'_\nu\}$ with respect to their branch dependencies $\{\mu, \nu\}$. Encoding this branch dependency in a 2×2 matrix and then projecting the time arguments back on the real-time axis results in

$$G(t, t') = \begin{pmatrix} G^{++}(t, t') & G^{+-}(t, t') \\ G^{-+}(t, t') & G^{--}(t, t') \end{pmatrix} = \begin{pmatrix} G^T(t, t') & G^<(t, t') \\ G^>(t, t') & G^{\tilde{T}}(t, t') \end{pmatrix} . \quad (8.8)$$

The off-diagonal components $G^{<,>}$ are called lesser and greater GFs while the diagonal ones $G^{T,\tilde{T}}$ are called causal and anticausal GFs. All names refer to the ordering of the fields with respect to their projected times. On the one hand, times from the “−” branch are always “greater” than the ones from the “+” branch and vice versa. On the other hand we have forward time evolution on the “+” branch, associated with causality, and antitimeevolution on the “−” branch giving rise to anticausality. The exact definitions are:

$$G^<(t, t') = -i \langle \xi^\dagger(t') \xi(t) \rangle \quad ; \quad G^>(t, t') = -i \langle \xi(t) \xi^\dagger(t') \rangle , \quad (8.9)$$

$$\begin{aligned} G^T(t, t') &= \theta(t-t')G^>(t, t') & ; & & G^{\tilde{T}}(t, t') &= \theta(t-t')G^<(t, t') \\ &+ \theta(t'-t)G^<(t, t') & & & &+ \theta(t'-t)G^>(t, t') . \end{aligned} \quad (8.10)$$

For completeness we also introduce the retarded and advanced GFs usually encountered in equilibrium theories and needed within the Meir Wingreen formula, later introduced in Eq. (8.18).

$$G^R(t, t') = \theta(t-t')[G^>-G^<](t, t') \quad ; \quad G^A(t, t') = \theta(t'-t)[G^<-G^>](t, t') . \quad (8.11)$$

Their connection to the four Keldysh blocks defined in Eq. (8.8) is given by the relation

$$\begin{pmatrix} G^T & G^< \\ G^> & G^{\tilde{T}} \end{pmatrix} = \begin{pmatrix} (G^R + G^<) & G^< \\ (G^R - G^A + G^<) & (G^< - G^A) \end{pmatrix} . \quad (8.12)$$

The identity above is easily shown by exploiting the fact that the four Keldysh components are not independent but fulfill the cyclic relations

$$G^R - G^A = G^> - G^< \quad ; \quad G^R + G^A = G^T - G^{\tilde{T}} \quad ; \quad G^T - G^{\tilde{T}} = G^> + G^< . \quad (8.13)$$

This dependency allows for a basis transformation called Keldysh rotation which eliminates one component of the 2×2 Keldysh substructure and simplifies analytical calculations. However we stay in the unrotated basis which is more convenient for our later numerics.

¹⁶Cf. Fig. 6.1. Contour time ordering equals normal time ordering along the contour. With respect to normal time two operators from the upper (lower) contour must be timeordered (antitimeordered).

8.2.2 Continuous frequency representation of GFs

We switch now to frequency space by Fourier transformation and exploit the fact that for a steady state situation all GF only depend on time differences. We rename $t - t' = t$ and $t' - t = -t$. While the off-diagonal blocks of Eq. (8.8) are related to their Fourier-transform by the definition

$$G^{\pm\mp}(t) = \int \frac{d\omega}{2\pi} e^{-i\omega t} G^{<, >}(\omega) , \quad (8.14)$$

the relation for the diagonal blocks needs some calculation. We first introduce continuous versions of the Heaviside step function and its derivative, the delta distribution

$$\theta(t) = -\lim_{\eta \rightarrow 0} \int \frac{d\omega}{2\pi i} \frac{e^{-i\omega t}}{\omega + i\eta} \quad ; \quad \delta(t) = \frac{d\theta(t)}{dt} = \int \frac{d\omega}{2\pi} e^{-i\omega t} . \quad (8.15)$$

Analogously, we get in frequency space

$$\theta(\omega) = +\lim_{\eta \rightarrow 0} \int \frac{dt}{2\pi i} \frac{e^{+i\omega t}}{t - i\eta} \quad ; \quad \delta(\omega) = \frac{d\theta(\omega)}{d\omega} = \int \frac{dt}{2\pi} e^{+i\omega t} . \quad (8.16)$$

The $G^{\pm\pm}$ components of Eq. (8.8) in frequency space are given by

$$\begin{aligned} G^{\pm\pm}(\omega) &= \int dt e^{i\omega t} [\theta(\pm t)G^>(t) + \theta(\mp t)G^<(t)] \\ &= -\int \frac{d\omega_1}{2\pi} \int \frac{d\omega_2}{2\pi i} \int dt e^{i\omega t} \left[\frac{e^{\mp i\omega_2 t}}{\omega_2 + i\eta} e^{-i\omega_1 t} G^>(\omega_1) + \frac{e^{\pm i\omega_2 t}}{\omega_2 + i\eta} e^{-i\omega_1 t} G^<(\omega_1) \right] \\ &= -\int \frac{d\omega_1}{2\pi} \int \frac{d\omega_2}{2\pi i} \int dt \left[\frac{e^{i(\omega - \omega_1 \mp \omega_2)t}}{\omega_2 + i\eta} G^>(\omega_1) + \frac{e^{i(\omega - \omega_1 \pm \omega_2)t}}{\omega_2 + i\eta} G^<(\omega_1) \right] \\ &= \int \frac{d\omega_1}{2\pi i} \left[\frac{G^>(\omega_1)}{\pm(\omega_1 - \omega) - i\eta} - \frac{G^<(\omega_1)}{\pm(\omega_1 - \omega) + i\eta} \right] . \end{aligned} \quad (8.17)$$

To conclude, the knowledge of the greater and lesser GFs in frequency space allows for computing the whole GF and thus a comparison with known results from [64].

8.2.3 The Meir Wingreen formula

The current formula for a transport setup, consisting of metallic leads and a central interacting region was worked out in general by Meir and Wingreen [41]. It is expressed in terms of Keldysh GFs and shifts the problem of current computation to the problem of evaluating GFs. We already stated a Meir Wingreen formula for the MSCT in the first part of the thesis. For the full interacting AH model in wide band approximation and with $\Gamma_L + \Gamma_R = \Gamma$, it reads

$$I(V) = \frac{2e}{h} \frac{\Gamma_L \Gamma_R}{\Gamma} \int d\epsilon \mathcal{A}(\omega) \left(n_F(\omega - \mu_L) - n_F(\omega - \mu_R) \right) , \quad (8.18)$$

and depends again on a spectral function, defined from the retarded GF

$$\mathcal{A}(\omega) = -2 \text{Im}(G^R(\omega)) \quad ; \quad G^R(\omega) = G^{++}(\omega) - G^{+-}(\omega) . \quad (8.19)$$

For the AH model we get a dependency on only one spectral function which is again not known in general. Within the next section we will show how to get it exactly in the limit $\lambda = 0$ from the retarded GF of the RL model. How to get it the limit $\lambda \ll \Gamma$ will be demonstrated in chapter 10 by a perturbative expansion of the self-energy in terms of the electron-phonon coupling.

8.2.4 The GF of the RL model

We will now perform the limit ($N \rightarrow \infty$) to Eq. (8.6). Let us first focus on the self-energy. The discrete definition of $\Sigma_0^{(+)}$ is given in Eq. (6.63). We also insert the definition of $X^{(+)}$ and regroup the product

$$\Sigma_0^{(+)} = \delta_t^2 \sum_{\alpha} (t_{\alpha} \sigma R) (G_{\alpha}) (t_{\alpha} \sigma R) \quad ; \quad G_{\alpha} = \sum_{\mathbf{k}} G_{\mathbf{k}\alpha} . \quad (8.20)$$

For ($N \rightarrow \infty$) we have to drop the prefactor δ_t^2 since it will become the measure of a contour-time integration. The product σR encodes the branch dependent forward and backward direction of real-time evolution including periodic boundary conditions. A small timeshift ($\propto \delta_t$) originating from the discrete path-integral is encoded in R . The correct continuum limit for this product is $R \rightarrow \mathbb{1}$ and due to the (usually hidden) boundary conditions $\sigma \rightarrow \sigma_z$ with a standard Pauli matrix σ_z in the 2×2 Keldysh space

$$t_{\alpha} \sigma R \rightarrow \begin{pmatrix} t_{\alpha} & 0 \\ 0 & -t_{\alpha} \end{pmatrix} . \quad (8.21)$$

For a continuous version of the GF of lead α we remember our previous definition $G_{\alpha} = \frac{X_{\alpha}}{i|t_{\alpha}|^2}$ and start from Eq. (7.4) which represents one matrix element

$$(G_{\alpha})_{i,j}^{\mu,\nu} \equiv -i C_{i,j}^{\mu,\nu} \int_{-\infty}^{+\infty} d\epsilon \nu_{\alpha}(\epsilon) n_F[-C_{i,j}^{\mu,\nu}(\epsilon - \mu_{\alpha})] e^{-i\epsilon \Delta T_{i,j}} . \quad (8.22)$$

We choose the infinite flat band model from Eq. (7.5), and the discrete time structure within Eq.(7.4) is removed by the following replacements

$$\Delta T_{i,j} \rightarrow (t-t') \quad ; \quad C_{i,j} \rightarrow C(t-t') = \theta(t-t') \begin{pmatrix} +1 & -1 \\ +1 & -1 \end{pmatrix} + \theta(t'-t) \begin{pmatrix} -1 & -1 \\ +1 & +1 \end{pmatrix} . \quad (8.23)$$

The result is a continuous expressions for all four Keldysh components. The Heavisides from the off-diagonals just add to one and we can directly read off the greater and lesser GF of the leads in energy space

$$G_{\alpha}^{\pm\mp}(t, t') = \int \frac{d\epsilon}{2\pi} \left(\pm i \frac{\Gamma_{\alpha}}{|t_{\alpha}|^2} 2n_F(\pm(\epsilon - \mu_{\alpha})) \right) e^{-i\epsilon(t-t')} = \int \frac{d\epsilon}{2\pi} e^{-i\epsilon(t-t')} G_{\alpha}^{<, >}(\epsilon) . \quad (8.24)$$

Now the knowledge of $G_{\alpha}^{<, >}(\epsilon)$ and Eq. (8.17) allow for the computation of $G_{\alpha}^{\pm\pm}(\epsilon)$:

$$\begin{aligned} G_{\alpha}^{\pm\pm}(\epsilon) &= \int \frac{d\epsilon_1}{2\pi i} \left[\frac{G_{\alpha}^{>}(\epsilon_1)}{\pm(\epsilon_1 - \epsilon) - i\eta} - \frac{G_{\alpha}^{<}(\epsilon_1)}{\pm(\epsilon_1 - \epsilon) + i\eta} \right] \\ &= \frac{\Gamma_{\alpha}}{|t_{\alpha}|^2} \int \frac{d\epsilon_1}{\pi} \left[n_F(\epsilon_1 - \mu_{\alpha}) \left(\frac{1}{\pm(\epsilon_1 - \epsilon) - i\eta} - \frac{1}{\pm(\epsilon_1 - \epsilon) + i\eta} \right) - \frac{1}{\pm(\epsilon_1 - \epsilon) - i\eta} \right] \\ &= i \frac{\Gamma_{\alpha}}{|t_{\alpha}|^2} (2n_F(\epsilon - \mu_{\alpha}) - 1) . \end{aligned} \quad (8.25)$$

In the last step we used the Cauchy formula [see Eq. (8.26)] together with the fact that the principal part of $(1/\epsilon')$ is zero and the principal parts of the integrals involving the Fermi-function cancel each other:

$$\int \frac{d\epsilon'}{\pi} \frac{f(\epsilon')}{\epsilon' - \epsilon \pm i\eta} = \mathcal{P} \int \frac{d\epsilon'}{\pi} \left(\frac{f(\epsilon')}{\epsilon' - \epsilon} \right) \mp i \int d\epsilon' \delta(\epsilon' - \epsilon) f(\epsilon'). \quad (8.26)$$

An analogous argumentation holds for $G_\alpha^{--}(\epsilon)$ and adding all Keldysh components we end up with the full Keldysh GF of the leads

$$G_\alpha(\epsilon) = i \frac{\Gamma_\alpha}{|t_\alpha|^2} \begin{pmatrix} 2n_F(\epsilon - \mu_\alpha) - 1 & 2n_F(\epsilon - \mu_\alpha) \\ 2n_F(\epsilon - \mu_\alpha) - 2 & 2n_F(\epsilon - \mu_\alpha) - 1 \end{pmatrix}. \quad (8.27)$$

Getting now back to Eq. (8.20), we can replace all parts by their continuous representations. Consistent with [64] we finally get the continuous self-energy of lead α

$$\Sigma_\alpha = \begin{pmatrix} t_\alpha & 0 \\ 0 & -t_\alpha \end{pmatrix} \cdot G_\alpha \cdot \begin{pmatrix} t_\alpha & 0 \\ 0 & -t_\alpha \end{pmatrix} = i\Gamma_\alpha \begin{pmatrix} 2n_F(\epsilon - \mu_\alpha) - 1 & -2n_F(\epsilon - \mu_\alpha) \\ 2 - 2n_F(\epsilon - \mu_\alpha) & 2n_F(\epsilon - \mu_\alpha) - 1 \end{pmatrix}. \quad (8.28)$$

The continuous version of the dot's inverse GF in energy space is

$$G_d^{-1}(\epsilon) = \begin{pmatrix} +(\epsilon - \epsilon_0) & \\ & -(\epsilon - \epsilon_0) \end{pmatrix}. \quad (8.29)$$

Defining now $N_F = n_F(\epsilon - \mu_L) + n_F(\epsilon - \mu_R)$, setting symmetric conditions for the tunneling $\Gamma_L = \Gamma_R = \Gamma/2$, the bias $\mu_L = -\mu_R = eV/2$ and using again the Dyson equation $G_0(\epsilon) = (G_d^{-1}(\epsilon) - \Sigma_L(\epsilon) - \Sigma_R(\epsilon))^{-1}$ we get the full GF of the RL model

$$G_0(\epsilon) = \frac{1}{(\epsilon - \epsilon_0)^2 + \Gamma^2} \begin{pmatrix} (\epsilon - \epsilon_0) + i\Gamma(N_F - 1) & i\Gamma N_F \\ i\Gamma(N_F - 2) & -(\epsilon - \epsilon_0) + i\Gamma(N_F - 1) \end{pmatrix}. \quad (8.30)$$

8.2.5 The analytical current for the RL model

From Eq. (8.30) and the definition (8.19) we get the spectral function

$$\mathcal{A}(\epsilon) = -2 \text{Im} \left\{ \frac{\epsilon - \epsilon_0 + i\Gamma(N_F - 1) - i\Gamma N_F}{(\epsilon - \epsilon_0)^2 + \Gamma^2} \right\} = \frac{2\Gamma}{(\epsilon - \epsilon_0)^2 + \Gamma^2}. \quad (8.31)$$

Finally, Eq. (8.18) provides the exact $I(V)$ relation for the RL model.

$$I(V) = \frac{e\Gamma}{h} \int d\epsilon \frac{\Gamma}{\Gamma^2 + (\epsilon - \epsilon_0)^2} \left(n_F(\epsilon - \mu_L) - n_F(\epsilon - \mu_R) \right). \quad (8.32)$$

The resonant level model is now completely solved, in the sense that we know analytically the full Green's function and also know the exact analytical current-voltage relation. In the next chapter we proceed solving the AH model by extending the numerical ISPI scheme to it.

9 Extension of the ISPI scheme to the AH model

We will now get back to our approach for the AH model and develop the numerical scheme to solve the spin summation in Eq. (6.66). In principle one could directly implement Eq. (6.66) using standard numerical routines for determinant computation¹⁷ but the problem is the resulting runtime. By discretizing the Keldysh contour and constructing a path-integral along it, we introduced a spin summation for almost all time points, each running over three values $S_j \in \{0, \pm 1\}$. To be precise, we introduced $3^{2(N-1)}$ possible spin combinations to sum over. For each individual combination we have to compute a determinant of a $2N \times 2N$ matrix. To estimate an appropriate value for N one has to consider the following things. First of all we introduced a Trotter discretization error, which can and will be extrapolated out but nevertheless assumes δ_t to be in principle small. We restrict ourselves to $\delta_t \Gamma \leq 0.5$. The next scale to consider is the time interval between our initial equilibrium state encoded in ρ_0 and the measurement time t_m itself. We start in the “distant past” and evolve the system along the contour. We are interested in a stationary current and therefore the initial switching of interactions must be far enough away from the measurement time. Otherwise we would measure the transient behavior of the system which might be also dependent on the details of the initial conditions encoded in ρ_0 , cf. [76]. The data we will present later was computed for $t_m \Gamma = 12$. One further numerical detail to consider is to place the measurement time roughly in the middle of the upper Keldysh branch so that the source term contribution does not end up at the borders of the GF matrices which might give rise to discretization artifacts (cf. [64]). In total this gives a lower bound of $2N \gtrsim 100$. Decreasing the time-discretization increases this lower bound. A direct implementation leads to at least $3^{2N-2} \approx 10^{47}$ matrices which need to be filled, and their determinants to be summed up to get $\mathcal{Z}[\eta]$. Without a significant decrease of the number of summations it is (at the moment) impossible to numerically solve this problem.

In the next sections we present the extension of the ISPI scheme from [64] to the AH model, i.e., we create a scheme to compute $\mathcal{Z}[\eta]$ numerically. To mark our starting point, we cite Eq. (6.66) once again

$$\mathcal{Z}[\eta] = \sum_{\vec{S} \in \mathbb{S}^{2N}} \det \left\{ B[\vec{S}] (\mathfrak{i}\mathcal{G}[\vec{S}])^{-1} \right\} .$$

The ISPI scheme exploits the exponential decay of long time correlations at finite temperature. Based on this, a maximal correlation time τ_c is introduced which leads to a band structure of correlation matrices with respect to time space. Finally this band structure will allow to decouple some of the spin summations of Eq. (6.66) and rewrite it as a product of sums over determinants of matrices with lower dimension. A dramatic reduction of the number of total summations is the consequence and a numerical solution of Eq. (6.66)

¹⁷We use a QR decomposition [38] for computing the determinants remaining in the final ISPI scheme from Eq. (9.22).

becomes feasible. In the following we will develop the ISPI scheme for the AH model in four steps. First we create the necessary band structure by a cut-off scheme. Afterwards we decouple the fermionic and the bosonic part of Eq. (6.66) separately. And finally we present a strategy to eliminate all remaining systematic errors from the scheme, i.e., the Trotter error and the memory truncation error induced by the introduction of τ_c .

9.1 Change to the ISPI basis-ordering

The first step before defining a truncation rule is to perform a change in the basis-ordering from “Keldysh \otimes time”, used so far and also in [40], to the ISPI basis-ordering “time \otimes Keldysh”, used in [64]. All time dependent matrix-objects Y (GFs, Self-energies, their inverse counterparts,...) are relabeled after the basis transformation. In index notation the transformation reads

$$Y_{i,j}(t_i, t_j)|_{i,j \in \{1, 2N\}} \rightarrow Y_{k,l}^{\sigma, \sigma'}(t_k^\sigma, t_l^{\sigma'}) \Big|_{\substack{\sigma, \sigma' \in \{\pm\} \\ k, l \in \{1, N\}}} . \quad (9.1)$$

Every time argument gets a subscript index $\{1, \dots, N\}$ representing its real-time projection and a superscript index $\{\pm\}$ labeling the Keldysh branch-dependence. See also Fig. 6.1 for the exact mapping of time indices. Consequently, from now on the vector \vec{S} is also changed to the new basis ordering

$$\vec{S} = (S_1^\pm, \dots, S_N^\pm) \in \mathbb{S}^{\pm N} := \prod_{i=1}^N \prod_{\sigma=\pm} \mathbb{S}_i^\sigma ; \quad \mathbb{S}_i^\sigma := \begin{cases} \{0, \pm 1\} & ; (i, \sigma) \notin \{(1, +), (N, -)\} \\ \{0\} & ; (i, \sigma) \in \{(1, +), (N, -)\} \end{cases} .$$

9.2 Cut-off scheme

We already mentioned that we use the natural decay of correlations for a truncation. For the spinless AH model we use the decay of the self-energy $\Sigma_0^{(+)}$ (shown in Fig. 9.1) to justify the truncation of \mathcal{G}^{-1} to a band structure in real-time. We define the maximal correlation time $\tau_c = K\delta_t$ and the explicit truncation rule is

$$(\mathcal{G}^{-1})_{i,j}^{\sigma, \sigma'} \longrightarrow \theta(K - |i - j|)(\mathcal{G}^{-1})_{i,j}^{\sigma, \sigma'} ; \quad \theta(0) = 1 . \quad (9.2)$$

Since G_s^{-1} is almost¹⁸ diagonal in time, the decay of $\Sigma_0^{(+)}$ is sufficient to justify Eq. (9.2). Furthermore to be consistent with this cancellation of long time-time correlations, we also have to introduce the maximal spin-spin correlation which will lead to a consistent scheme

$$S_i^\pm \cdot S_j^{\pm'} = \begin{cases} S_i^\pm \cdot S_j^{\pm'} & ; |i - j| \leq K \\ 0 & ; |i - j| > K \end{cases} . \quad (9.3)$$

This spin-spin correlation relation can be also motivated by the fact that the truncation of \mathcal{G}^{-1} is equivalently achieved by performing the transformation of Eq. (6.60) prior to the Gaussian integration (6.59) accompanied by the introduction of a maximal field-field correlation time for the (appropriately transformed) fields $\bar{\zeta}(t)$ and $\zeta(t')$.

¹⁸Only the diagonal and the sub-diagonal with respect to time are occupied. Each time element possesses a 2×2 Keldysh substructure.

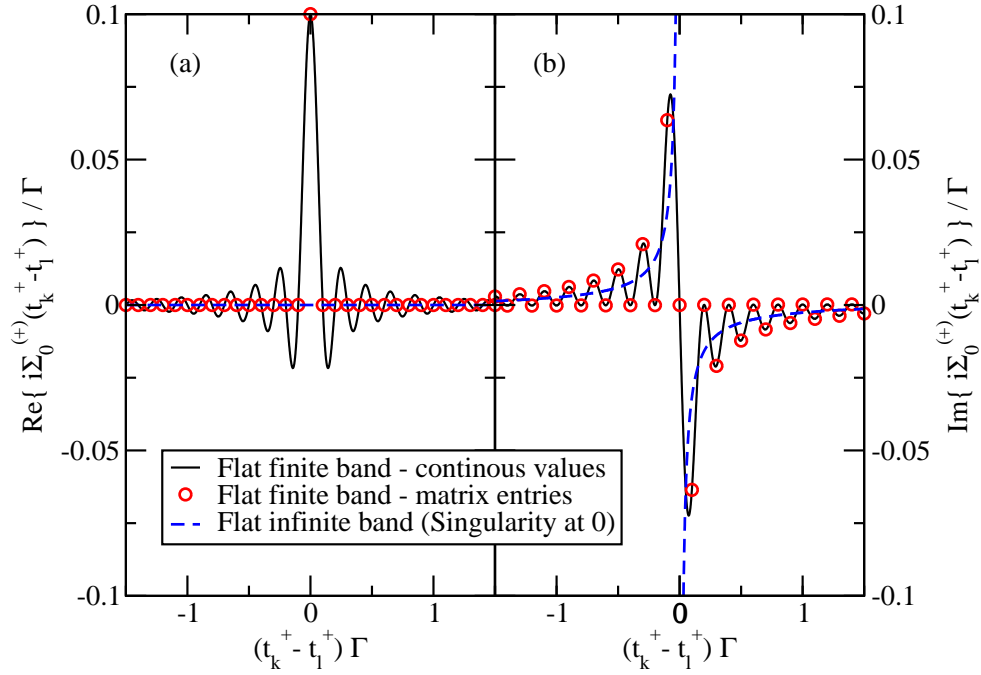


Figure 9.1: (a) Real and (b) imaginary part of $i\Sigma_0^{(+)}(t_k^+ - t_1^+)$ for $\delta_t\Gamma = 0.1$; $\beta\Gamma = 5$; $eV = \Gamma$; $D = \frac{\pi}{\delta_t}$. Black lines: Continuous solutions from our flat finite band model used for the leads (cf. Sec. 7.3). Red circles: Values of the self-energy entering our matrix representation when calculating the discrete path sum (6.66). Blue dashed line: Flat infinite band model – divergent for zero correlation time and not suitable for our numerics (cf. Sec. 7.2).

9.3 Construction of the ISPI scheme - fermionic part

The starting point for the fermionic part of the iterative scheme is the application of Eq. (9.2) on \mathcal{G}^{-1} and the grouping of the remaining occupied bands into blocks of time dimension $K \times K$ with $N_K = N/K$ chosen integer. For a shorter notation and since the resulting object only depends on the fermionic degrees of freedom we abbreviate it with F only

$$F = (i\mathcal{G})^{-1} = \begin{pmatrix} \boxed{F^{11}} & \boxed{F^{12}} & 0 & \dots & 0 \\ \boxed{F^{21}} & \boxed{F^{22}} & \boxed{F^{23}} & \ddots & \vdots \\ 0 & \boxed{F^{32}} & \boxed{F^{33}} & \ddots & 0 \\ \vdots & \ddots & \ddots & \ddots & \boxed{F^{N_K-1 N_K}} \\ 0 & \dots & 0 & \boxed{F^{N_K N_K-1}} & \boxed{F^{N_K N_K}} \end{pmatrix}. \quad (9.4)$$

The band structure implies that blocks $F^{l,l+1}$ ($F^{l+1,l}$) correspond to lower (upper) triangular matrices while the blocks on the diagonal are fully occupied.

The exact structure is

$$\boxed{F^{ll'}} = \begin{pmatrix} F_{(l-1)K+1, (l'-1)K+1} & \cdots & F_{(l-1)K+1, l'K} \\ \vdots & \ddots & \vdots \\ F_{lK, (l'-1)K+1} & \cdots & F_{lK, l'K} \end{pmatrix} ; \quad F_{i,j} = -\mathfrak{i} \begin{pmatrix} (\mathcal{G}^{-1})_{i,j}^{++} & (\mathcal{G}^{-1})_{i,j}^{+-} \\ (\mathcal{G}^{-1})_{i,j}^{-+} & (\mathcal{G}^{-1})_{i,j}^{--} \end{pmatrix} . \quad (9.5)$$

Each element of these blocks still possesses a 2×2 Keldysh substructure kept implicitly. Due to $((\mathfrak{i}\mathcal{G})^{-1})_{i,j}^{\pm} = ((\mathfrak{i}\mathcal{G})^{-1})_{i,j}^{\pm}[S_i^{\pm}]$, cf. Eq. (6.66), each block is in general dependent on $2K$ different pseudo-spins

$$F^{ll'}[S_{(l-1)K+1}^{\pm}, \dots, S_{lK}^{\pm}] =: F^{ll'}[\vec{S}^{(l)}] . \quad (9.6)$$

We store them in vectors/arrays $\vec{S}^{(l)}$ which are elements of spin-sets of cardinality¹⁹ 3^{2K} .

$$\vec{S}^{(l)} := (S_{(l-1)K+1}^{\pm}, \dots, S_{lK}^{\pm}) \in \mathbb{S}^{(l)} := \mathbb{S}_{(l-1)K+1}^{+} \times \mathbb{S}_{(l-1)K+1}^{-} \times \cdots \times \mathbb{S}_{lK}^{+} \times \mathbb{S}_{lK}^{-} . \quad (9.7)$$

Based on the block-wise spin dependence [cf. Eq. (9.5)] and the spin correlation relation (9.3) we get a block-product cancellation rule which also holds if inverse blocks are involved

$$F^{ii'}[\vec{S}^{(i)}] F^{jj'}[\vec{S}^{(j)}] = \begin{cases} F^{ii'} F^{jj'} & ; |i-j| \leq K \\ 0 & ; |i-j| > K \end{cases} . \quad (9.8)$$

The block structure introduced together with the block-block correlation relation and the spin-spin correlation relation [see Eq. (9.3)] are the fundamental ingredients to develop an iterative scheme similar to the one for the Anderson model in [64]. Keep in mind that $\mathcal{Z}[\eta]$ also depends on a bosonic part $B[\vec{S}]$ which we will address later.

The idea of the ISPI-scheme is to perform a block wise Gaussian elimination on F under application of the block-block correlation relation. In the end the matrix F is transformed to an upper triangular matrix with respect to the $K \times K$ -blocks. The determinant of F therefore corresponds to the product of the determinants of all (transformed) $K \times K$ -blocks on the diagonal. Due to the block-block correlation relation each of these blocks will only depend on $4K$ different pseudo spins and therefore the summation in Eq. (6.66) can be decoupled.

¹⁹Except for $|\mathbb{S}^{(1)}| = 3^{2K-2}$ due to the Keldysh boundary conditions.

Gaussian elimination on F :

The whole Gaussian elimination scheme will be applied in time space. Therefore each element still possesses a 2×2 Keldysh substructure kept implicit and we are only dealing with $N \times N$ block matrices from now on. The starting point of the elimination is $F_{(1)}$ alias F itself. Whenever needed, we attach the iteration step as a subscript in brackets to an object. The whole scheme will need $N_K = N/K$ transformations, performed by a transformation-matrix $L_{(l)}$ with the convention that $F_{(l+1)} = L_{(l)}F_{(l)}$. The scheme is finished when $F_{(N_K)}$ is reached, which will be an upper triangular block matrix. Each block has dimension $K \times K$ in time space.

Let us begin with a definition on how to divide $F_{(l)}$ into a 2×2 block matrix in time space with varying sizes for each iteration step l

$$F_{(l)} = \left(\begin{array}{c|c} \alpha_{(l)} & \beta_{(l)} \\ \hline \gamma_{(l)} & \delta_{(l)} \end{array} \right) ; \quad \alpha_{(l)} = \begin{pmatrix} (F_{(l)})_{1,1} & \cdots & (F_{(l)})_{1,lK} \\ \vdots & \ddots & \vdots \\ (F_{(l)})_{lK,1} & \cdots & (F_{(l)})_{lK,lK} \end{pmatrix}. \quad (9.9)$$

Note that the definition of $\alpha_{(l)}$ implies the definition of all other blocks. The transformation matrix is defined as

$$L_{(l)} := \left(\begin{array}{c|c} \mathbb{1}_{lK} & 0 \\ \hline -\gamma_{(l)}\alpha_{(l)}^{-1} & \mathbb{1}_{N_K-lK} \end{array} \right) ; \quad \det(L_{(l)}) = 1 \quad (9.10)$$

and performs one Gaussian elimination step from $F_{(l)}$ to $F_{(l+1)}$

$$F_{(l+1)} = L_{(l)}F_{(l)} = \left(\begin{array}{c|c} \alpha_{(l)} & \beta_{(l)} \\ \hline 0 & \delta_{(l)} - \gamma_{(l)}\alpha_{(l)}^{-1}\beta_{(l)} \end{array} \right). \quad (9.11)$$

With respect to the 2×2 block matrix the element $\delta_{(l)} - \gamma_{(l)}\alpha_{(l)}^{-1}\beta_{(l)}$ is called Schur complement. When the Gaussian elimination scheme is finished we can rewrite $\det F$ based on the fact, that $F_{(N_K)}$ is an upper diagonal block matrix with respect to $K \times K$ blocks in time space and that all applied transformation matrices have a determinant equal one

$$\det F = \det F_{(N_K)} = \prod_{i=1}^{N_K} \det \boxed{F_{(N_K)}^{ii}}. \quad (9.12)$$

This was the first step on the way to achieve a decoupling of the summations in Eq. (6.66). We rewrote the determinant of one $N \times N$ matrix into a product of determinants of $K \times K$ matrices. Due to the iterative construction of the Schur complements, all diagonal blocks do in general still dependent on the complete spin-vector \vec{S} . A decoupling of the summations of Eq. (6.66) is achieved by carefully inspecting the spin-dependencies and applying the block-block correlation relation from Eq. (9.8) in each elimination step when constructing the Schur-complement. For more insight the first two elimination steps are presented in detail in the following. We start with $F_{(1)}$ grouped in the corresponding four

blocks

$$F_{(1)} = \left(\begin{array}{c|cccc} \boxed{F_{(1)}^{11}} & \boxed{F_{(1)}^{12}} & 0 & \dots & 0 \\ \boxed{F_{(1)}^{21}} & \boxed{F_{(1)}^{22}} & \boxed{F_{(1)}^{23}} & \ddots & \vdots \\ 0 & \boxed{F_{(1)}^{32}} & \boxed{F_{(1)}^{33}} & \ddots & 0 \\ \vdots & \ddots & \ddots & \ddots & \boxed{F_{(1)}^{N_K-1 N_K}} \\ 0 & \dots & 0 & \boxed{F_{(1)}^{N_K N_K-1}} & \boxed{F_{(1)}^{N_K N_K}} \end{array} \right) \equiv \left(\begin{array}{c|c} \alpha_{(1)} & \beta_{(1)} \\ \gamma_{(1)} & \delta_{(1)} \end{array} \right).$$

The first elimination step transforms $F_{(1)}$ to

$$F_{(2)} = \left(\begin{array}{c|cccc} \boxed{F_{(1)}^{11}} & \boxed{F_{(1)}^{12}} & 0 & \dots & \\ 0 & \boxed{F_{(1)}^{22} - F_{(1)}^{21}(F_{(1)}^{11})^{-1}F_{(1)}^{12}} & \boxed{F_{(1)}^{23}} & 0 & \dots \\ 0 & \boxed{F_{(1)}^{32}} & \boxed{F_{(1)}^{33}} & \boxed{F_{(1)}^{34}} & \\ \vdots & 0 & \boxed{F_{(1)}^{43}} & \boxed{F_{(1)}^{44}} & \ddots \\ \vdots & \vdots & & \ddots & \ddots \end{array} \right) \equiv \left(\begin{array}{c|c} \alpha_{(2)} & \beta_{(2)} \\ \gamma_{(2)} & \delta_{(2)} \end{array} \right).$$

Despite setting $\gamma_{(1)} = 0$ we only get one replacement in the $\delta_{(1)}$ -block

$$\boxed{F_{(2)}^{22}[\vec{S}^{(2)}, \vec{S}^{(1)}]} = \boxed{F_{(1)}^{22}[\vec{S}^{(2)}] - F_{(1)}^{21}[\vec{S}^{(2)}](F_{(1)}^{11}[\vec{S}^{(1)}])^{-1}F_{(1)}^{12}[\vec{S}^{(1)}]}. \quad (9.13)$$

In the next elimination step the block-block correlation enters the scheme and reduces the spin dependencies

$$F_{(3)} = \left(\begin{array}{c|cccc} \boxed{F_{(1)}^{11}} & \boxed{F_{(1)}^{12}} & 0 & \dots & \\ 0 & \boxed{F_{(2)}^{22}} & \boxed{F_{(1)}^{23}} & 0 & \dots \\ 0 & 0 & \boxed{F_{(3)}^{33}} & \boxed{F_{(1)}^{34}} & \\ \vdots & \vdots & \boxed{F_{(1)}^{43}} & \boxed{F_{(1)}^{44}} & \ddots \\ \vdots & \vdots & & \ddots & \ddots \end{array} \right) \equiv \left(\begin{array}{c|c} \alpha_{(2)} & \beta_{(2)} \\ 0 & \delta_{(2)} - \gamma_{(2)}\alpha_{(2)}^{-1}\beta_{(2)} \end{array} \right).$$

The application of the the block-block correlation relation (9.8) inside the second and all upcoming Schur complements now leads to a consistent iterative scheme. In the actual step, the dependence on $\vec{S}^{(1)}$ is canceled from $F_{(3)}^{33}$

$$\boxed{F_{(3)}^{33}[\vec{S}^{(2)}, \vec{S}^{(3)}]} = \boxed{F_{(1)}^{33} - F_{(1)}^{32}(F_{(2)}^{22} - F_{(1)}^{21}(F_{(1)}^{11})^{-1}F_{(1)}^{12})^{-1}F_{(1)}^{23}}. \quad (9.14)$$

The complete factorization of $\det(F[\vec{S}])$ including the spin dependence reads

$$\det(F[\vec{S}]) = \prod_{l=1}^{N_K} \det \boxed{F_{(l)}^l[\vec{S}^{(l-1)}; \vec{S}^{(l)}]} = \prod_{l=1}^{N_K} \det \boxed{F_{(N_K)}^l[\vec{S}^{(l-1)}; \vec{S}^{(l)}]} . \quad (9.15)$$

All relevant remaining blocks are Schur-complements and obey the rule

$$F_{(l)}^l[\vec{S}^{(l-1)}; \vec{S}^{(l)}] = F^{lK,lK}[\vec{S}^{(l)}] - F^{lK,(l-1)K}[\vec{S}^{(l)}] \left(F^{(l-1)K,(l-1)K}[\vec{S}^{(l-1)}] \right)^{-1} F^{(l-1)K,lK}[\vec{S}^{(l-1)}] ,$$

in the sense that contributions coming from blocks $F^{i,j}$ with indices $i, j \notin \{1, \dots, N_K\}$ vanish. With this factorization of $\det(F[\vec{S}])$ we achieved a decoupling of the spin dependencies. This is also possible for the bosonic part $\det(B[\vec{S}])$ which we derive next.

9.4 Construction of the ISPI scheme - bosonic part

Analyzing now the dependencies of $\det(B)$ from Eq. (6.56), one finds for the $\lambda = 0$ part

$$B_0[\vec{S}] = \prod_{i=1}^{N_K} B_0^{(i)}[\vec{S}^{(i)}] \quad ; \quad B_0^{(i)}[\vec{S}^{(i)}] = \prod_{i=(l-1)K+1}^{lK} \prod_{\sigma=\pm} \left(\frac{S_i^\sigma}{2} e^{-i\delta_t \sigma \epsilon_0} \right)^{|S_i^\sigma|} . \quad (9.16)$$

Although the $\lambda \neq 0$ part of B seems to couple all spins with each other, we can again exploit the truncation scheme to achieve a decoupling. Based on $|S_i^\pm| \in \{0, \pm 1\}$, we write

$$B_\lambda[\vec{S}] = M^{|\vec{S}|^2} e^{\vec{S}^T (S\Lambda S) \vec{S}} . \quad (9.17)$$

Due to the spin-spin correlation length (9.3) and also motivated by the highly oscillatory behavior of Λ [cf. Eq. (6.55)], it is justified to cut it consistently with Eq. (9.4) to band structure. Consequently, also the product $S\Lambda S$ is reduced to a band structure since S is diagonal

$$S\Lambda S = \begin{pmatrix} \boxed{(S\Lambda S)^{11}} & \boxed{(S\Lambda S)^{12}} & & & \\ \boxed{(S\Lambda S)^{21}} & \ddots & & \ddots & \\ & \ddots & & \ddots & \boxed{(S\Lambda S)^{N_{K-1}N_K}} \\ & & & \boxed{(S\Lambda S)^{N_K N_{K-1}}} & \boxed{(S\Lambda S)^{N_K N_K}} \end{pmatrix} . \quad (9.18)$$

By analyzing the exponent of Eq. (9.17) with respect to its spin-dependencies

$$\vec{S}^T (S\Lambda S) \vec{S} = \sum_{i=1}^{N_K} \vec{S}^{(i+1)} (S\Lambda S)^{i+1,i} \vec{S}^{(i)} + \vec{S}^{(i)} (S\Lambda S)^{i,i} \vec{S}^{(i)} + \vec{S}^{(i)} (S\Lambda S)^{i,i+1} \vec{S}^{(i+1)} , \quad (9.19)$$

we factorize B_λ

$$B_\lambda^{(l)}[\vec{S}^{(l+1)}, \vec{S}^{(l)}] = M^{|\vec{S}^{(l)}|^2} e^{\vec{S}^{(l+1)} (S\Lambda S)^{l+1,l} \vec{S}^{(l)} + \vec{S}^{(l)} (S\Lambda S)^{l,l} \vec{S}^{(l)} + \vec{S}^{(l)} (S\Lambda S)^{l,l+1} \vec{S}^{(l+1)}} , \quad (9.20)$$

keeping in mind the boundary condition $(S\Lambda S)^{N_K+1, N_K} = (S\Lambda S)^{N_K, N_K+1} = 0$. The whole bosonic contribution to the generating function gets decoupled with respect to its spin dependencies and factorizes

$$\det(B[\vec{S}]) = \prod_{l=1}^{N_K} \underbrace{B_\lambda^{(l)}[\vec{S}^{(l+1)}, \vec{S}^{(l)}] B_0^{(l)}[\vec{S}^{(l)}]}_{:=B^{(l)}[\vec{S}^{(l+1)}, \vec{S}^{(l)}]} . \quad (9.21)$$

Each factor depends on maximal $2K$ spins and we use again the boundary condition $\vec{S}^{(N+1)} = \emptyset$ to shorten notations. Now we can collect everything to gain our final iterative result. The number of summations needed is given in the red boxes

$$\begin{aligned} \mathcal{Z}[\eta] &= \sum_{\vec{S} \in \mathbb{S}_N^\pm} \det B[\vec{S}] \cdot \det F[\vec{S}, \eta] && \boxed{\# = 3^{2N-2}} \\ &= \sum_{\vec{S}^{(N_K)} \in \mathbb{S}^{(N_K)}} \prod_{l=1}^{N_K} \sum_{\vec{S}^{(l-1)} \in \mathbb{S}^{(l-1)}} B^{(l)}[\vec{S}^{(l+1)}, \vec{S}^{(l)}] \det F_{(l)}^{ll}[\vec{S}^{(l-1)}; \vec{S}^{(l)}] && \boxed{\# = \left(N_K - \frac{8}{9}\right) 3^{2K}} . \end{aligned} \quad (9.22)$$

Since the summation over all configurations of a spin-vector can be performed successively and only runs over all combinations of a $2K$ -dimensional vector in each iterative step, the numerical effort is dramatically reduced from $3^{2N-2} \rightarrow \left(N_K - \frac{8}{9}\right) \cdot 3^{2K}$ summations.

9.5 Data handling, extrapolation and convergence

A priori, our numerical scheme is affected by two systematic errors. First we generate a Trotter error, which appears in Eq. (6.21), when the short-time propagator is split into noncommuting parts over a finite noninfinitesimal interval of length δ_t . Second, we had to introduce a maximal memory time $\tau_c = K\delta_t$ for field-field correlations to partly disentangle the spin-summations and hereby we introduced a “memory error”.

For a given set of physical parameters, i.e., $(T/\Gamma, eV/\Gamma, \lambda/\Gamma, \epsilon_0/\Gamma)$, and fixed numerical parameters, i.e., (δ_t, K) , we obtain the tunneling current from Eq. (6.7). We explicitly calculate the generating function in the presence as well as in the absence of the source term $\eta \approx 10^{-3}$ and then perform a numerical derivative according to Eq. (6.7). This yields a numerical value $I = I(K\delta_t, \delta_t)$ which is still afflicted with the two systematic errors described above. We repeat this procedure for different values of K and δ_t while keeping the physical parameters fixed and refer to the generated set of currents as raw data for a single physical data point. An example of such a set of raw data is shown in Fig. 9.2. To extract the physical single data point from this raw data set, we employ the following systematic extrapolation procedure.

In contrast to Ref. [64], we use a least-dependence approach [77, 78] for the further evaluation here. From Fig. 9.2 we see that for $\delta_t\Gamma \in [0.3, 0.4]$ the data points lie within a few per cent range, also for $\delta_t\Gamma \in [0.18, 0.22]$. For $\delta_t\Gamma \in [0.3, 0.35]$ the deviations among the points are small as well. We take all currents computed for a given interval $[\delta_{t,I}, \delta_{t,F}]$ and calculate the mean value

$$\langle I \rangle_{[\delta_{t,I}, \delta_{t,F}]} = N_I^{-1} \sum_{I \in \mathbb{I}_{[\delta_{t,I}, \delta_{t,F}]}} I \quad ; \quad N_I = |\mathbb{I}_{[\delta_{t,I}, \delta_{t,F}]}| \quad ; \quad \mathbb{I}_{[\delta_{t,I}, \delta_{t,F}]} = \{I(K\delta_t, \delta_t) \mid \delta_t \in [\delta_{t,I}, \delta_{t,F}]\} .$$

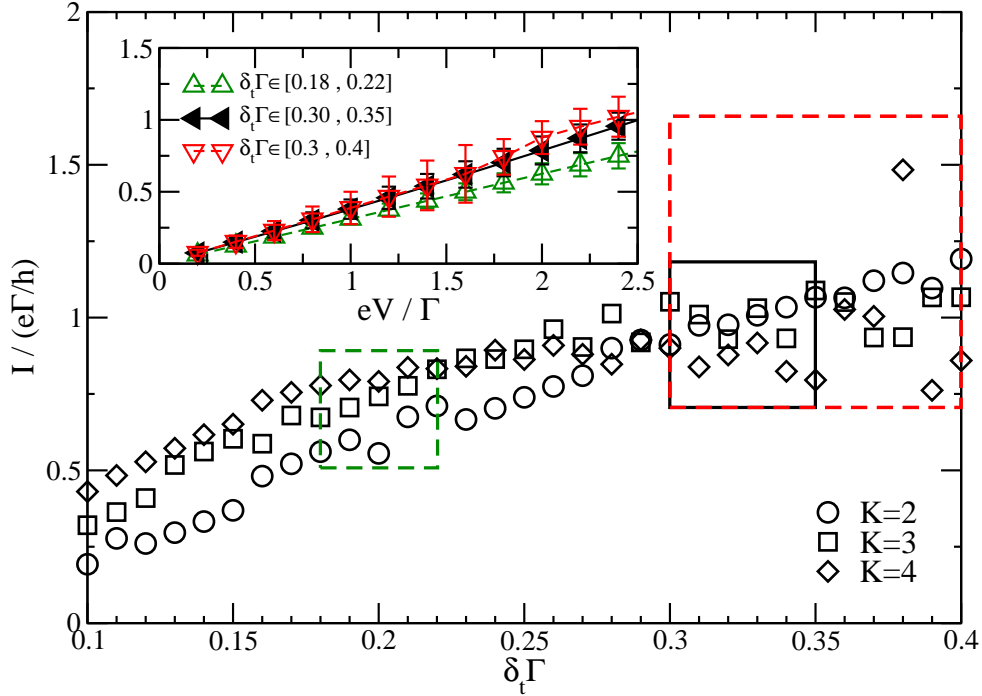


Figure 9.2: Raw data obtained by the ISPI scheme for the spinless AH model. The parameters are ($T = 0.33\Gamma$, $eV = 2.4\Gamma$, $\lambda = \Gamma$, $\omega_0 = \Gamma/2$, $\epsilon_0 = 0$). The boxes in the plot mark the three regions for which we have obtained the current values, i.e., solid line box $0.3 \leq \delta_t\Gamma \leq 0.35$, dashed large box $0.3 \leq \delta_t\Gamma \leq 0.4$ and the small dashed box $0.18 \leq \delta_t\Gamma \leq 0.22$. The corresponding IV characteristics is shown in the inset.

Usually we vary $\delta_t\Gamma$ within the interval using a step-size of 0.01. Together with the corresponding standard deviation we get the ISPI value for the current and an error bar

$$I_{[\delta_t, I, \delta_t, F]}^{ISPI} = \langle I(K\delta_t, \delta_t) \rangle_{[\delta_t, I, \delta_t, F]} \pm \sqrt{\langle I(K\delta_t, \delta_t)^2 \rangle_{[\delta_t, I, \delta_t, F]} - \langle I(K\delta_t, \delta_t) \rangle_{[\delta_t, I, \delta_t, F]}^2}. \quad (9.23)$$

Necessarily, all results presented later are obtained from the same δ_t -interval and $K \in \{2, 3, 4\}$. In the inset of Fig. 9.2 we show as example one $I(V)$ data set averaged over all three different intervals, precisely taking into account different amounts of memory for the respective curves. Note that the color code of the data in the inset corresponds to the colors of the rectangles marking raw-data points taken into account for the different fit-ranges at one fixed voltage. Once, two or more curves match we are sure that the data is converged. In the example $0.3 \leq \delta_t\Gamma \leq 0.35$ is sufficient, moreover all results presented here are obtained within this memory window. As long as error bars are not shown, they are in the order of the symbol size.

We were limited to $K = 4$ since the total number of summations is exponentially dependent on it [cf. Eq. (9.22)]. For typical parameters and $K = 4$, our ISPI code yielding a single raw-data point $I(\delta_t, K)$ runs for ≈ 11 CPU hours on a 2.93 GHz Xeon processor. We already used special optimized libraries for matrix and vector operations but a further parallelization of the code could increase its performance.

10 Analytical approaches to the AH model

Before turning to a detailed discussion of our numerical results obtained from the ISPI scheme, we briefly summarize the analytical approaches to the AH model that we employ to benchmark our method. The following sections will explain each approach. Since our ISPI approach is only valid for $T > 0$, we also present all necessary calculations to extend some of the methods to finite temperature.

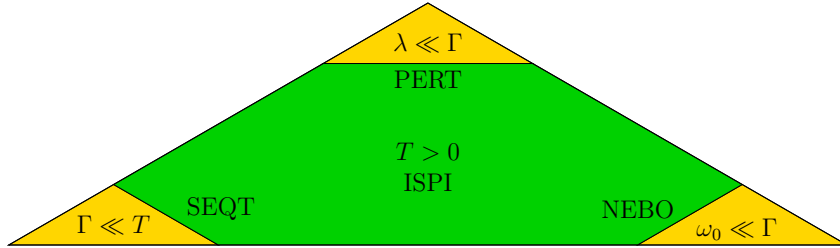


Figure 10.1: Parameter regimes of the AH model, accessible by different analytical approaches compared to ISPI. The abbreviations and exact limitations of each approach are explained in the listing below.

- (i) PERT: For $\lambda \ll \Gamma$, perturbation theory in the electron-phonon coupling applies and yields a closed IV expression for arbitrary values of all other parameters [79]. We note that the solution of the AH model with a very broad dot level [80, 81] corresponds to this small- λ regime.
- (ii) SEQT: For high temperatures, $T \gg \Gamma$, a description in terms of a rate equation is possible [35]. We here use the simplest sequential tunneling version with golden rule rates [82]. For small λ , the corresponding results will match those of perturbation theory, while in the opposite strong-coupling limit, the Franck-Condon blockade occurs and implies a drastic current suppression at low bias voltage [51, 83].
- (iii) NEBO: For small oscillator frequency, $\omega_0 \ll \min(\Gamma, eV)$, the nonequilibrium Born-Oppenheimer (NEBO) approximation is controlled and allows to obtain I from a Langevin equation for the oscillator [84, 85]. For small λ , this approach is also consistent with perturbative theory, while for high T , NEBO and rate equation results will be found to agree.
- (iv) ISPI: For finite temperature $T > 0$ correlations within the relevant GF decay exponentially and our ISPI approach is applicable (cf. 9.2). Despite this hard limit we must assume the following soft limits: $\delta_t^2 \omega_0 \Gamma \ll 1$ and $\delta_t^2 \epsilon_0 \Gamma \ll 1$ [cf. Eqs. (6.44) and (8.5)]. For the leads $\delta_t^2 \epsilon_{\mathbf{k}} \Gamma \ll 1$ is required but always guaranteed by the cut-off $|\epsilon| \leq D = \frac{\pi}{\delta_t}$ and the limited δ_t range used. They are soft because increasing computational power would allow for decreasing δ_t while keeping $\tau_c = K \delta_t$ constant at the price of higher K .

10.1 Perturbative expansion in the phonon coupling

In the regime of a small electron phonon coupling ($\lambda \ll \Gamma$) we can compare the current emerging from our ISPI approach with the results from a perturbation in λ , worked out in Ref. [79]. Up to second order and in the limit of $T = 0$ the expressions for the resulting current correction $\delta I(\lambda)$ are given in [79]. Since our ISPI approach is not valid in the regime $T = 0$ we need to compare to a perturbative result at finite temperature which we develop in this section by following and extending the derivations from [79].

The analytic expression for the current given by Eq. (8.32) was derived from the Meir Wingreen formula [Eq. (8.18)] which still holds in the presence of a phonon. The exact retarded GF is unknown but obeys its own Dyson equation. By a diagrammatic expansion of the self-energy up to the lowest nonvanishing order ($\propto \lambda^2$) we get (see also [79])

$$G^R = G_0^R + G_0^R \Sigma^R G^R = G_0^R + G_0^R \Sigma_{\lambda^2}^R G_0^R + \mathcal{O}(\lambda^3). \quad (10.1)$$

By inserting Eq. (10.1) into Eq. (8.18) we recover Eq. (8.32) plus a correction δI due to the presence of the phonon. The corresponding self-energy corresponds to two diagrams (tadpole and rainbow) but only the rainbow will give a contribution to the current, since the effect of the tadpole can be absorbed by a shift in the chemical potential. The leading correction from $\Sigma_{\lambda^2}^R$ is

$$\delta I(V) = -\frac{e\Gamma}{h} \int d\omega [n_F(\omega - \mu_L) - n_F(\omega - \mu_R)] \text{Im} \left\{ \frac{\Sigma_{\lambda^2}^R(\omega)}{(\omega - \epsilon_0 + i\Gamma)^2} \right\}. \quad (10.2)$$

The denominator follows from the already known GF of the RL model [Eq. (8.30)]

$$\begin{aligned} (G_0^R(\omega))^2 &= (G_0^{++}(\omega) - G_0^{+-}(\omega))^2 \\ &= \left(\frac{\omega - \epsilon_0 + i\Gamma(N_F(\omega) - 1) - i\Gamma N_F(\omega)}{(\omega - \epsilon_0)^2 + \Gamma^2} \right)^2 = \frac{1}{(\omega - \epsilon_0 + i\Gamma)^2}. \end{aligned} \quad (10.3)$$

Like the retarded GF before, also the second order retarded self-energy is composed of two Keldysh components of the full second order self-energy

$$\Sigma_{\lambda^2}^R(\omega) = \Sigma_{\lambda^2}^T(\omega) + \Sigma_{\lambda^2}^<(\omega) = \Sigma_{\lambda^2}^{++}(\omega) + \Sigma_{\lambda^2}^{+-}(\omega). \quad (10.4)$$

The individual components are derived in Ref. [79] from a diagrammatic expansion leading to their definition in terms of components of the full noninteracting GF $G_0(\omega)$ and the full GF of the “free” phonon $G_Q(\omega)$

$$\Sigma_{\lambda^2}^{+\pm}(\omega) = \pm i\lambda^2 \int \frac{d\omega'}{2\pi} G_Q^{+\pm}(\omega') G_0^{+\pm}(\omega - \omega'). \quad (10.5)$$

The GF of the “free” phonon is defined in a standard way as contour ordered displacement correlator

$$G_Q(t, t') = -i \langle T_C \{ \hat{Q}(t) \hat{Q}(t') \} \rangle. \quad (10.6)$$

The frequency representation follows by Fourier transformation

$$G_Q(\omega) = (n_B(\omega_0) + 1) \begin{pmatrix} \frac{1}{\omega - \omega_0 + i\delta} - \frac{1}{\omega + \omega_0 - i\delta} & -2\pi i\delta(\omega + \omega_0) \\ -2\pi i\delta(\omega - \omega_0) & \frac{1}{\omega + \omega_0 + i\delta} - \frac{1}{\omega - \omega_0 - i\delta} \end{pmatrix} \\ + (n_B(\omega_0)) \begin{pmatrix} \frac{1}{\omega + \omega_0 + i\delta} - \frac{1}{\omega - \omega_0 - i\delta} & -2\pi i\delta(\omega - \omega_0) \\ -2\pi i\delta(\omega + \omega_0) & \frac{1}{\omega - \omega_0 + i\delta} - \frac{1}{\omega + \omega_0 - i\delta} \end{pmatrix}. \quad (10.7)$$

The explicit transformation is given in appendix B. The frequency integration within Eq. (10.5) is also carried out in appendix B and we cite here only the final result (B.19)

$$\Sigma_{\lambda^2}^R(\omega) = \Sigma_{\lambda^2}^{++}(\omega) + \Sigma_{\lambda^2}^{+-}(\omega) \\ = \sum_{s_0=\pm 1} \sum_{s_1=\pm 1} \lambda^2 \left(n_B(\omega_0) + \left| \frac{s_0 + s_1}{2} \right| \right) \left[\frac{\frac{1}{2} N_F(-s_1(\omega - s_0\omega_0))}{\omega - s_0\omega_0 - \epsilon_0 + i\Gamma} \right. \\ + \frac{i s_1}{4\pi(\omega - s_0\omega_0 - \epsilon_0 - i\Gamma + s_1 i\delta)} (\Psi(\epsilon_0 + i\Gamma) - \Psi(\omega - s_0\omega_0 + s_1 i\delta)) \\ \left. - \frac{i s_1}{4\pi(\omega - s_0\omega_0 - \epsilon_0 + i\Gamma + s_1 i\delta)} (\bar{\Psi}(\epsilon_0 - i\Gamma) - \bar{\Psi}(\omega - s_0\omega_0 + s_1 i\delta)) \right]. \quad (10.8)$$

The solution is based on the definition

$$\Psi(x) = \psi_0 \left(\frac{1}{2} - \frac{\beta i}{2\pi}(x - \mu_L) \right) + \psi_0 \left(\frac{1}{2} - \frac{\beta i}{2\pi}(x - \mu_R) \right) \quad (10.9)$$

$$\bar{\Psi}(x) = \psi_0 \left(\frac{1}{2} + \frac{\beta i}{2\pi}(x - \mu_L) \right) + \psi_0 \left(\frac{1}{2} + \frac{\beta i}{2\pi}(x - \mu_R) \right), \quad (10.10)$$

with $\psi_0(z)$ being the digamma function.

10.2 Sequential tunneling approximation

Using the sequential tunneling approximation for the spinless AH model allows to access another limit of the parameter space, namely the limit $\Gamma \ll 1/\beta$. The rate equation approach we compare with was published in [86] and here we only summarize the exact adoption to our model. Things get even simpler for our case compared to the model studied in [86] since we neglect spin and have no external bath coupled to our system. For convenience and better comparison we will introduce rescaled quantities to match the definitions of the paper instead of rescaling all of their equations. The differences emerge from a freedom of choice for the hybridization and the units used to describe the oscillator position times its coupling constant. Introducing l_0 , the characteristic length of the oscillator (which will later drop out again), we define

$$\tilde{\Gamma}_\alpha = 2\Gamma_\alpha = 2\pi\nu_\alpha(\epsilon_F)|t_\alpha|^2 \quad ; \quad \tilde{\lambda} = \frac{\sqrt{2}}{l_0}\lambda. \quad (10.11)$$

The basic ingredient of this approach are the sequential tunneling rates which are derived using Fermi's golden rule like also done for the MSCT in the first part of the thesis.

The steady state distribution P_Q is defined by the master equation

$$\dot{\vec{P}} = W\vec{P} = 0 \quad ; \quad \sum_Q P_Q = 1 . \quad (10.12)$$

The above master equation is quite simple because it describes the population of the dot which can only be empty or full, corresponding to only two states $|0\rangle$ and $|1\rangle$.

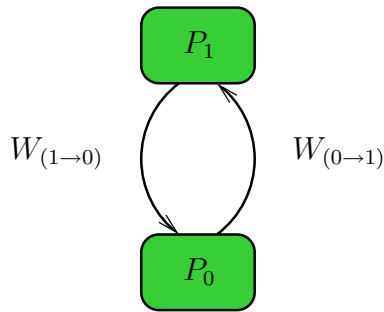


Figure 10.2: Schematic illustration of all levels and rates involved. The states are labeled by their occupation probabilities P_Q .

In contrast to the MSCT we can solve Eq. (10.12) analytically. We replace one redundant rate equation by the normalization condition and get the exactly solvable system

$$\begin{pmatrix} -W_{(0 \rightarrow 1)} & +W_{(1 \rightarrow 0)} \\ 1 & 1 \end{pmatrix} \begin{pmatrix} P_0 \\ P_1 \end{pmatrix} = \begin{pmatrix} 0 \\ 1 \end{pmatrix} . \quad (10.13)$$

The solution is given by

$$P_0 = \frac{W_{(1 \rightarrow 0)}}{W_{(0 \rightarrow 1)} + W_{(1 \rightarrow 0)}} \quad ; \quad P_1 = \frac{W_{(0 \rightarrow 1)}}{W_{(0 \rightarrow 1)} + W_{(1 \rightarrow 0)}} . \quad (10.14)$$

Let us now turn to the rates. Their computation in [86] starts with a polaron transformation followed by a golden rule calculation. The result are the lead dependent sequential tunneling rates

$$W_{(0 \rightarrow 1)} = \sum_{\alpha} \Gamma_{(0 \rightarrow 1)}^{\alpha} \quad ; \quad \Gamma_{(0 \rightarrow 1)}^{\alpha} = \tilde{\Gamma}_{\alpha} \int \frac{d\omega}{2\pi} F_0(+\omega) n_F(+(\tilde{\epsilon}_0 + \omega - \mu_{\alpha})) , \quad (10.15)$$

$$W_{(1 \rightarrow 0)} = \sum_{\alpha} \Gamma_{(1 \rightarrow 0)}^{\alpha} \quad ; \quad \Gamma_{(1 \rightarrow 0)}^{\alpha} = \tilde{\Gamma}_{\alpha} \int \frac{d\omega}{2\pi} F_0(-\omega) n_F(-(\tilde{\epsilon}_0 + \omega - \mu_{\alpha})) . \quad (10.16)$$

Although the AH model used in [86] is spinful, the transition rates are the same like for our spinless system. This stems from the fact, that Braig et al. assume to have an infinite Coulomb repulsion energy and therefore a three state model with only single occupied levels. The difference between the three state and two state approach enters in the dimensionality of the master equation but not within the rates.

Due to the polaron transformation used in Ref. [86], the rates are dependent on a level energy $\tilde{\epsilon}_0$ which results from shifting ϵ_0 by the polaron energy²⁰ ϵ_P , with

$$\tilde{\epsilon}_0 = \epsilon_0 - \epsilon_P \quad ; \quad \epsilon_P = \frac{1}{2}\tilde{\lambda}l \quad ; \quad l = \frac{\tilde{\lambda}}{\omega_0}l_0^2 . \quad (10.17)$$

The function $F_0(\omega)$ is defined by its Fourier transformation

$$F_0(\pm\omega) = \int_{-\infty}^{\infty} e^{\pm i\omega t} F_0(t) \quad ; \quad F_0(t) = \langle e^{+ip_0(t)l} e^{-ip_0(0)l} \rangle . \quad (10.18)$$

For the spinless AH model without external bath $F_0(t)$ is given by

$$F_0(t) = \exp\{g[(e^{+i\omega_0 t} - 1)n_B(+\omega_0) - (e^{-i\omega_0 t} - 1)n_B(-\omega_0)]\} , \quad (10.19)$$

with g being determined from the ratio of the classical displacement length and the quantum mechanical oscillator length

$$g = \frac{1}{2} \left(\frac{\tilde{\lambda}l_0}{\omega_0} \right)^2 . \quad (10.20)$$

Braig et al. claim that the evaluation of $F_0(\omega)$ from Eqs. (10.19) and (10.18) is equivalent to the independent boson model [87], and thus the solution is given by

$$F_0(\omega) = 2\pi \sum_{n=-\infty}^{\infty} P_n(g) \delta(\omega - n\omega_0) , \quad (10.21)$$

where

$$P_n(g) = \mathcal{I}_n \left(\frac{g}{\sinh(\Omega)} \right) e^{n\Omega - g \coth(\Omega)} \quad ; \quad \Omega = \frac{\beta\omega_0}{2} \quad (10.22)$$

and \mathcal{I}_n is the modified Bessel function of the first kind. Inserting the solution into the rates reduces them to the simple form

$$\Gamma_{(0 \rightarrow 1)}^\alpha = \tilde{\Gamma}_\alpha \tilde{n}_\alpha \quad ; \quad \Gamma_{(1 \rightarrow 0)}^\alpha = \Gamma_{(0 \rightarrow 1)}^\alpha e^{\beta(\tilde{\epsilon}_0 - \mu_\alpha)} , \quad (10.23)$$

with

$$\tilde{n}_\alpha = \int_{-\infty}^{\infty} \frac{d\omega}{2\pi} F_0(\omega) n_F(\omega + \tilde{\epsilon}_0) = \sum_{n=-\infty}^{\infty} P_n(g) n_F(\tilde{\epsilon}_0 + n\omega_0 - \mu_\alpha) . \quad (10.24)$$

Knowing the rates and the occupation probabilities immediately yields the expression for the current through the system from the net flow between the left lead and the dot²¹

$$I_L = e(P_0\Gamma_{(0 \rightarrow 1)}^L - P_1\Gamma_{(1 \rightarrow 0)}^L) = -I_R = \frac{I_L - I_R}{2} = I . \quad (10.25)$$

Due to current conservation in the sequential tunneling picture this current is equivalent to the symmetrized current computed by the ISPI method.

²⁰The definition here is consistent with the one later used after back-substituting λ .

²¹Note that in the sequential tunneling picture the relation $\dot{N}_L = -\dot{N}_d$ holds between the lead and dot occupation. The definition (10.25) is consistent with our initial current definition from Eq. (5.5).

10.3 Slow phonon limit - Nonequilibrium Born Oppenheimer approximation (NEBO)

The details of this approximation were developed in [88] and extended in [84]. We just summarize the expressions needed to recover the data we later use for comparison to our ISPI approach and refer to the original publication for more details.

In the limit $\omega_0 \ll \Gamma$ the electronic dynamics of the AH model are much faster than the oscillation of the phonon mode and we can separate the timescales and apply a form of Born-Oppenheimer approximation. From the viewpoint of the “fast” electronic system the oscillator position only enters as a parameter which will slowly change in time. Therefore the electron-phonon coupling is interpreted as a position dependent renormalization of the level energy.

$$\epsilon_\lambda(x) = \epsilon_0 + \lambda x . \quad (10.26)$$

Under these assumptions the electronic system is governed by an adiabatically changing and position dependent GF which directly follows from Eq. (8.30) with the replacement $\epsilon_0 \rightarrow \epsilon_\lambda(x)$

$$G_{0,ad}^{\pm\mp}[\omega, x] = \pm 2i \sum_{\alpha} \Gamma_{\alpha} \frac{n_F(\pm(\omega - \mu_{\alpha}))}{(\omega - \epsilon_{\lambda}(x))^2 + \Gamma^2} . \quad (10.27)$$

On the other hand the electronic system influences the almost classical slow phonon-mode and the oscillator is therefore governed by a Langevin equation in terms of the oscillators coordinate x and a Gaussian noise field $\xi(t)$

$$m\ddot{x}_c + A(x)\dot{x} + m\omega_0^2 x = F(x) + \xi(t) . \quad (10.28)$$

Despite the usual kinetic and potential terms, additionally a position-dependent force $F(x)$ and a damping $A(x)$ enter in the equation of motion for the oscillator. Together with the intensity D of the white noise ($\langle \xi(t)\xi(t') \rangle = D(X)\delta(t-t')$) everything can be expressed by the Keldysh components $G_{0,ad}^{\pm\mp}[\omega, x]$ of the adiabatic electronic GF

$$F(x) = -\frac{\lambda}{2\pi i} \int d\omega G_{0,ad}^{+-}[\omega, x] , \quad (10.29)$$

$$A(x) = +\frac{\lambda^2}{2\pi} \int d\omega G_{0,ad}^{+-}[\omega, x] \partial_{\omega} G_{0,ad}^{-+}[\omega, x] , \quad (10.30)$$

$$D(x) = +\frac{\lambda^2}{2\pi} \int d\omega G_{0,ad}^{+-}[\omega, x] G_{0,ad}^{-+}[\omega, x] . \quad (10.31)$$

The description of the dynamics in terms of a Langevin equation is equivalent to the description by a Fokker-Planck-equation for the probability $\mathcal{P}(x, p, t)$ that at a given time t the displacement and the momentum of the phonon mode are given by x and $p = m\dot{x}$

$$\partial_t \mathcal{P} = -\frac{p}{m} \partial_x \mathcal{P} - F(x) \partial_p \mathcal{P} + \frac{A(x)}{m} \partial_p (p \mathcal{P}) + \frac{D(x)}{2} \partial_p^2 \mathcal{P} \quad ; \quad \mathcal{P} = \mathcal{P}(x, p, t) . \quad (10.32)$$

Due to the position dependence of the adiabatic electronic GF also the corresponding spectral function becomes position dependent and from Eq. (8.18) we get a position

dependent current formula

$$I(x) = \frac{e\Gamma}{h} \int d\epsilon \frac{\Gamma}{\Gamma^2 + (\epsilon - \epsilon_0 - \lambda x)^2} \left(n_F(\epsilon - \mu_L) - n_F(\epsilon - \mu_R) \right). \quad (10.33)$$

By solving the Fokker Planck equation numerically and then averaging Eq. (10.33) over the distribution \mathcal{P} we get our final NEBO result for the current

$$I(t) = \int dx dp \mathcal{P}(x, p, t) I(x). \quad (10.34)$$

In the next sections we present extrapolated and converged numerical results, starting from the noninteracting AH model as first check, then benchmarking against the other analytical methods presented within this chapter and finally accessing the quantum coherent low temperature regime, inaccessible by any kind of perturbative approximation.

11 Numerical results

All numerical results throughout this chapter are computed for the symmetric problem, defined by $\mu_L = -\mu_R = eV/2$, and the hybridization strengths $\Gamma_L = \Gamma_R = \Gamma/2$.

11.1 Check against the RL model

We start with the noninteracting problem ($\lambda = 0$) and depict the result in Fig. 11.1, where the symmetrized tunneling current I is shown as a function of the bias voltage V .

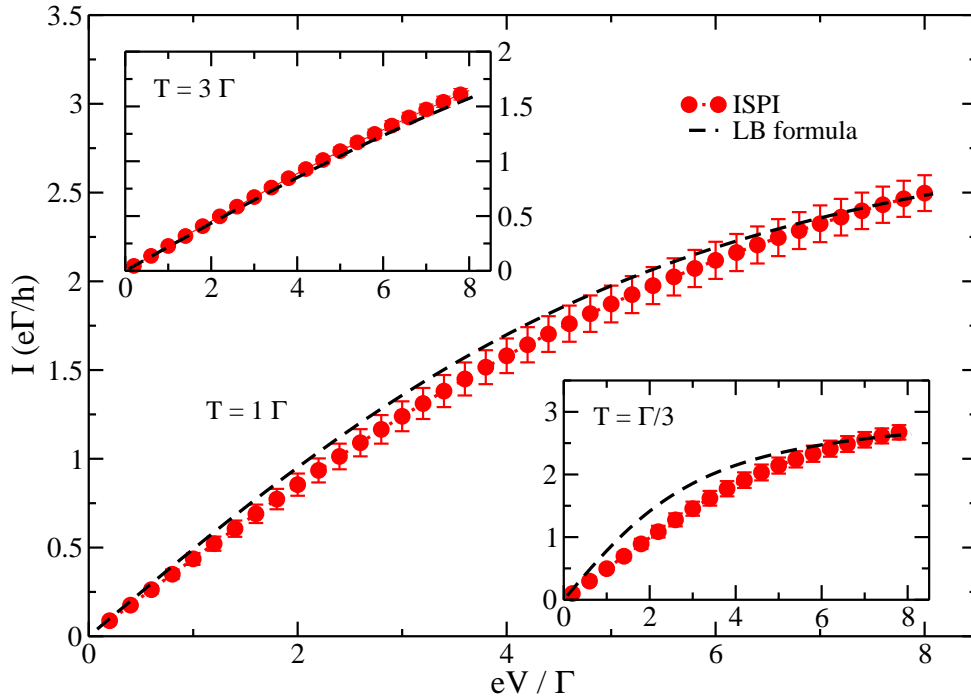


Figure 11.1: $I(V)$ characteristics of the RL model ($\epsilon_0 = \lambda = \omega_0 = 0$). The ISPI data agrees well with the analytical $\lambda = 0$ result for different temperatures and bias voltages.

The fixed parameters are in the main panel $T = \Gamma$, $\epsilon_0 = \lambda = \omega_0 = 0$. For the lower (upper) inset only the temperature is changed to $T = \Gamma/3$ ($T = 3\Gamma$). The analytical results for the RL model are given by Eq. (8.32) which is equal to the Landauer-Büttiker formula for it. Figure 11.1 states excellent agreement between both. For $T = 3$ the overlap of ISPI with the exact result is almost perfect and the small deviations for lower temperatures reflect the fact that by lowering temperature and entering the deep quantum regime, long range correlations become more important. Nevertheless our memory extrapolation scheme works well and keeps these deviations small and controllable. Let us now turn to the full interacting spinless AH model.

11.2 Benchmark against approximative analytics

Next we show that the numerical ISPI results are consistent with different analytical theories valid in special regions of the parameter space (cf. yellow corners in Fig. 10.1 and see explanations at the beginning of chapter 10.) For clarity, we focus on a resonant level with $\epsilon = 0$ here.

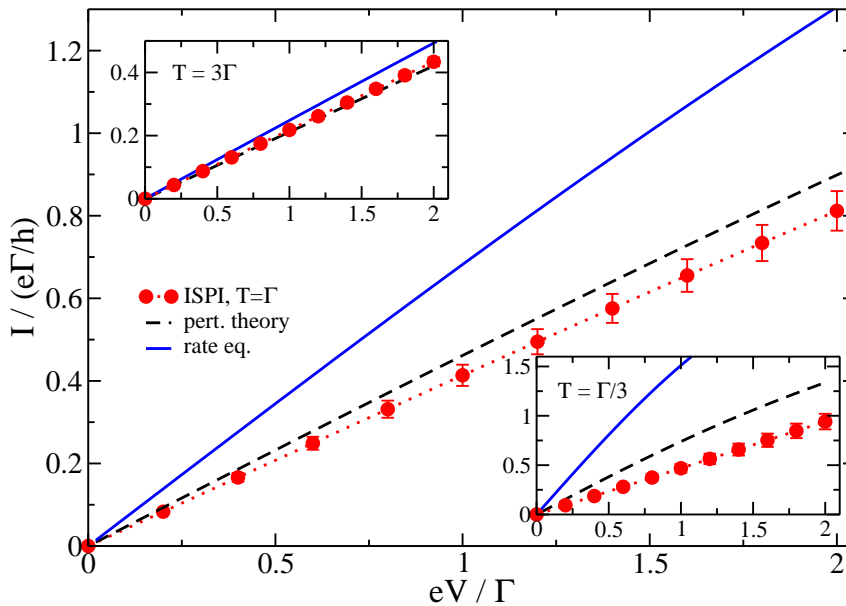


Figure 11.2: Current I (in units of $e\Gamma/h$) vs bias voltage eV (in units of Γ) for $\lambda = 0.5\Gamma$, $\omega_0 = \Gamma$, $\epsilon = 0$, and $T = \Gamma$. The ISPI data are depicted as filled red circles, where the dotted red curve is a guide to the eye only and the error bars are explained in the main text. We also show the results of perturbation theory in λ (dashed black curve) and of the rate equation (solid blue curve). The upper (lower) inset shows the corresponding result for $T = 3\Gamma$ ($T = \Gamma/3$).

Let us start with the case of weak electron-phonon coupling, $\lambda = 0.5\Gamma$. Figure 11.2 compares our ISPI data for $\omega_0 = \Gamma$ to the respective results of perturbation theory in λ and of the rate equation. As expected, for this parameter choice, perturbation theory essentially reproduces the ISPI data. The rate equation is quite accurate for high temperatures, but quantitative agreement with ISPI was obtained only for $T \gtrsim 10\Gamma$. Note that the ISPI error bars increase when lowering T due to the growing memory time (τ_c) demands.

The effect of changing the phonon frequency ω_0 is illustrated in Fig. 11.3, taking $T = \Gamma$ but otherwise identical parameters. Again perturbation theory is well reproduced. Next, Fig. 11.4 shows ISPI results for a slow phonon mode, $\omega_0 = \Gamma/2$, with stronger electron-phonon coupling, $\lambda = \Gamma$. In that case, perturbation theory in λ is not reliable and the rate equation is only accurate at the highest temperature ($T = 3\Gamma$) studied, cf. the upper left inset of Fig. 11.4. However, we observe from Fig. 11.4 that for such a slow phonon mode, NEBO provides a good approximation for all temperatures and/or voltages of interest.

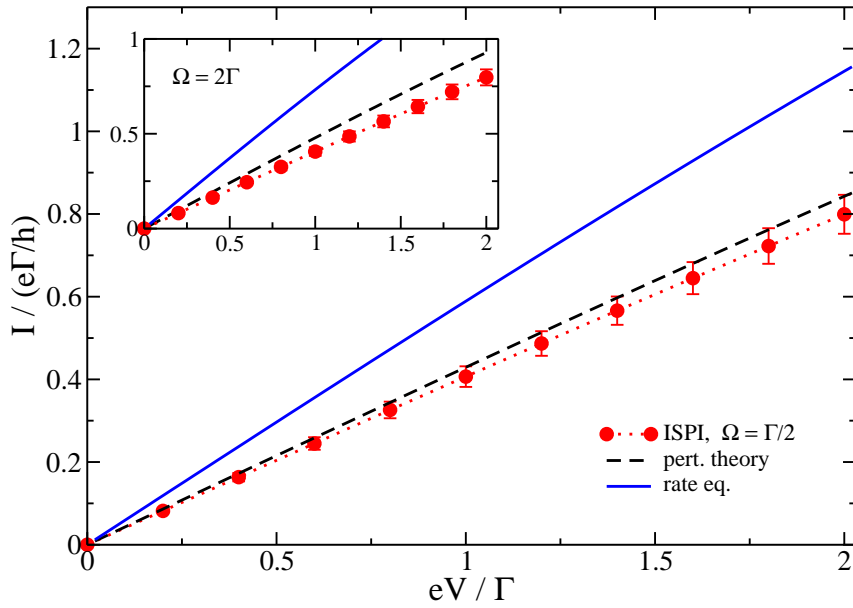


Figure 11.3: Same as Fig. 11.2 but for $\omega_0 = 0.5\Gamma$ (main panel) and $\omega_0 = 2\Gamma$ (inset), both for $T = \Gamma$.

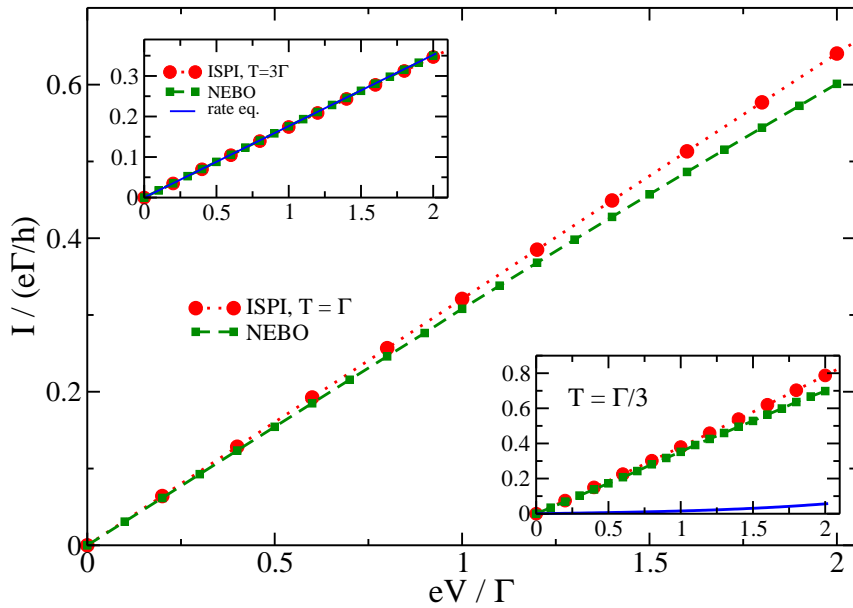


Figure 11.4: Same as Fig. 11.2 but for $\omega_0 = 0.5\Gamma$ and $\lambda = \Gamma$. The main panel is for $T = \Gamma$ and compares the ISPI results to NEBO predictions. The insets are for $T = 3\Gamma$ and $T = \Gamma/3$, respectively, where also the rate equation results are shown. Notice that in contrast to ISPI, the rate equation predicts an unphysical current blockade for $T = \Gamma/3$.

We conclude that the ISPI technique is capable of accurately describing three different analytically tractable parameter regimes.

11.3 Franck-Condon (FC) blockade

Next we address the limit of strong electron-phonon coupling λ , where the rate equation approach yields a FC blockade of the current for low bias and $T \gg \Gamma$ [83]. Sufficiently large λ can be realized experimentally, and the FC blockade has indeed been observed in suspended carbon nanotube quantum dots [51]. Before we proceed with our own results we first provide a qualitative understanding of the physics behind the FC blockade from a sequential tunneling picture, illustrated and explained in Fig. 11.5.

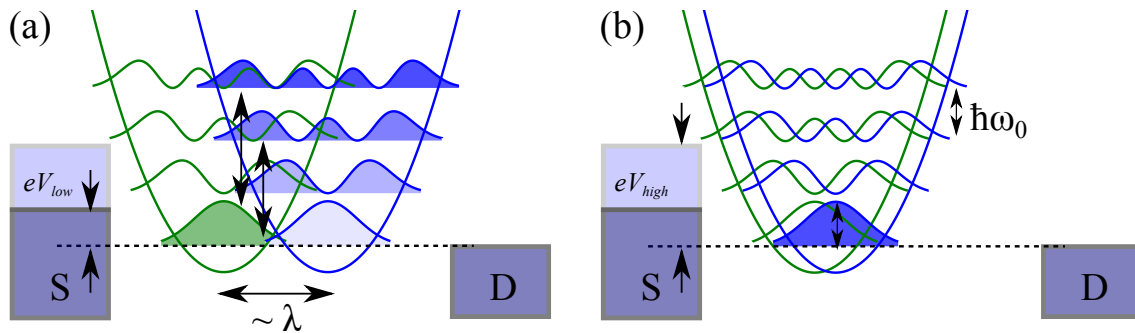


Figure 11.5: Schematic illustration of the FC blockade within a sequential tunneling picture. Regime (a): Large displacement of the oscillator potential for strong electron-phonon coupling ($\lambda \gg \Gamma$). Regime (b): Weak electron-phonon coupling ($\lambda \ll \Gamma$). The shifted parabola (blue) represents a filled and the unshifted (green) an empty dot level. The displacement originates from the direct coupling of the phonon to the dot occupation [cf. Eq. (5.1)]. The shift for $\lambda \gg 1$ in (a) suppresses the transitions between low-lying vibronic states and thus causes the FC blockade of the current in a low-bias regime (eV_{low}). In a high-bias regime (eV_{high}) the same mechanism causes transitions to excited vibronic states (black vertical arrows) yielding vibrational sidebands and a current. For regime (b) there is almost no displacement and thus higher vibronic states stay almost orthogonal to the ground state and suppress sideband excitations. Figure based on [51].

The schematic explanation of the Franck-Condon blockade within Fig. 11.5 is based on some underlying assumptions. First of all one assumes a NEBO limit where electronic transitions are much faster than the resulting shift of the oscillator to adapt to the changed charge state. A factorization of the molecular wave function into an electronic and a vibronic part is justified in this limit and allows for the argumentation based on the vibronic overlaps only. Second, the illustration from Fig. 11.5 only takes into account sequential transitions. The FC blockade is most likely visible in a strong coupling regime, where the displacement of the phonon mode for a charged electronic state with respect to the empty electronic state is large [cf. Fig. 11.5 (a)], but not limited to this strong interacting regime only.

After this qualitative short description let us get back to our approach for the AH model. For an unequilibrated phonon mode with intermediate-to-large λ , understanding the FC blockade in the quantum-coherent low-temperature regime, $T < \Gamma$, is an open theoretical problem. Here multiple phonon excitation and deexcitation effects imply a complicated (unknown) nonequilibrium phonon distribution function, and the one-step tunneling interpretation in terms of FC matrix elements between shifted oscillator parabolas [83] is not applicable anymore. We study this question using our ISPI simulation, which automatically takes into account quantum coherence effects.

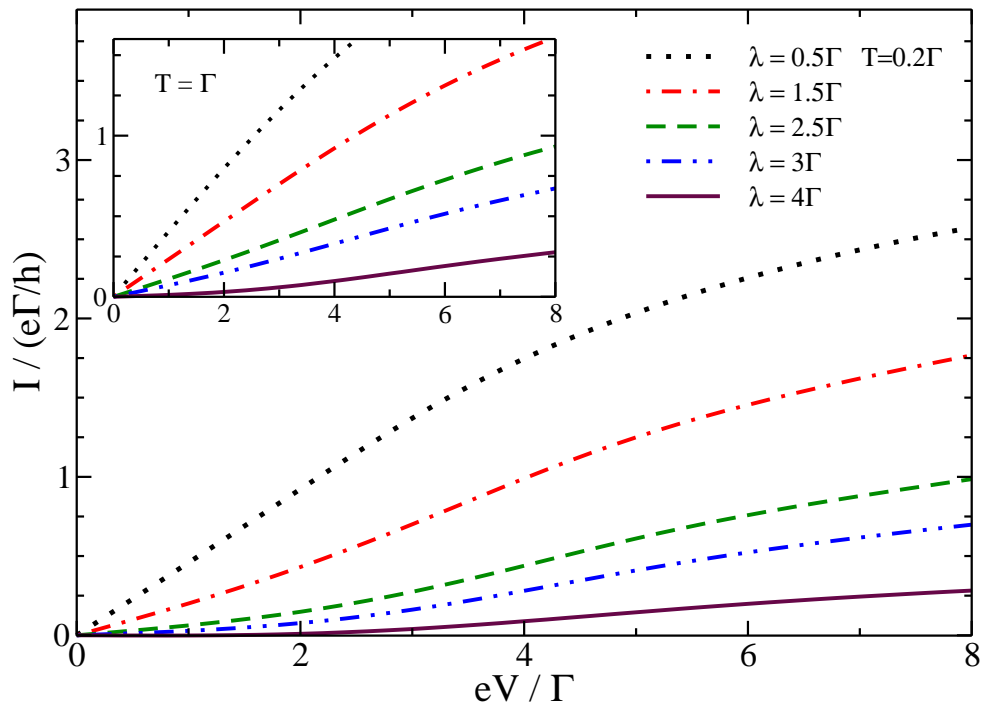


Figure 11.6: ISPI data for the IV curves from weak ($\lambda = 0.5\Gamma$) to strong ($\lambda = 4\Gamma$) electron-phonon coupling, with $\omega_0 = 2\Gamma$. The main panel is for $T = 0.2\Gamma$, the inset for $T = \Gamma$. We used a dense voltage grid yielding smooth IV curves. Error bars are not shown but remain small, cf. Fig. 11.2.

In Fig. 11.6, the crossover from weak to strong electron-phonon coupling λ is considered. The inset shows IV curves for $T = \Gamma$, where we observe a current blockade for low voltages once $\lambda \gtrsim 2\Gamma$. The blockade becomes more pronounced when increasing λ and is lifted for voltages above the polaron energy λ^2/ω_0 [83]. Remarkably, the FC blockade persists and becomes even sharper as one enters the quantum-coherent regime (here, $T = 0.2\Gamma$), despite of the breakdown of the sequential tunneling picture. We also observe a nonequilibrium smearing of phonon step features in the IV curves in Fig. 11.6, cf. also Refs. [51, 83].

12 Conclusions

We have extended the iterative simulation of path integrals (ISPI) technique to the Anderson-Holstein model, which is the simplest nonequilibrium model for quantum dots or molecules with an intrinsic bosonic (phonon) mode. Our formulation exploits a mapping to an effective three-state system which could also be of interest to quantum Monte Carlo schemes. A main difference to the ISPI scheme from [64] is the usage of discrete Green's functions, directly constructed from the real-time path-integral approach instead of gaining them by discretizing continuous Green's functions. We demonstrated how to overcome divergence and convergence problems resulting from the need to use the leads self-energy as stand alone object instead of the full Green's function of the RL model like done in [64]. Extending the ISPI approach from the spinful Anderson model including Coulomb interaction on the dot to the spinless Anderson-Holstein model involving a phonon mode demonstrated also the capability of the ISPI approach to handle interactions which are nonlocal in time. We carefully checked our scheme against the exact solution of the RL model remaining from the AH model in the noninteracting limit and reproduced three analytical approximations valid in different parameter regions of the full interacting AH model. Namely a sequential tunneling approach, a perturbation in the electron-phonon coupling and a nonequilibrium Born Oppenheimer approximation. Our extension of the ISPI approach to the Anderson-Holstein model captures the full crossover between those limits unless both T and V are very small. For a strong electron-phonon coupling and an unequilibrated phonon mode, we find that the Franck-Condon blockade becomes even more pronounced as one enters the quantum coherent regime inaccessible by the three analytical theories. Despite the presented extension of the ISPI scheme and the results shown, there are still open questions. We only presented on resonance results ($\epsilon_0 = 0$) since we still encounter difficulties in perfectly reproducing expected symmetries like $I(\epsilon_0) = I(-\epsilon_0)$ for the RL model within the accessible parameter space of ISPI. We can overcome these problems by smaller δ_t values within the direct current method which ensures that our defined objects are correct but limits us in memory time. A possible way to improve our scheme to become more symmetric could be the usage of a symmetric trotter breakup instead of the naive one, but this might also complicate the iterative scheme and give rise to other complications. Despite of these technical aspects an increase of computational power in the form of more CPUs or an intrinsic parallelization of the code will extend the possible memory-time τ_c and provide further access into the deep quantum regime of the AH model. For a complete review about the ISPI method we also recommend [65] which is to be published soon.

Appendix A: MSCT

A Regularization scheme for cotunneling rates

The infinitesimal complex parts $0+$ introduced during the rate derivation in chapter 2.2.1 are now replaced by $\tilde{\Gamma}_{1,2}$ which reflects the fact, that two different sequential transitions are broadened and virtually involved in each cotunneling rate. Despite this replacement the rates still have to be understood in the limit $\tilde{\Gamma}_{1,2} \rightarrow 0$.

A.1 General structure of the cotunneling rates

The elastic cotunneling rate, transferring an electron from lead j to lead $-j$ (without changing the dot-state) becomes

$$\Gamma_{j,Q}^{(\text{EC})} = \frac{\Gamma_L \Gamma_R}{8\pi} \int d\epsilon n_F[+(\epsilon - \mu_j)] n_F[-(\epsilon - \mu_{-j})] \quad (\text{A.1})$$

$$\times \left| \frac{1}{\epsilon - \epsilon_{(Q \rightarrow Q+1)} + i\tilde{\Gamma}_1} - \frac{1}{\epsilon - \epsilon_{(Q \rightarrow Q-1)} - i\tilde{\Gamma}_2} \right|^2.$$

The inelastic local $j = j'$: $\left\{ \begin{array}{l} s_{jj'} = +1 \\ \rho_{jj'} = 1/2 \end{array} \right\}$ and nonlocal $j \neq j'$: $\left\{ \begin{array}{l} s_{jj'} = -1 \\ \rho_{jj'} = 1 \end{array} \right\}$ rates are

$$\Gamma_{j,j',Q \rightarrow Q \pm 2}^{(\text{AR})} = \rho_{jj'} \frac{\Gamma_j \Gamma_{j'}}{8\pi} \int d\epsilon n_F[\pm(\epsilon - \mu_j)] n_F[\pm(\epsilon_{(Q \rightarrow Q \pm 2)} - \epsilon - \mu_{j'})]$$

$$\times \left| \frac{1}{\epsilon - \epsilon_{(Q \rightarrow Q \pm 1)} \pm i\tilde{\Gamma}_1} - \frac{s_{jj'}}{\epsilon_{(Q \pm 1 \rightarrow Q \pm 2)} - \epsilon \pm i\tilde{\Gamma}_2} \right|^2. \quad (\text{A.2})$$

All cotunneling rates are based on the same integral $K = \int d\epsilon \kappa(\epsilon)$ after introducing

$$\kappa(\epsilon) = n_F[\alpha(\epsilon - \mu_1)] n_F[\alpha(\epsilon_{(a)} - \epsilon - \mu_2)] \left| \frac{1}{\epsilon - \epsilon_{(b)} + \alpha i\tilde{\Gamma}_1} - \frac{s}{\epsilon_{(c)} - \epsilon + \alpha i\tilde{\Gamma}_2} \right|^2. \quad (\text{A.3})$$

Note that we will later exploit the fact that $\alpha, s \in \{\pm\}$ holds and therefore their square equals one. The exact mapping of the rates to this generalized integral is

$$\Gamma_{j,Q}^{(\text{EC})} = \frac{\Gamma_L \Gamma_R}{8\pi} K \left| \begin{array}{l} \left\{ \begin{array}{l} \alpha = 1; \mu_1 = \mu_j; \mu_2 = -\mu_{-j}; s = -1 \\ \epsilon_{(a)} = 0; \epsilon_{(b)} = \epsilon_{(Q \rightarrow Q+1)}; \epsilon_{(c)} = \epsilon_{(Q \rightarrow Q-1)} \end{array} \right\} \end{array} \right., \quad (\text{A.4})$$

$$\Gamma_{j,j',Q \rightarrow Q \pm 2}^{(\text{AR})} = \rho_{jj'} \frac{\Gamma_j \Gamma_{j'}}{8\pi} K \left| \begin{array}{l} \left\{ \begin{array}{l} \alpha = \pm; \mu_1 = \mu_j; \mu_2 = \mu_{j'}; s = s_{jj'} \\ \epsilon_{(a)} = \epsilon_{(Q \rightarrow Q \pm 2)}; \epsilon_{(b)} = \epsilon_{(Q \rightarrow Q \pm 1)}; \epsilon_{(c)} = \epsilon_{(Q \pm 1 \rightarrow Q \pm 2)} \end{array} \right\} \end{array} \right|. \quad (\text{A.5})$$

In the next section we deduce the regularization scheme needed for nondivergent cotunneling rates in the limit $\tilde{\Gamma}_{1,2} \rightarrow 0$.

A.2 Isolation of divergent residuals

The denominator of Eq. (A.3) has leading order ϵ^2 and allows for applying residual theory and therefore isolating the divergences in terms of single divergent residual contributions. After choosing a positive/negative oriented closed contour in the upper/lower complex plane including the real axis and enclosing the poles

$$\begin{aligned} \epsilon_{(b)}^\pm &= \epsilon_{(b)} \pm i\alpha\tilde{\Gamma}_1 \quad ; \quad \epsilon_{(c)}^\pm = \epsilon_{(c)} \pm i\alpha\tilde{\Gamma}_2 \\ \epsilon_{0,a}^\pm(n) &= \mu_1 \pm i\frac{\pi}{\alpha\beta}(2n+1) \quad ; \quad \epsilon_{0,b}^\pm(n) = \epsilon_{(a)} - \mu_2 \pm i\frac{\pi}{\alpha\beta}(2n+1) \quad ; \quad n \in \mathbb{N}^0, \end{aligned}$$

the general (divergent) solution of the integral is the average of both contour-integrations:

$$\begin{aligned} K &= \frac{1}{2} \sum_{s=\pm} (K_{div}^s + K_{reg}^s) \quad ; \quad K_{div}^\pm = \pm 2\pi i \left(\text{Res}(\kappa, \epsilon_{(b)}^\pm) + \text{Res}(\kappa, \epsilon_{(c)}^\pm) \right) \\ K_{reg}^\pm &= \pm 2\pi i \sum_{n=0}^{\infty} \text{Res}(\kappa, \epsilon_{0,a}^\pm(n)) + \text{Res}(\kappa, \epsilon_{0,b}^\pm(n)) . \end{aligned}$$

In principle the average is not necessary here but turns out to be useful, because calculations involve more symmetries to exploit and we stay consistent with [37] where the same idea is used for regularization. The argumentation to justify the regularization scheme is the following: the divergence is only caused by the four residuals

$$\begin{aligned} \text{Res}(\kappa, \epsilon_{(b)}^\pm) &= \frac{\pm i \left((\epsilon_{(c)} - \epsilon_{(b)}) \mp i\alpha \left((1+2s)\tilde{\Gamma}_1 - \tilde{\Gamma}_2 \right) \right) / 2\alpha\tilde{\Gamma}_1}{\left(e^{\alpha\beta(\epsilon_{(b)} - \mu_1)} + e^{\mp i\beta\tilde{\Gamma}_1} \right) \left(e^{\alpha\beta(\epsilon_{(a)} - \epsilon_{(b)} - \mu_2)} + e^{\pm i\beta\tilde{\Gamma}_1} \right) (\epsilon_{(b)} - \epsilon_{(c)} \pm i\alpha(\tilde{\Gamma}_1 - \tilde{\Gamma}_2))} \\ \text{Res}(\kappa, \epsilon_{(c)}^\pm) &= \frac{\pm i \left(((\epsilon_{(b)} - \epsilon_{(c)}) \mp i\alpha \left((1+2s)\tilde{\Gamma}_2 - \tilde{\Gamma}_1 \right)) \right) / 2\alpha\tilde{\Gamma}_2}{\left(e^{\alpha\beta(\epsilon_{(c)} - \mu_1)} + e^{\mp i\beta\tilde{\Gamma}_2} \right) \left(e^{\alpha\beta(\epsilon_{(a)} - \epsilon_{(c)} - \mu_2)} + e^{\pm i\beta\tilde{\Gamma}_2} \right) (\epsilon_{(c)} - \epsilon_{(b)} \pm i\alpha(\tilde{\Gamma}_2 - \tilde{\Gamma}_1))} . \end{aligned}$$

They can be approximated²² by their leading order in $\mathcal{O}(1/\tilde{\Gamma}_{1,2})$ for $\tilde{\Gamma}_{1,2} \rightarrow 0$:

$$\begin{aligned} K_{div}^\pm &= \frac{\pi}{\alpha\tilde{\Gamma}_1} n_F[\alpha(\epsilon_{(b)} - \mu_1)] n_F[\alpha(\epsilon_{(a)} - \epsilon_{(b)} - \mu_2)] \\ &\quad + \frac{\pi}{\alpha\tilde{\Gamma}_2} n_F[\alpha(\epsilon_{(c)} - \mu_1)] n_F[\alpha(\epsilon_{(a)} - \epsilon_{(c)} - \mu_2)] + \mathcal{O}(\tilde{\Gamma}_{1,2}) . \end{aligned}$$

The remaining contributions to the integral are all nondivergent and encoded in K_{reg} , evaluated later. Having now the exact expression for K_{div} we have to justify why it is physically necessary to omit this part in the rates.

²²Anyway one can also show that the $\mathcal{O}(1/\tilde{\Gamma}_{1,2})$ terms will cancel each other and do not contribute to K at all.

A.3 The regularization scheme - Physical motivation

The idea from [37], is to argue that whatever is explicitly chosen for $\tilde{\Gamma}_{1,2}$ must be constructed out of sequential rates and therefore has a leading order of Γ . Plugging this into the divergent part of the cotunneling rates, reduces their leading order from Γ^2 to only Γ . But this corresponds per definition to something in first order, which is already fully included in the sequential rates. Since the limit $\tilde{\Gamma}_{1,2}$ will be performed for the nondivergent part, the exact expression for $\tilde{\Gamma}_{1,2}$ is not of interest, and the rates using K_{reg} in the limit of $\tilde{\Gamma}_{1,2} \rightarrow 0$ are the desired regularized rates.

A numerical and analytical verification of this way of regularization is given in section 2.4.1, where we have computed the linear conductance for $E_c = 0$ from the regularized rates analytically and numerically and compared it to the exact solution from Eq. (2.76) and found a very good agreement.

A.4 The regularized integral

From the two Fermi-distributions we get the following infinite sets of residues from their poles located in the upper/lower complex plane dependent on the choice of the $+/-$ sign

$$\begin{aligned} \text{Res}(\kappa, \epsilon_{0,a}^{\pm}(n)) &= + \frac{n_B[\alpha(\epsilon_{(a)} - \mu_1 - \mu_2)]}{\alpha\beta} \\ &\times \frac{\frac{i\pi(2n+1)(1+s)}{\alpha\beta} \mp \left(\epsilon_{(c)} + \epsilon_{(b)}s - \mu_1(1+s) \pm i\alpha(\tilde{\Gamma}_1s - \tilde{\Gamma}_2)\right)}{\left(\frac{i\pi}{\alpha\beta}(2n+1) \mp (\epsilon_{(b)} - \mu_1 \pm i\alpha\tilde{\Gamma}_1)\right) \left(\frac{i\pi}{\alpha\beta}(2n+1) \mp (\epsilon_{(b)} - \mu_1 \mp i\alpha\tilde{\Gamma}_1)\right)} \\ &\times \frac{\frac{i\pi(2n+1)(1+s)}{\alpha\beta} \mp \left(\epsilon_{(c)} + \epsilon_{(b)}s - \mu_1(1+s) \mp i\alpha(\tilde{\Gamma}_1s - \tilde{\Gamma}_2)\right)}{\left(\frac{i\pi}{\alpha\beta}(2n+1) \mp (\epsilon_{(c)} - \mu_1 \pm i\alpha\tilde{\Gamma}_2)\right) \left(\frac{i\pi}{\alpha\beta}(2n+1) \mp (\epsilon_{(c)} - \mu_1 \mp i\alpha\tilde{\Gamma}_2)\right)}, \end{aligned} \quad (\text{A.6})$$

$$\begin{aligned} \text{Res}(\kappa, \epsilon_{0,b}^{\pm}(n)) &= - \frac{n_B[\alpha(\epsilon_{(a)} - \mu_1 - \mu_2)]}{\alpha\beta} \\ &\times \frac{\frac{i\pi(2n+1)(1+s)}{\alpha\beta} \pm \left(\epsilon_{(a)}(1+s) - \epsilon_{(b)}s - \epsilon_{(c)} - \mu_2(1+s) \mp i\alpha(\tilde{\Gamma}_1s - \tilde{\Gamma}_2)\right)}{\left(\frac{i\pi}{\alpha\beta}(2n+1) \pm (\epsilon_{(a)} - \epsilon_{(b)} - \mu_2 \mp i\alpha\tilde{\Gamma}_1)\right) \left(\frac{i\pi}{\alpha\beta}(2n+1) \pm (\epsilon_{(a)} - \epsilon_{(b)} - \mu_2 \pm i\alpha\tilde{\Gamma}_1)\right)} \\ &\times \frac{\frac{i\pi(2n+1)(1+s)}{\alpha\beta} \pm \left(\epsilon_{(a)}(1+s) - \epsilon_{(b)}s - \epsilon_{(c)} - \mu_2(1+s) \pm i\alpha(\tilde{\Gamma}_1s - \tilde{\Gamma}_2)\right)}{\left(\frac{i\pi}{\alpha\beta}(2n+1) \pm (\epsilon_{(a)} - \epsilon_{(c)} - \mu_2 \mp i\alpha\tilde{\Gamma}_2)\right) \left(\frac{i\pi}{\alpha\beta}(2n+1) \pm (\epsilon_{(a)} - \epsilon_{(c)} - \mu_2 \pm i\alpha\tilde{\Gamma}_2)\right)}. \end{aligned} \quad (\text{A.7})$$

Inserting these residuals in $K_{reg} = \lim_{\tilde{\Gamma}_{1,2} \rightarrow 0} (K_{reg}^+ + K_{reg}^-)/2$ will result in a sum of convergent series.

Based on the identity 8.363 (3.) from [74]

$$\sum_{n=0}^{\infty} \left(\frac{1}{y+k} - \frac{1}{x+k} \right) = \psi_0(x) - \psi_0(y) \quad (\text{A.8})$$

it is possible to express K_{reg} in terms of the digamma-function ψ_0 and it's derivative, the trigamma-function ψ_1 :

$$\begin{aligned} \lim_{\tilde{\Gamma}_{1,2} \rightarrow 0} K_{reg,a}^{\pm} &= \pm 2\pi i \sum_{n=0}^{\infty} \lim_{\tilde{\Gamma}_{1,2} \rightarrow 0} \text{Res}(\kappa, \epsilon_{0,a}^{\pm}) = n_B[\alpha(\epsilon_{(a)} - \mu_1 - \mu_2)] \\ &\times \left(\frac{2s}{(\epsilon_{(b)} - \epsilon_{(c)})} \left(\psi_0 \left[\frac{1}{2} \pm \frac{i\alpha\beta}{2\pi}(\epsilon_{(c)} - \mu_1) \right] - \psi_0 \left[\frac{1}{2} \pm \frac{i\alpha\beta}{2\pi}(\epsilon_{(b)} - \mu_1) \right] \right) \right. \\ &\left. \pm \frac{\alpha\beta}{2\pi i} \left(\psi_1 \left[\frac{1}{2} \pm \frac{i\alpha\beta}{2\pi}(\epsilon_{(c)} - \mu_1) \right] + \psi_1 \left[\frac{1}{2} \pm \frac{i\alpha\beta}{2\pi}(\epsilon_{(b)} - \mu_1) \right] \right) \right) \end{aligned} \quad (\text{A.9})$$

$$\begin{aligned} \lim_{\tilde{\Gamma}_{1,2} \rightarrow 0} K_{reg,b}^{\pm} &= \pm 2\pi i \sum_{n=0}^{\infty} \lim_{\tilde{\Gamma}_{1,2} \rightarrow 0} \text{Res}(\kappa, \epsilon_{0,b}^{\pm}) = n_B[\alpha(\epsilon_{(a)} - \mu_1 - \mu_2)] \\ &\times \left(\frac{2s}{(\epsilon_{(c)} - \epsilon_{(b)})} \left(\psi_0 \left[\frac{1}{2} \pm \frac{i\alpha\beta}{2\pi}(\epsilon_{(c)} - \epsilon_{(a)} + \mu_2) \right] - \psi_0 \left[\frac{1}{2} \pm \frac{i\alpha\beta}{2\pi}(\epsilon_{(b)} - \epsilon_{(a)} + \mu_2) \right] \right) \right. \\ &\left. \mp \frac{\alpha\beta}{2\pi i} \left(\psi_1 \left[\frac{1}{2} \pm \frac{i\alpha\beta}{2\pi}(\epsilon_{(c)} - \epsilon_{(a)} + \mu_2) \right] + \psi_1 \left[\frac{1}{2} \pm \frac{i\alpha\beta}{2\pi}(\epsilon_{(b)} - \epsilon_{(a)} + \mu_2) \right] \right) \right) . \end{aligned} \quad (\text{A.10})$$

By introducing shorthand notations with z^* being the complex conjugated of z

$$\text{Re}\psi_0[z] := \frac{1}{2}(\psi_0[z] + \psi_0[z^*]) \quad ; \quad \text{Im}\psi_1[z] := \frac{1}{2i}(\psi_1[z] - \psi_1[z^*]) \quad (\text{A.11})$$

and adding everything we end up at the final compact and regularized version of K :

$$\begin{aligned} K_{reg} &= n_B[\alpha(\epsilon_{(a)} - \mu_1 - \mu_2)] \\ &\times \left(\frac{2s}{(\epsilon_{(b)} - \epsilon_{(c)})} \left(\text{Re}\psi_0 \left[\frac{1}{2} + \frac{i\alpha\beta}{2\pi}(\epsilon_{(c)} - \mu_1) \right] - \text{Re}\psi_0 \left[\frac{1}{2} + \frac{i\alpha\beta}{2\pi}(\epsilon_{(b)} - \mu_1) \right] \right) \right. \\ &\quad \left. + \frac{\alpha\beta}{2\pi} \left(\text{Im}\psi_1 \left[\frac{1}{2} + \frac{i\alpha\beta}{2\pi}(\epsilon_{(c)} - \mu_1) \right] + \text{Im}\psi_1 \left[\frac{1}{2} + \frac{i\alpha\beta}{2\pi}(\epsilon_{(b)} - \mu_1) \right] \right) \right) \\ &+ \frac{2s}{(\epsilon_{(c)} - \epsilon_{(b)})} \left(\text{Re}\psi_0 \left[\frac{1}{2} + \frac{i\alpha\beta}{2\pi}(\epsilon_{(c)} - \epsilon_{(a)} + \mu_2) \right] - \text{Re}\psi_0 \left[\frac{1}{2} + \frac{i\alpha\beta}{2\pi}(\epsilon_{(b)} - \epsilon_{(a)} + \mu_2) \right] \right) \\ &\quad \left. - \frac{\alpha\beta}{2\pi} \left(\text{Im}\psi_1 \left[\frac{1}{2} + \frac{i\alpha\beta}{2\pi}(\epsilon_{(c)} - \epsilon_{(a)} + \mu_2) \right] + \text{Im}\psi_1 \left[\frac{1}{2} + \frac{i\alpha\beta}{2\pi}(\epsilon_{(b)} - \epsilon_{(a)} + \mu_2) \right] \right) \right) . \end{aligned} \quad (\text{A.12})$$

A.5 Special limits

Let us now also compute several limits of this expression. First there is still a singularity inside the Bose-distribution. Whenever this singularity is hit we switch to the following expression:

$$\lim_{\epsilon_{(a)} \rightarrow (\mu_1 + \mu_2)} K_{reg} = \frac{s}{(\epsilon_{(b)} - \epsilon_{(c)})\pi} \left(\text{Im}\psi_1 \left[\frac{1}{2} + \frac{i\alpha\beta}{2\pi}(\epsilon_{(b)} - \mu_1) \right] - \text{Im}\psi_1 \left[\frac{1}{2} + \frac{i\alpha\beta}{2\pi}(\epsilon_{(c)} - \mu_1) \right] \right) + \frac{\alpha\beta}{4\pi^2} \left(\text{Re}\psi_2 \left[\frac{1}{2} + \frac{i\alpha\beta}{2\pi}(\epsilon_{(b)} - \mu_1) \right] + \text{Re}\psi_2 \left[\frac{1}{2} + \frac{i\alpha\beta}{2\pi}(\epsilon_{(c)} - \mu_1) \right] \right) .$$

Secondly by carefully taking the limits $\epsilon_{(b)} \rightarrow \epsilon_{(c)}$ and $E_{0,2} \rightarrow 0$ we get the regularized $E_c = 0$ result used in section 2.4.1:

$$K_{reg}|_{E_c=0} = \lim_{E_{0,2} \rightarrow 0} \left[\lim_{\epsilon_{(b)} \rightarrow \epsilon_{(c)}} K_{reg} \right] \tag{A.13}$$

$$= \left[1 + n_B[\alpha(\mu_1 + \mu_2)] \right] \frac{\alpha\beta(1+s)}{\pi} \left[\text{Im}\psi_1 \left[\frac{1}{2} + i\frac{\alpha\beta}{2\pi}\mu_1 \right] + \text{Im}\psi_1 \left[\frac{1}{2} + i\frac{\alpha\beta}{2\pi}\mu_2 \right] \right] .$$

It only gives a contribution for $s \neq -1$, i.e., only processes not involving both leads can contribute in the $E_c = 0$ case. This can also be seen directly from Eq. (A.3) in the limit $E_c \rightarrow 0$ and accordingly $\tilde{\Gamma}_{1,2} \rightarrow \tilde{\Gamma}$. Again there is a singularity inside the Bose-distribution, and in the case when it is hit we will switch to the limit

$$\lim_{\mu_2 \rightarrow -\mu_1} (K_{reg}|_{E_c=0}) = \frac{\alpha\beta(1+s)}{2\pi^2} \left(\text{Re}\psi_2 \left[\frac{1}{2} + i\frac{\alpha\beta}{2\pi}\mu_1 \right] \right) . \tag{A.14}$$

Appendix B: ISPI

B Perturbation theory at finite temperature

B.1 Green's function of the "free" phonon

B.1.1 Time representation

We start from the standard definition with time-arguments defined on the Keldysh contour

$$G_Q(t, t') = -i \langle \mathcal{T}_C \{ \hat{Q}(t) \hat{Q}(t') \} \rangle \equiv \begin{pmatrix} G_Q^{++} & G_Q^{+-} \\ G_Q^{-+} & G_Q^{--} \end{pmatrix} \equiv \begin{pmatrix} G_Q^T(t, t') & G_Q^<(t, t') \\ G_Q^>(t, t') & G_Q^{\bar{T}}(t, t') \end{pmatrix}. \quad (\text{B.1})$$

The time evolution of the position operators follows from Heisenberg's equation of motion

$$\hat{Q}(t) = \hat{b}(t) + \hat{b}^\dagger(t) \quad ; \quad \hat{b}(t) = \hat{b} e^{-i\omega_0 t} \quad ; \quad \hat{b}^\dagger(t) = \hat{b}^\dagger e^{+i\omega_0 t}. \quad (\text{B.2})$$

As example we now write down the causal Green's function of the phonon:

$$G_Q^T(t, t') = -i \langle T \{ \hat{Q}(t) \hat{Q}(t') \} \rangle = -i \left[\theta(t - t') \langle \hat{Q}(t) \hat{Q}(t') \rangle + \theta(t' - t) \langle \hat{Q}(t') \hat{Q}(t) \rangle \right]. \quad (\text{B.3})$$

The individual correlators can be directly evaluated in terms of the Bose-distribution, e.g.

$$\begin{aligned} \langle \hat{Q}(t) \hat{Q}(t') \rangle &= \langle (\hat{b} e^{-i\omega_0 t} + \hat{b}^\dagger e^{+i\omega_0 t}) (\hat{b} e^{-i\omega_0 t'} + \hat{b}^\dagger e^{+i\omega_0 t'}) \rangle \\ &= \langle \hat{b} \hat{b} \rangle e^{-i\omega_0(t-t')} + \langle \hat{b}^\dagger \hat{b} \rangle e^{+i\omega_0(t-t')} \\ &= (n_B(\omega_0) + 1) e^{-i\omega_0(t-t')} + n_B(\omega_0) e^{+i\omega_0(t-t')}. \end{aligned} \quad (\text{B.4})$$

Analogously we get

$$\langle \hat{Q}(t') \hat{Q}(t) \rangle = (n_B(\omega_0) + 1) e^{+i\omega_0(t-t')} + n_B(\omega_0) e^{-i\omega_0(t-t')}. \quad (\text{B.5})$$

Collecting all terms leads to the full Keldysh component

$$G_Q^T(t, t') = -i \left[(n_B(\omega_0) + 1) e^{-i\omega_0|t-t'|} + n_B(\omega_0) e^{+i\omega_0|t-t'|} \right]. \quad (\text{B.6})$$

All other Keldysh components are derived similarly and we end up with

$$iG_Q(t, t') = (n_B(\omega) + 1) \begin{pmatrix} e^{-i\omega_0|t-t'|} & e^{+i\omega_0(t-t')} \\ e^{-i\omega_0(t-t')} & e^{+i\omega_0|t-t'|} \end{pmatrix} + n_B(\omega) \begin{pmatrix} e^{+i\omega_0|t-t'|} & e^{-i\omega_0(t-t')} \\ e^{+i\omega_0(t-t')} & e^{-i\omega_0|t-t'|} \end{pmatrix}. \quad (\text{B.7})$$

B.1.2 Frequency representation

For the computation of the self-energy correction according to Eq. (10.5) we need the Fourier transform of $G_Q(t, t')$. Since it only depends on time differences we substitute

$(t - t') \rightarrow t$. The Fourier transform will only affect the phase factors. The off-diagonal components are again simple and follow from

$$-\mathrm{i} \int dt e^{\mathrm{i}\omega t} e^{\pm \mathrm{i}\omega_0 t} = -2\pi \mathrm{i} \delta(\omega \pm \omega_0) . \quad (\text{B.8})$$

For the diagonal ones we need again a functional representation of the Heaviside step function

$$\theta(t) = -\lim_{\delta \rightarrow 0} \int \frac{dx}{2\pi \mathrm{i}} \frac{e^{-ixt}}{x + \mathrm{i}\delta} . \quad (\text{B.9})$$

We get:

$$\begin{aligned} -\mathrm{i} \int dt e^{\mathrm{i}\omega t} e^{\pm \mathrm{i}\omega_0 |t|} &= -\mathrm{i} \left[\int dt \{ \theta(t) e^{\mathrm{i}(\omega \pm \omega_0)t} + \theta(-t) e^{\mathrm{i}(\omega \pm \omega_0)t} \} \right] \\ &= \frac{1}{2\pi} \left[\int \frac{dx}{x + \mathrm{i}\delta} \int dt \{ e^{\mathrm{i}(\omega \pm \omega_0 - x)t} + e^{\mathrm{i}(\omega \pm \omega_0 + x)t} \} \right] \\ &= \int \frac{dx}{x + \mathrm{i}\delta} \{ \delta(\omega \pm \omega_0 - x) + \delta(\omega \pm \omega_0 + x) \} \\ &= \frac{1}{\omega \pm \omega_0 + \mathrm{i}\delta} - \frac{1}{\omega \mp \omega_0 - \mathrm{i}\delta} . \end{aligned} \quad (\text{B.10})$$

Finally, the complete bosonic Green's function in frequency space reads:

$$\begin{aligned} G_Q(\omega) &= (n_B(\omega_0) + 1) \begin{pmatrix} \frac{1}{\omega - \omega_0 + \mathrm{i}\delta} - \frac{1}{\omega + \omega_0 - \mathrm{i}\delta} & -2\pi \mathrm{i} \delta(\omega + \omega_0) \\ -2\pi \mathrm{i} \delta(\omega - \omega_0) & \frac{1}{\omega + \omega_0 + \mathrm{i}\delta} - \frac{1}{\omega - \omega_0 - \mathrm{i}\delta} \end{pmatrix} \\ &\quad + (n_B(\omega_0)) \begin{pmatrix} \frac{1}{\omega + \omega_0 + \mathrm{i}\delta} - \frac{1}{\omega - \omega_0 - \mathrm{i}\delta} & -2\pi \mathrm{i} \delta(\omega - \omega_0) \\ -2\pi \mathrm{i} \delta(\omega + \omega_0) & \frac{1}{\omega - \omega_0 + \mathrm{i}\delta} - \frac{1}{\omega + \omega_0 - \mathrm{i}\delta} \end{pmatrix} . \end{aligned} \quad (\text{B.11})$$

Due to $\omega_0 > 0$ and by setting $n_B(\omega_0) = -\theta(-\omega_0) = 0$ reproduces the correct $T = 0$ Green's function used in [79].

B.2 The second order retarded self-energy

In this section we perform all integrations needed to get the the second order retarded self-energy $\Sigma_{\lambda_2}^R(\omega) = \Sigma_{\lambda_2}^{++}(\omega) + \Sigma_{\lambda_2}^{+-}(\omega)$ at finite temperature by solving

$$\Sigma_{\lambda_2}^{\pm\pm}(\omega) = \pm \mathrm{i} \lambda^2 \int \frac{d\Omega}{2\pi} G_Q^{\pm\pm}(\Omega) G_0^{\pm\pm}(\omega - \Omega) . \quad (\text{B.12})$$

B.2.1 The causal component of the self energy

We start with the causal component, defined by

$$\begin{aligned} \Sigma_{\lambda_2}^{++}(\omega) &= \mathrm{i} \lambda^2 \int \frac{d\Omega}{2\pi} G_Q^{++}(\Omega) G_0^{++}(\omega - \Omega) \\ &= \mathrm{i} \lambda^2 \sum_{s_0, s_1 = \pm} s_1 \left(n_B(\omega_0) + \left| \frac{s_0 + s_1}{2} \right| \right) \underbrace{\int \frac{d\Omega}{2\pi} \frac{G_0^{++}(\omega - \Omega)}{\Omega - s_0 \omega_0 + s_1 \mathrm{i}\delta}}_{:= I_0[s_0, s_1]} . \end{aligned} \quad (\text{B.13})$$

The solution of $I_0[s_0, s_1]$ will be carried out later, but we already state the result:

$$\begin{aligned}
 I_0[s_0, s_1] &= \frac{\text{i} N_F(\omega - s_0\omega_0)}{2(\omega - s_0\omega_0 - \epsilon_0 + s_1\text{i}\Gamma)} - \frac{\delta_{s_1,1}\text{i}(\omega - s_0\omega_0 - \epsilon_0 - \text{i}\Gamma)}{(\omega - s_0\omega_0 - \epsilon_0)^2 + \Gamma^2} \\
 &+ \frac{1}{4\pi(\omega - s_0\omega_0 - \epsilon_0 - \text{i}\Gamma)} (\Psi(\epsilon_0 + \text{i}\Gamma) - \Psi(\omega - s_0\omega_0)) \\
 &- \frac{1}{4\pi(\omega - s_0\omega_0 - \epsilon_0 + \text{i}\Gamma)} (\bar{\Psi}(\epsilon_0 - \text{i}\Gamma) - \bar{\Psi}(\omega - s_0\omega_0)) . \tag{B.14}
 \end{aligned}$$

The above result involves the definition

$$\Psi(x) = \psi_0 \left(\frac{1}{2} - \frac{\beta\text{i}}{2\pi}(x - \mu_L) \right) + \psi_0 \left(\frac{1}{2} - \frac{\beta\text{i}}{2\pi}(x - \mu_R) \right) \tag{B.15}$$

$$\bar{\Psi}(x) = \psi_0 \left(\frac{1}{2} + \frac{\beta\text{i}}{2\pi}(x - \mu_L) \right) + \psi_0 \left(\frac{1}{2} + \frac{\beta\text{i}}{2\pi}(x - \mu_R) \right) , \tag{B.16}$$

based on the digamma function $\psi_0(z)$.

B.2.2 The lesser component of the self-energy

We can now write $\Sigma_{\lambda^2}^{+-}$ in a form, analogous to (B.13)

$$\begin{aligned}
 \Sigma_{\lambda^2}^{+-}(\omega) &= -\text{i}\lambda^2 \int \frac{d\Omega}{2\pi} G_Q^{+-}(\Omega) G_0^{+-}(\omega - \Omega) \\
 &= -\text{i}\lambda^2 \int \frac{d\Omega}{2\pi} \frac{2\pi\Gamma N_F(\omega - \Omega)}{(\omega - \Omega - \epsilon_0)^2 + \Gamma^2} [(n_B(\omega_0) + 1)\delta(\Omega + \omega_0) + n_B(\omega_0)\delta(\Omega - \omega_0)] \\
 &= -\text{i}\Gamma\lambda^2 \left\{ \frac{(n_B(\omega_0) + 1)N_F(\omega + \omega_0)}{(\omega + \omega_0 - \epsilon_0)^2 + \Gamma^2} + \frac{n_B(\omega_0)N_F(\omega - \omega_0)}{(\omega - \omega_0 - \epsilon_0)^2 + \Gamma^2} \right\} \\
 &= \text{i}\lambda^2 \sum_{s_0, s_1 = \pm 1} s_1 \left(n_B(\omega_0) + \left| \frac{s_0 + s_1}{2} \right| \right) \frac{\delta_{s_1, -1}\Gamma N_F(\omega - s_0\omega_0)}{(\omega - s_0\omega_0 - \epsilon_0)^2 + \Gamma^2} . \tag{B.17}
 \end{aligned}$$

B.2.3 The retarded self-energy

Let us first calculate an auxiliary relation

$$\begin{aligned}
 &\frac{\text{i} N_F(\omega - s_0\omega_0)}{2(\omega - s_0\omega_0 - \epsilon_0 + s_1\text{i}\Gamma)} - \frac{\delta_{s_1,1}\text{i}(\omega - s_0\omega_0 - \epsilon_0 - \text{i}\Gamma)}{(\omega - s_0\omega_0 - \epsilon_0)^2 + \Gamma^2} + \frac{\delta_{s_1,-1}\Gamma N_F(\omega - s_0\omega_0)}{(\omega - s_0\omega_0 - \epsilon_0)^2 + \Gamma^2} \\
 &= \frac{1}{(\omega - s_0\omega_0 - \epsilon_0)^2 + \Gamma^2} \left\{ \delta_{s_1,1} \frac{\text{i}}{2} N_F(\omega - s_0\omega_0)(\omega - s_0\omega_0 - \epsilon_0 - \text{i}\Gamma) - \delta_{s_1,1}\text{i}(\omega - s_0\omega_0 - \epsilon_0 - \text{i}\Gamma) \right. \\
 &\quad \left. + \delta_{s_1,-1} \frac{\text{i}}{2} N_F(\omega - s_0\omega_0)(\omega - s_0\omega_0 - \epsilon_0 + \text{i}\Gamma) + \delta_{s_1,-1}\Gamma N_F(\omega - s_0\omega_0) \right\} \\
 &= \frac{1}{(\omega - s_0\omega_0 - \epsilon_0)^2 + \Gamma^2} \left\{ \delta_{s_1,1} \frac{\text{i}}{2} [N_F(\omega - s_0\omega_0) - 2](\omega - s_0\omega_0 - \epsilon_0 - \text{i}\Gamma) \right. \\
 &\quad \left. + \delta_{s_1,-1} \frac{\text{i}}{2} N_F(\omega - s_0\omega_0)(\omega - s_0\omega_0 - \epsilon_0 - \text{i}\Gamma) \right\} \\
 &= \frac{\text{i}}{2} \frac{[-s_1 N_F(-s_1(\omega - s_0\omega_0))]}{\omega - s_0\omega_0 - \epsilon_0 + \text{i}\Gamma} . \tag{B.18}
 \end{aligned}$$

Now we can collect everything and arrive at the final result for the retarded self-energy:

$$\begin{aligned}
 \Sigma_{\lambda^2}^R(\omega) &= \Sigma_{\lambda^2}^{++}(\omega) + \Sigma_{\lambda^2}^{+-}(\omega) \\
 &= \sum_{s_0=\pm 1} \sum_{s_1=\pm 1} \lambda^2 \left(n_B(\omega_0) + \left| \frac{s_0 + s_1}{2} \right| \right) \left[\frac{\frac{1}{2} N_F(-s_1(\omega - s_0\omega_0))}{\omega - s_0\omega_0 - \epsilon_0 + i\Gamma} \right. \\
 &\quad + \frac{i s_1}{4\pi(\omega - s_0\omega_0 - \epsilon_0 - i\Gamma)} (\Psi(\epsilon_0 + i\Gamma) - \Psi(\omega - s_0\omega_0)) \\
 &\quad \left. - \frac{i s_1}{4\pi(\omega - s_0\omega_0 - \epsilon_0 + i\Gamma)} (\bar{\Psi}(\epsilon_0 - i\Gamma) - \bar{\Psi}(\omega - s_0\omega_0)) \right]. \tag{B.19}
 \end{aligned}$$

In the next sections we perform the still missing integrations.

B.3 Solving the remaining integrals

In this appendix we will solve $I_0[s_0, s_1]$ using residual theory. Remember the definition:

$$I_0[s_0, s_1] = \int \frac{d\Omega}{2\pi} \frac{G_0^{++}(\omega - \Omega)}{\Omega - s_0\omega_0 + s_1 i\delta} ; \quad s_{0,1} = \pm 1. \tag{B.20}$$

For simplifying the calculation, we first split up

$$G_0^{++}(\omega - \Omega) = \frac{\omega - \Omega - \epsilon_0 + i\Gamma(N_F(\omega - \Omega) - 1)}{(\omega - \Omega - \epsilon_0)^2 + \Gamma^2} = \frac{1}{\omega - \Omega - \epsilon_0 + i\Gamma} + \frac{i\Gamma N_F(\omega - \Omega)}{(\omega - \Omega - \epsilon_0)^2 + \Gamma^2},$$

and rewrite $I_0[s_0, s_1] := I_1[s_0, s_1] + I_2[s_0, s_1]$ as sum of two integrals to be solved separately within the next two sections.

Solving $I_1[s_0, s_1]$

The integral we want to solve is

$$I_1[s_0, s_1] = \int \frac{d\Omega}{2\pi} \frac{-1}{\Omega - (s_0\omega_0 - s_1 i\delta)} \frac{1}{\Omega - (\omega - \epsilon_0 + i\Gamma)}. \tag{B.21}$$

We use residual theory since the denominator has leading order Ω^2 and therefore the integrand vanishes for integrating from infinity to minus infinity over a semicircle with infinite radius. This can be shown using the parametrization

$$\Omega(\phi) = R e^{i\phi} \quad \rightarrow \quad d\Omega = R i e^{i\phi} d\phi \tag{B.22}$$

and a general polynomial of degree two:

$$\begin{aligned}
 \int_{\text{semicircle}} d\Omega \frac{1}{a\Omega^2 + b\Omega + c} &= \lim_{R \rightarrow \infty} \int_0^{2\pi} d\phi \frac{R i e^{i\phi}}{aR^2 e^{2i\phi} + bR e^{i\phi} + c} \\
 &= \lim_{R \rightarrow \infty} \int_0^{2\pi} d\phi \frac{1}{R} \frac{i e^{i\phi}}{a e^{2i\phi} + \frac{1}{R} b e^{i\phi} + \frac{c}{R^2}} = 0. \tag{B.23}
 \end{aligned}$$

Since the same argumentation is valid for the lower semicircle one can choose one of them. The integrand of $I_1[s_0, s_1]$ has two simple poles

$$\Omega_1[s_0, s_1] = s_0\omega_0 - s_1i\delta \quad ; \quad \Omega_2 = \omega - \epsilon_0 + i\Gamma \quad (\text{B.24})$$

which correspond to the following residues:

$$\text{Res}(\Omega_1) = \lim_{\Omega \rightarrow \Omega_1} \frac{-1}{2\pi} \frac{\Omega - \Omega_1}{(\Omega - \Omega_1)(\Omega - \Omega_2)} = -\frac{1}{2\pi(\Omega_1 - \Omega_2)} \quad , \quad (\text{B.25})$$

$$\text{Res}(\Omega_2) = \lim_{\Omega \rightarrow \Omega_2} \frac{-1}{2\pi} \frac{\Omega - \Omega_2}{(\Omega - \Omega_1)(\Omega - \Omega_2)} = +\frac{1}{2\pi(\Omega_1 - \Omega_2)} \quad . \quad (\text{B.26})$$

The pole of $\Omega_1[s_0, -1]$ and of Ω_2 are in the upper half-plane and the pole of $\Omega_1[s_0, +1]$ is in the lower half-plane. Choosing a closed contour along the real axis and in the upper half-plane with positive orientation, the integral is:

$$I_1[s_0, +1] = 2\pi i(\text{Res}(\Omega_2)) = -\frac{i}{\omega - s_0\omega_0 - \epsilon_0 + i\Gamma + i\delta} \quad , \quad (\text{B.27})$$

$$I_1[s_0, -1] = 2\pi i(\text{Res}(\Omega_1) + \text{Res}(\Omega_2)) = 0 \quad . \quad (\text{B.28})$$

Solving $I_2[s_0, s_1]$

The first step is to do a partial fraction decomposition on the integrand of $I_2[s_0, s_1]$, which can be done in a symmetric way. (Note that s_1 is written as \pm and N_F is decomposed with respect to its lead dependence

$$I_2[s_0, \pm] = \sum_{\alpha=L/R} \int \frac{d\Omega}{2\pi} \frac{1}{\Omega - (s_0\omega_0 \mp i\delta)} \frac{i\Gamma n_F(\omega - \Omega - \mu_\alpha)}{(\omega - \Omega - \epsilon_0)^2 + \Gamma^2} = \sum_{\alpha=L/R} I_2^\alpha[s_0, \pm] \quad . \quad (\text{B.29})$$

The substitution $\omega - \Omega = x$ leads to

$$I_2^\alpha[s_0, \pm] = \int \frac{dx}{2\pi} \frac{1}{\omega - s_0\omega_0 \pm i\delta - x} \frac{i\Gamma n_F(x - \mu_\alpha)}{(x - \epsilon_0)^2 + \Gamma^2} \quad . \quad (\text{B.30})$$

The poles of the integrand are:

$$x_0^\pm = \omega - s_0\omega_0 \pm i\delta \quad ; \quad x_1^\pm = \epsilon_0 \pm i\Gamma \quad ; \quad x_2^\pm = \pm i\frac{\pi}{\beta}(2n+1) + \mu_\alpha \quad . \quad (\text{B.31})$$

After a partial fraction decomposition

$$\begin{aligned} I_2^\alpha[s_0, \pm] &= - \int \frac{dx}{2\pi} \frac{i\Gamma n_F(x - \mu_\alpha)}{(x - x_0^\pm)(x - x_1^+)(x - x_1^-)} \\ &= - \int \frac{dx}{2\pi} \frac{i\Gamma}{2i\Gamma} \left(\underbrace{\frac{n_F(x - \mu_\alpha)}{(x - x_0^\pm)(x - x_1^+)}}_{g^+(x)} - \underbrace{\frac{n_F(x - \mu_\alpha)}{(x - x_0^\pm)(x - x_1^-)}}_{g^-(x)} \right) \end{aligned} \quad (\text{B.32})$$

we need the following residues:

$$\begin{aligned} \text{Res}(g^+, x_0^\pm) &= \frac{n_F(x_0^\pm - \mu_\alpha)}{x_0^\pm - x_1^\pm} & ; & \quad \text{Res}(g^-, x_0^\pm) = \frac{n_F(x_0^\pm - \mu_\alpha)}{x_0^\pm - x_1^\mp} & \quad (\text{B.33}) \\ \text{Res}(g^+, x_2^-) &= -\frac{1}{\beta} \frac{1}{(x_2^- - x_0^\pm)(x_2^- - x_1^\pm)} & ; & \quad \text{Res}(g^-, x_2^+) = -\frac{1}{\beta} \frac{1}{(x_2^+ - x_0^\pm)(x_2^+ - x_1^\mp)}. \end{aligned}$$

All poles are of first order. For example the last residuum follows from:

$$\begin{aligned} \text{Res}(g^-, x_2^+) &= \lim_{x \rightarrow x_2^+} \frac{(x - x_2^+)n_F(x - \mu_\alpha)}{(x - x_0^\pm)(x - x_1^\mp)} = \frac{1}{(x_2^+ - x_0^\pm)(x_2^+ - x_1^\mp)} \lim_{\eta \rightarrow 0} \frac{\eta}{e^{\beta(x_2^+ + \eta)} + 1} \\ &= \frac{1}{(x_2^+ - x_0^\pm)(x_2^+ - x_1^\mp)} \lim_{\eta \rightarrow 0} \frac{\eta}{-e^{\beta\eta} + 1} = -\frac{1}{\beta} \frac{1}{(x_2^+ - x_0^\pm)(x_2^+ - x_1^\mp)}. \end{aligned} \quad (\text{B.34})$$

Following the same argumentation as for I_1 we choose a semicircle contour $\mathcal{C}^{+(-)}$ in the upper (lower) half of the complex plane for the integration of $g^{-(+)}$. The upper (lower) contour has a winding number of $+(-)1$ and we end up with:

$$\begin{aligned} I_2^\alpha[s_0, \pm] &= -\frac{1}{4\pi} \left\{ \int_{\mathcal{C}_\pm^-} \frac{n_F(x - \mu_\alpha)}{(x - x_0^\pm)(x - x_1^\pm)} - \int_{\mathcal{C}_\pm^+} \frac{n_F(x - \mu_\alpha)}{(x - x_0^\pm)(x - x_1^\mp)} \right\} \\ &= -\frac{1}{4\pi} \left\{ (-2\pi i) (\text{Res}(g^+, x_0^-) \delta_{\pm,-} + \sum_{n=0}^{\infty} \text{Res}(g^+, x_2^-)) \right. \\ &\quad \left. - (2\pi i) (\text{Res}(g^-, x_0^+) \delta_{\pm,+} + \sum_{n=0}^{\infty} \text{Res}(g^-, x_2^+)) \right\} \\ &= \frac{i}{2} \left\{ \text{Res}(g^\mp, x_0^\pm) + \sum_{n=0}^{\infty} \text{Res}(g^+, x_2^-) + \text{Res}(g^-, x_2^+) \right\}. \end{aligned} \quad (\text{B.35})$$

Back-substitution for the first summand leads to:

$$\text{Res}(g^\mp, x_0^\pm) = \frac{n_F(x_0^\pm - \mu_\alpha)}{x_0^\pm - x_1^\mp} = \frac{n_F(\omega - s_0\omega_0 - \mu_\alpha \pm i\delta)}{\omega - s_0\omega_0 - \epsilon_0 \pm i\Gamma \pm i\delta}. \quad (\text{B.36})$$

Next we have to evaluate the series we got from the poles of the Fermi-function. We will again use the relation Eq. (A.8) to get a solution in terms of the digamma function $\psi_0(x)$.

Thus, the result is

$$\begin{aligned}
 I_{2,\psi}^\alpha[s_0, \pm] &= \frac{\mathfrak{i}}{2} \left(\sum_{n=0}^{\infty} \text{Res}(g^+, x_2^-) + \text{Res}(g^-, x_2^+) \right) \\
 &= \sum_{n=0}^{\infty} \left(\frac{1}{2\beta\mathfrak{i}} \right) \left[\frac{1}{(x_2^- - x_0^\pm)(x_2^- - x_1^+)} + \frac{1}{(x_2^+ - x_0^\pm)(x_2^+ - x_1^-)} \right] \\
 &= \sum_{n=0}^{\infty} \left(\frac{1}{2\beta\mathfrak{i}} \right) \left[\frac{1}{-x_1^+ + x_0^\pm} \left(\frac{1}{x_2^- - x_0^\pm} - \frac{1}{x_2^- - x_1^+} \right) + \frac{1}{-x_1^- + x_0^\pm} \left(\frac{1}{x_2^+ - x_0^\pm} - \frac{1}{x_2^+ - x_1^-} \right) \right] \\
 &= \sum_{n=0}^{\infty} \left(\frac{1}{2\beta\mathfrak{i}} \right) \left[\frac{-\beta}{2\pi\mathfrak{i}(-x_1^+ + x_0^\pm)} \left(\frac{1}{n + \frac{1}{2} - \frac{\beta}{2\pi\mathfrak{i}}(\mu_\alpha - x_0^\pm)} - \frac{1}{n + \frac{1}{2} - \frac{\beta}{2\pi\mathfrak{i}}(\mu_\alpha - x_1^+)} \right) \right. \\
 &\quad \left. + \frac{\beta}{2\pi\mathfrak{i}(-x_1^- + x_0^\pm)} \left(\frac{1}{n + \frac{1}{2} + \frac{\beta}{2\pi\mathfrak{i}}(\mu_\alpha - x_0^\pm)} - \frac{1}{n + \frac{1}{2} + \frac{\beta}{2\pi\mathfrak{i}}(\mu_\alpha - x_1^-)} \right) \right] \\
 &= \frac{\psi_0 \left(\frac{1}{2} - \frac{\beta}{2\pi\mathfrak{i}}(\mu_\alpha - \epsilon_0 - \mathfrak{i}\Gamma) \right) - \psi_0 \left(\frac{1}{2} - \frac{\beta}{2\pi\mathfrak{i}}(\mu_\alpha - \omega + s_0\omega_0 \mp \mathfrak{i}\delta) \right)}{4\pi(-\epsilon_0 - \mathfrak{i}\Gamma + \omega - s_0\omega_0 \pm \mathfrak{i}\delta)} \\
 &\quad - \frac{\psi_0 \left(\frac{1}{2} + \frac{\beta}{2\pi\mathfrak{i}}(\mu_\alpha - \epsilon_0 + \mathfrak{i}\Gamma) \right) - \psi_0 \left(\frac{1}{2} + \frac{\beta}{2\pi\mathfrak{i}}(\mu_\alpha - \omega + s_0\omega_0 \mp \mathfrak{i}\delta) \right)}{4\pi(-\epsilon_0 + \mathfrak{i}\Gamma + \omega - s_0\omega_0 \pm \mathfrak{i}\delta)}. \quad (\text{B.37})
 \end{aligned}$$

Now we can perform the limit $\delta \rightarrow 0$ and collect all terms:

$$I_{2,f}^\alpha[s_0, \pm] = \frac{\mathfrak{i}}{2} \text{Res}(g^\mp, x_0^\pm) = \frac{\mathfrak{i} n_F(x_0^\pm - \mu_\alpha)}{2(x_0^\pm - x_1^\mp)} = \frac{\mathfrak{i} n_F(\omega - s_0\omega_0 - \mu_\alpha)}{2(\omega - s_0\omega_0 - \epsilon_0 \pm \mathfrak{i}\Gamma)}. \quad (\text{B.38})$$

The whole integral reads $I_2[s_0, s_1] = \sum_{\alpha=L/R} I_{2,f}^\alpha[s_0, s_1] + I_{2,\psi}^\alpha[s_0, s_1]$ and with the definitions from Eq. (B.15) we end up at the final result:

$$\begin{aligned}
 I_2[s_0, s_1] &= \frac{\mathfrak{i} N_F(\omega - s_0\omega_0)}{2(\omega - s_0\omega_0 - \epsilon_0 + s_1\mathfrak{i}\Gamma)} + \frac{\Psi(\epsilon_0 + \mathfrak{i}\Gamma) - \Psi(\omega - s_0\omega_0)}{4\pi(\omega - s_0\omega_0 - \epsilon_0 - \mathfrak{i}\Gamma)} \\
 &\quad - \frac{\bar{\Psi}(\epsilon_0 - \mathfrak{i}\Gamma) - \bar{\Psi}(\omega - s_0\omega_0)}{4\pi(\omega - s_0\omega_0 - \epsilon_0 + \mathfrak{i}\Gamma)}. \quad (\text{B.39})
 \end{aligned}$$

Bibliography

- [1] M. Hasan and C. Kane. *Colloquium: Topological insulators*. Reviews of Modern Physics **82**, 3045 (2010).
- [2] X.-L. Qi and S.-C. Zhang. *Topological insulators and superconductors*. Reviews of Modern Physics **83**, 1057 (2011).
- [3] A. Kitaev. *Unpaired Majorana fermions in quantum wires*. Physics-Uspekhi **44**, 131 (2001).
- [4] L. Fu and C. Kane. *Superconducting Proximity Effect and Majorana Fermions at the Surface of a Topological Insulator*. Physical Review Letters **100**, 096407 (2008).
- [5] M. Sato and S. Fujimoto. *Topological phases of noncentrosymmetric superconductors: Edge states, Majorana fermions, and non-Abelian statistics*. Physical Review B **79**, 094504 (2009).
- [6] C. Beenakker. *Search for Majorana Fermions in Superconductors*. Annual Review of Condensed Matter Physics **4**, 113 (2013).
- [7] M. Leijnse and K. Flensberg. *Introduction to topological superconductivity and Majorana fermions*. Semiconductor Science and Technology **27**, 124003 (2012).
- [8] C. Bolech and E. Demler. *Observing Majorana bound States in p-Wave Superconductors Using Noise Measurements in Tunneling Experiments*. Physical Review Letters **98**, 237002 (2007).
- [9] J. Nilsson, A. R. Akhmerov and C. W. J. Beenakker. *Splitting of a Cooper Pair by a Pair of Majorana Bound States*. Physical Review Letters **101**, 120403 (2008).
- [10] K. Law, P. A. Lee and T. Ng. *Majorana Fermion Induced Resonant Andreev Reflection*. Physical Review Letters **103**, 237001 (2009).
- [11] K. Flensberg. *Tunneling characteristics of a chain of Majorana bound states*. Physical Review B **82**, 180516(R) (2010).
- [12] M. Wimmer, A. R. Akhmerov, J. P. Dahlhaus and C. W. J. Beenakker. *Quantum point contact as a probe of a topological superconductor*. New Journal of Physics **13**, 053016 (2011).
- [13] V. Mourik, K. Zuo, S. M. Frolov, S. R. Plissard, E. P. a. M. Bakkers and L. P. Kouwenhoven. *Signatures of Majorana Fermions in Hybrid Superconductor-Semiconductor Nanowire Devices*. Science **336**, 1003 (2012).

- [14] L. P. Rokhinson, X. Liu and J. K. Furdyna. *The fractional a.c. Josephson effect in a semiconductor-superconductor nanowire as a signature of Majorana particles*. Nature Physics **8**, 795 (2012).
- [15] A. Das, Y. Ronen, Y. Most, Y. Oreg, M. Heiblum and H. Shtrikman. *Zero-bias peaks and splitting in an AlInAs nanowire topological superconductor as a signature of Majorana fermions*. Nature Physics **8**, 887 (2012).
- [16] M. T. Deng, C. L. Yu, G. Y. Huang, M. Larsson, P. Caroff and H. Q. Xu. *Anomalous zero-bias conductance peak in a Nb-InSb nanowire-Nb hybrid device*. Nano letters **12**, 6414 (2012).
- [17] R. Lutchyn, J. Sau and S. Das Sarma. *Majorana Fermions and a Topological Phase Transition in Semiconductor-Superconductor Heterostructures*. Physical Review Letters **105**, 077001 (2010).
- [18] Y. Oreg, G. Refael and F. von Oppen. *Helical Liquids and Majorana Bound States in Quantum Wires*. Physical Review Letters **105**, 177002 (2010).
- [19] J. Alicea. *New directions in the pursuit of Majorana fermions in solid state systems*. Reports on progress in physics **75**, 076501 (2012).
- [20] D. Bagrets and A. Altland. *Class D Spectral Peak in Majorana Quantum Wires*. Physical Review Letters **109**, 227005 (2012).
- [21] J. Liu, A. C. Potter, K. T. Law and P. a. Lee. *Zero-Bias Peaks in the Tunneling Conductance of Spin-Orbit-Coupled Superconducting Wires with and without Majorana End-States*. Physical Review Letters **109**, 267002 (2012).
- [22] S. Gangadharaiah, B. Braunecker, P. Simon and D. Loss. *Majorana Edge States in Interacting One-Dimensional Systems*. Physical Review Letters **107**, 036801 (2011).
- [23] E. M. Stoudenmire, J. Alicea, O. A. Starykh and M. P. A. Fisher. *Interaction Effects in Topological Superconducting Wires Supporting Majorana Fermions*. Physical Review B **84**, 014503 (2011).
- [24] E. Sela, A. Altland and A. Rosch. *Majorana fermions in strongly interacting helical liquids*. Physical Review B **84**, 085114 (2011).
- [25] A. Zazunov, A. L. Yeyati and R. Egger. *Coulomb blockade of Majorana-fermion-induced transport*. Physical Review B **84**, 165440 (2011).
- [26] L. Fu. *Electron Teleportation via Majorana Bound States in a Mesoscopic Superconductor*. Physical Review Letters **104**, 056402 (2010).
- [27] N. Didier, M. Gibertini, A. G. Moghaddam, J. König and R. Fazio. *Josephson-Majorana cycle in topological single-electron hybrid transistors*. Physical Review B **88**, 024512 (2013).
- [28] P. a. M. Dirac. *The Quantum Theory of the Electron*. Proceedings of the Royal Society A: Mathematical, Physical and Engineering Sciences **117**, 610 (1928).

-
- [29] C. Anderson. *The Positive Electron*. Physical Review **43**, 491 (1933).
- [30] E. Majorana. *Teoria simmetrica dell'elettrone e del positrone*. Il Nuovo Cimento **14**, 171 (1937).
- [31] Y. Bychkov and E. Rashba. *Oscillatory effects and the magnetic susceptibility of carriers in inversion layers*. Journal of physics C: Solid state ... **17**, 6039 (1984).
- [32] J. Alicea, Y. Oreg, G. Refael, F. von Oppen and M. P. a. Fisher. *Non-Abelian statistics and topological quantum information processing in 1D wire networks*. Nature Physics **7**, 412 (2011).
- [33] A. Zazunov and R. Egger. *Supercurrent blockade in Josephson junctions with a Majorana wire*. Physical Review B **85**, 104514 (2012).
- [34] A. Altland and B. Simons. *Condensed matter field theory* (Cambridge University Press, Cambridge, 2010), 2nd edn.
- [35] Y. V. Nazarov and Y. Blanter. *Quantum transport: introduction to nanoscience* (Cambridge University Press, Cambridge, 2009).
- [36] M. Turek and K. Matveev. *Cotunneling thermopower of single electron transistors*. Physical Review B **65**, 115332 (2002).
- [37] J. Koch, F. von Oppen, Y. Oreg and E. Sela. *Thermopower of single-molecule devices*. Physical Review B **70**, 195107 (2004).
- [38] W. Press, S. Teukolsky, W. Vetterling and B. Flannery. *Numerical recipes: The art of scientific computing* (Cambridge University Press, Cambridge, 2007), 3rd edn.
- [39] R. Hützen, A. Zazunov, B. Braunecker, A. L. Yeyati and R. Egger. *Majorana single-charge transistor*. Physical Review Letters **109**, 166403 (2012).
- [40] A. Kamenev and A. Levchenko. *Keldysh technique and non-linear sigma-model: basic principles and applications*. arXiv:0901.3586v3 (2009).
- [41] Y. Meir and N. S. Wingreen. *Landauer formula for the current through an interacting electron region*. Physical Review Letters **68**, 2512 (1992).
- [42] S. Tewari, C. Zhang, S. Das Sarma, C. Nayak and D.-H. Lee. *Testable Signatures of Quantum Nonlocality in a Two-Dimensional Chiral p-Wave Superconductor*. Physical Review Letters **100**, 027001 (2008).
- [43] J. C. Cuevas and E. Scheer. *Molecular electronics: An Introduction to Theory and Experiment* (World Scientific, Singapore, 2010).
- [44] N. A. Zimbovskaya and M. R. Pederson. *Electron transport through molecular junctions*. Physics Reports **509**, 1 (2011).
- [45] M. Galperin, M. A. Ratner and A. Nitzan. *Molecular transport junctions: vibrational effects*. Journal of Physics: Condensed Matter **19**, 103201 (2007).

- [46] H. G. Craighead. *Nanoelectromechanical Systems*. Science **290**, 1532 (2000).
- [47] M. Roukes. *Nanoelectromechanical systems face the future*. Phys. World **14**, 25 (2001).
- [48] O. Tal, M. Krieger, B. Leerink and J. van Ruitenbeek. *Electron-Vibration Interaction in Single-Molecule Junctions: From Contact to Tunneling Regimes*. Physical Review Letters **100**, 196804 (2008).
- [49] G. A. Steele, A. K. Hüttel, B. Witkamp, M. Poot, H. B. Meerwaldt, L. P. Kouwenhoven and H. S. J. van der Zant. *Strong coupling between single-electron tunneling and nanomechanical motion*. Science **325**, 1103 (2009).
- [50] B. Lassagne, Y. Tarakanov, J. Kinaret, D. Garcia-Sanchez, D. Garcia-Sanchez and A. Bachtold. *Coupling mechanics to charge transport in carbon nanotube mechanical resonators*. Science **325**, 1107 (2009).
- [51] R. Leturcq, C. Stampfer, K. Inderbitzin, L. Durrer, C. Hierold, E. Mariani, M. G. Schultz, F. von Oppen and K. Ensslin. *Franck-Condon blockade in suspended carbon nanotube quantum dots*. Nature Physics **5**, 327 (2009).
- [52] A. K. Hüttel, B. Witkamp, M. Leijnse, M. Wegewijs and H. S. J. van der Zant. *Pumping of Vibrational Excitations in the Coulomb-Blockade Regime in a Suspended Carbon Nanotube*. Physical Review Letters **102**, 225501 (2009).
- [53] T. Holstein. *Studies of polaron motion: Part I. The molecular-crystal model*. Annals of Physics **342**, 325 (1959).
- [54] T. Holstein. *Studies of polaron motion: Part II. The small polaron*. Annals of Physics **8**, 343 (1959).
- [55] A. Mitra, I. Aleiner and A. J. Millis. *Phonon effects in molecular transistors: Quantal and classical treatment*. Physical Review B **69**, 245302 (2004).
- [56] H. Wang and M. Thoss. *Numerically exact quantum dynamics for indistinguishable particles: the multilayer multiconfiguration time-dependent Hartree theory in second quantization representation*. The Journal of chemical physics **131**, 024114 (2009).
- [57] P. Cornaglia, H. Ness and D. Grempel. *Many-Body Effects on the Transport Properties of Single-Molecule Devices*. Physical Review Letters **93**, 147201 (2004).
- [58] L. Arrachea and M. Rozenberg. *Quantum Monte Carlo method for models of molecular nanodevices*. Physical Review B **72**, 041301(R) (2005).
- [59] E. Gull, A. J. Millis, A. Lichtenstein, A. Rubtsov, M. Troyer and P. Werner. *Continuous-time Monte Carlo methods for quantum impurity models*. Reviews of Modern Physics **83**, 349 (2011).
- [60] J. E. Han. *Nonequilibrium electron transport in strongly correlated molecular junctions*. Physical Review B **81**, 113106 (2010).

-
- [61] A. Dirks, P. Werner, M. Jarrell and T. Pruschke. *Continuous-time quantum Monte Carlo and maximum entropy approach to an imaginary-time formulation of strongly correlated steady-state transport*. Physical Review E **82**, 026701 (2010).
- [62] L. Muehlbacher and E. Rabani. *Real-Time Path Integral Approach to Nonequilibrium Many-Body Quantum Systems*. Physical Review Letters **100**, 176403 (2008).
- [63] M. Schiró and M. Fabrizio. *Real-time diagrammatic Monte Carlo for nonequilibrium quantum transport*. Physical Review B **79**, 153302 (2009).
- [64] S. Weiss, J. Eckel, M. Thorwart and R. Egger. *Iterative real-time path integral approach to nonequilibrium quantum transport*. Physical Review B **77**, 195316 (2008).
- [65] S. Weiss, R. Hützen, D. Becker, J. Eckel, R. Egger and M. Thorwart. *Iterative path integral summation for nonequilibrium quantum transport*. preprint arXiv:1304.6919 (2013).
- [66] J. Eckel, F. Heidrich-Meisner, S. G. Jakobs, M. Thorwart, M. Pletyukhov and R. Egger. *Comparative study of theoretical methods for non-equilibrium quantum transport*. New Journal of Physics **12**, 043042 (2010).
- [67] D. Segal, A. J. Millis and D. Reichman. *Numerically exact path-integral simulation of nonequilibrium quantum transport and dissipation*. Physical Review B **82**, 205323 (2010).
- [68] D. Becker, S. Weiss, M. Thorwart and D. Pfannkuche. *Non-equilibrium quantum dynamics of the magnetic Anderson model*. New Journal of Physics **14**, 073049 (2012).
- [69] J. Koch, F. von Oppen and A. Andreev. *Theory of the Franck-Condon blockade regime*. Physical Review B **74**, 205438 (2006).
- [70] L. Keldysh. *Diagram technique for nonequilibrium processes*. Sov. Phys. JETP **20**, 1018 (1965).
- [71] J. Negele and H. Orland. *Quantum many-particle systems* (Westview Press, Boulder, 1998).
- [72] M. Suzuki. *Generalized Trotter's formula and systematic approximants of exponential operators and inner derivations with applications to many-body problems*. Communications in Mathematical Physics **51**, 183 (1976).
- [73] H. De Raedt and B. De Raedt. *Applications of the generalized Trotter formula*. Physical Review A **28**, 3575 (1983).
- [74] I. S. Gradshteyn and I. M. Ryzhik. *Table of integrals, series and products* (Elsevier, 2007), 7th edn.
- [75] R. Hützen, S. Weiss, M. Thorwart and R. Egger. *Iterative summation of path integrals for nonequilibrium molecular quantum transport*. Physical Review B **85**, 121408(R) (2012).

- [76] K. F. Albrecht, A. Martin-Rodero, R. C. Monreal, L. Mühlbacher and A. Levy Yeyati. *Long transient dynamics in the Anderson-Holstein model out of equilibrium*. Physical Review B **87**, 085127 (2013).
- [77] J. Eckel, S. Weiss and M. Thorwart. *Phonon-induced decoherence and dissipation in donor-based charge qubits*. The European Physical Journal B **53**, 91 (2006).
- [78] M. Thorwart, P. Reimann and P. Haenggi. *Iterative algorithm versus analytic solutions of the parametrically driven dissipative quantum harmonic oscillator*. Physical Review E **62**, 5808 (2000).
- [79] R. Egger and A. Gogolin. *Vibration-induced correction to the current through a single molecule*. Physical Review B **77**, 113405 (2008).
- [80] B. Dóra and A. Halbritter. *Temperature-dependent conductance of deformable molecular devices*. Physical Review B **80**, 155402 (2009).
- [81] Y. Vinkler, A. Schiller and N. Andrei. *Quantum quenches and driven dynamics in a single-molecule device*. Physical Review B **85**, 035411 (2012).
- [82] K. Flensberg. *Tunneling broadening of vibrational sidebands in molecular transistors*. Physical Review B **68**, 205323 (2003).
- [83] J. Koch and F. von Oppen. *Franck-Condon blockade and giant Fano factors in transport through single molecules*. Physical Review Letters **94**, 206804 (2005).
- [84] F. Pistolesi, Y. Blanter and I. Martin. *Self-consistent theory of molecular switching*. Physical Review B **78**, 085127 (2008).
- [85] N. Bode, S. Kusminskiy, R. Egger and F. von Oppen. *Scattering Theory of Current-Induced Forces in Mesoscopic Systems*. Physical Review Letters **107**, 036804 (2011).
- [86] S. Braig and K. Flensberg. *Vibrational sidebands and dissipative tunneling in molecular transistors*. Physical Review B **68**, 205324 (2003).
- [87] G. Mahan. *Many-particle physics* (Plenum Press, New York, 1981).
- [88] D. Mozyrsky, M. Hastings and I. Martin. *Intermittent polaron dynamics: Born-Oppenheimer approximation out of equilibrium*. Physical Review B **73**, 035104 (2006).

Danksagung

Zunächst gilt mein besonderer Dank meinem Betreuer Herrn Prof. Dr. Egger, der diese Arbeit durch das Vertrauen in mich, die Auswahl interessanter Themen und seine stete Offenheit für Diskussionen erst ermöglichte.

Herrn Prof. Dr. Horbach danke ich sehr für die Bereitschaft zur Koreferenz dieser Arbeit.

I am also grateful to Prof. Dr. Levy Yeyati for providing me the opportunity to apply for the “INC Young Researchers Prize”, a great visit to Madrid and for the fruitful collaborative work.

Ebenfalls danke ich Herrn Prof. Dr. Thorwart für seine Unterstützung gerade in der ersten Zeit meiner Arbeit und für die Ermöglichung produktiver Forschungsaufenthalte in Freiburg und die gute Zusammenarbeit.

Ebenfalls für die tolle Zusammenarbeit möchte ich Dr. Bernd Braunecker und Dr. Alex Zazunov danken. Gerade die vielen Diskussionen mit Alex waren mir immer eine Freude und Inspiration (Question?!...). Ich werde die nachmittäglichen Diskussionen vermissen.

Für die tolle Arbeitsatmosphäre am Institut möchte ich allen Kollegen danken. Im speziellen Frau Wildhagen für ihre stete Hilfsbereitschaft bei allem Organisatorischen, Jens für seine Geduld bei meinen Installationsanfragen und Aldo für das tolle Essen am Wochenende während des Zusammenschreibens, seine Durchsicht des Manuskripts und die vielen Diskussionen.

Meinen wechselnden Bürokollegen und Nachbarn Jens Eckel, Andreas Schulz, Denis Klöpfer und Stephan Weiss schulde ich Dank für die stets nette Arbeitsatmosphäre und ihr unaufhörliches Interesse zu diskutieren. Gerade für die Zusammenarbeit und Freundschaft mit Stephan, die mich auch durch alle Tiefphasen meiner Arbeit begleitet hat, bin ich sehr Dankbar, ebenso wie für die Durchsicht des Manuskripts. Auch Sylvia möchte ich für ihre Freundschaft und die sorgfältige Durchsicht des Manuskripts danken.

Nicht zu vergessen ist natürlich auch die stete Ablenkung in meiner Freizeit, für die ich allen meinen Freunden, die mich durch die letzten vier Jahre begleitet haben sehr danke. Namentlich möchte ich an dieser Stelle erwähnen: Anne, Anna-Lena, Daniel, Daniela, Gjlsha, Holger, Jan, Jessi, Johanna, Julia, Katharina, Katrin, Lisa, Olga, Olivia, Philipp, Phuong, und Renate.

Ein riesen Dank geht an meine liebe Mitbewohnerin Isabel die mich in allen Phasen meiner Arbeit ertragen und unterstützt hat ;-)

Der größte Dank gilt natürlich meinen Eltern, die stets an mich glaubten und mir mein Studium und damit diese Arbeit überhaupt erst ermöglicht haben und mich in jeder erdenklichen Weise unterstützen.

Erklärung

Die vorliegende Dissertation habe ich eigenständig und ohne Verwendung unerlaubter Hilfsmittel angefertigt. Sie wurde bisher nicht in identischer oder ähnlicher Form bei einer anderen Institution eingereicht. Ich habe bisher keine erfolglosen Promotionsversuche unternommen.

Düsseldorf, 29. Mai 2013

(Roland Hützen)